ASPECTS OF PROCESSING AND ANALYSIS OF HUMAN GAIT DATA

BY

MOHAMED SAID ABDEL-AZIM

B.Sc.(Eng.), B.Sc.(Math.), M.Eng.

A Thesis

Submitted to the Faculty of Graduate Studies

in Partial Fulfilment of the Requirements

for the Degree

Doctor of Philosophy

McMaster University

April, 1979

ASPECTS OF PROCESSING AND ANALYSIS OF HUMAN GAIT DATA

DOCTOR OF PHILOSOPHY (1979) McMASTER UNIVERSITY
(Electrical Engineering) Hamilton, Ontario

TITLE: Aspects of Processing and Analysis of Human Gait Data

AUTHOR: Mohamed Said Abdel-Azim

B.Sc. (Elect. Eng.) (Cairo University)

B.Sc. (Math.) (Ain Shams University)

M.Eng. (Elect. Eng.) (McMaster University)

SUPERVISORS: Professors E. Della Torre and N.K. Sinha

NUMBER OF PAGES: xii, 169

ABSTRACT

This thesis is mainly directed towards the developement of new techniques that can be used in the analysis of normal and pathological gaits. The kinematic aspects of human gait are studied, and a new technique for the derivation of spatial trajectories of joints from electrogoniometric measurements is presented. The technique relies on the fact that at any point in time, there is at least one point of either foot in contact with the floor. This point is used as an instantaneous reference from which the positions of the joints are calculated. The procedure is repeated for various points of contact during the walk cycles.

The spatial trajectories are used in the study of the kinetics of gait. Forces and moments acting at the joints are computed by considering the equations of motion of the segments of the lower extremity. Rates of energy exchange between the muscles crossing the joints and the segments connected by these joints are estimated, and the total energy expenditure by the leg muscles during swing is obtained. The relation between the speed of walking and energy expenditure by the muscles is studied for normal

subjects and hemiplegic patients. The outcome of this study is a new method that can be used in the assessment of normal and pathological gaits.

A study of the various electromyographic processing strategies is presented. The different processors are evaluated, and the processor that is most suitable for the analysis of gait is determined. This processor is used on EMG signals from various muscles, and the processed signals are used as inputs to systems whose outputs are the muscle torques at the joints. The transfer-function models of these systems are obtained for the swing phase, and then the same models are used to predict muscle torques and floor-reaction forces during the stance phase.

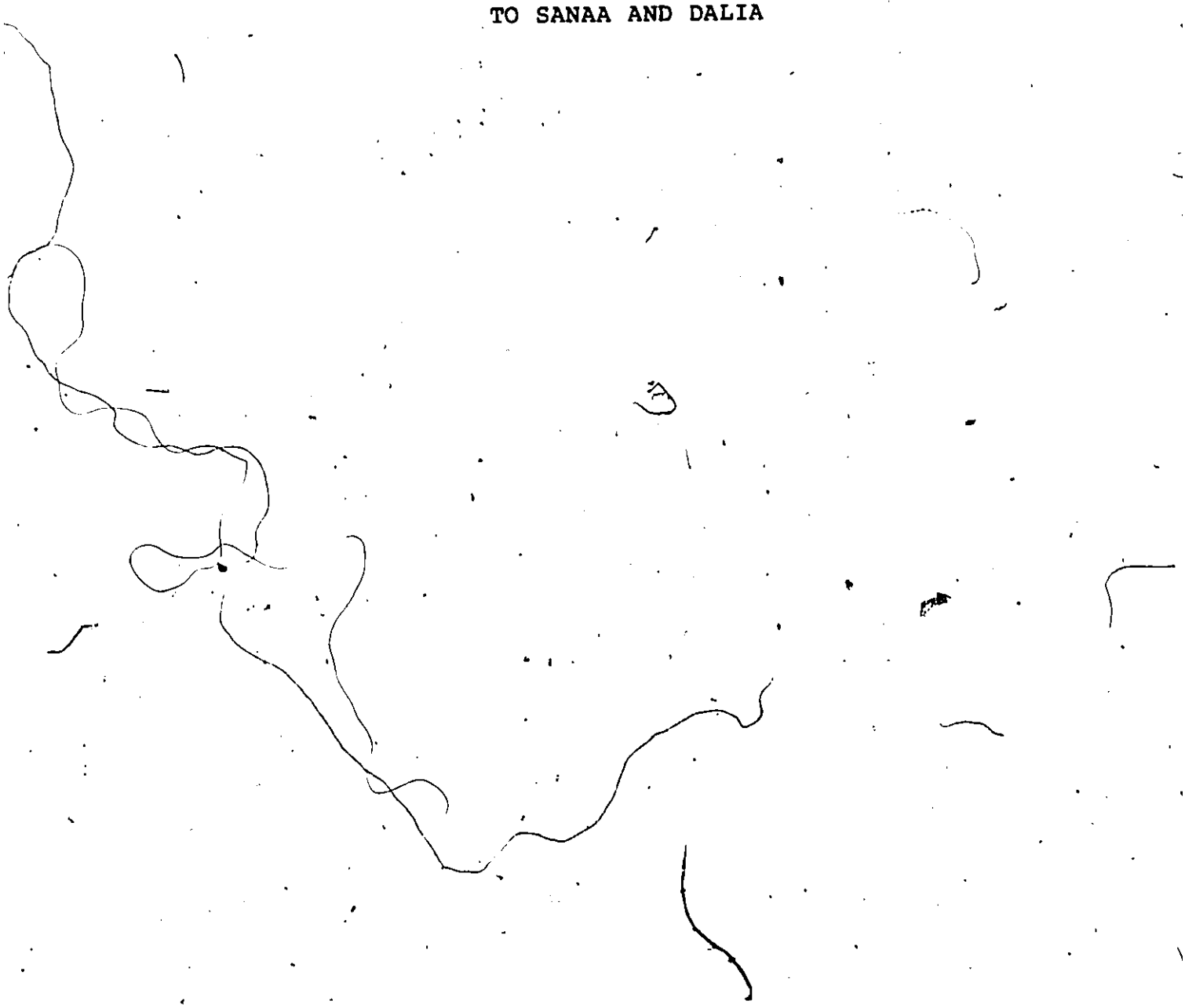
TO SANAA AND DALIA

ACKNOWLEDGEMENTS

With deep gratitude I wish to express my appreciation and thanks to Professor E. Della Torre for his guidance and support throughout this work. I am also sincerely thankful and indebted to Professor N.K. Sinha for his help and valuable suggestions.

The support and encouragement of Dr. M. Milner are greatly appreciated. I would also like to thank Dr. M. Brandstater for his helpful suggestions and discussions.

Further thanks are due to the entire Biomedical Engineering Department, Chedoke Rehabilitation Centre, and in particular to Dr. H. de Bruin, Dr. S. Naumann, Dr. C. Hershler, Mr. T. Wallace and Mr. S. Szarka.

Special thanks are due to Miss P. Dillon and Miss N. Sine for their invaluable help in typing this thesis.

Appreciation is gratefully expressed to McMaster University and the National Research Council of Canada for their financial support.

Finally, the understanding and patience of my wife and daughter are greatly appreciated.

TABLE OF CONTENTS

TABLE OF CONTENTS (cont'd)

TABLE OF CONTENTS (cont'd)

LIST OF ILLUSTRATIONS

LIST OF ILLUSTRATIONS (cont'd)

LIST OF ILLUSTRATIONS (cont'd)

LIST OF TABLES

CHAPTER 1

INTRODUCTION

Walking constitutes an essential part of everyday human activity. This has prompted many researchers to study the complex mechanisms involved in human gait. By gaining better understanding of these mechanisms, researchers could develop new methods for the quantitative assessment of gait. These methods could be used to assess the recovery of patients suffering from various locomotor disabilities. Another important objective of human gait research is the design of better prosthetic and orthotic devices. As researchers acquire more knowledge about the mechanics of normal gait, they will be able to design devices that will satisfactorily perform some of the functions of the limbs that they replace.

The modern study of human locomotion began in the 1930s and has drawn greater attention since then. Significant contributions during this time include the work of Elftman (1939), Liberson (1965), and Inman (1966). Due to complexity of the subject, most of the results obtained so far have been experimental in nature. Research activities to date appear to fall into two broad areas. The first area is concerned with the functional structure and operational

behaviour of the locomotor system. The second area is concerned with energy expenditure, oxygen consumption, and metabolism in general associated with walking.

This thesis includes original research on three of the major aspects of gait:

(1) Kinematics of gait: the relative angular variations between segments of the lower extremities are measured using electrogoniometers. A new technique is proposed which makes use of these measurements in the derivation of absolute spatial trajectories of joints of the legs.

(2) Kinetics of gait: the forces and torques acting at the joints during the swing phase are determined by solving the equations of motion of segments of the lower extremity. The total muscle torques at the joints are used to compute the energy expended by the leg muscles. By comparing the energies expended by normal subjects with those expended by hemiplegic patient, we arrive at a new method for the assessment of gait.

(3) Electromyography: EMG signals from various leg muscles are measured during walking. Various EMG processing strategies are evaluated using multiple-coherence functions, and the processor most suitable for gait analysis is found. The processed EMG

signals are then used to predict muscle torques and floor-reaction forces during the stance phase.

A brief description of the various mechanisms involved in human gait is given in Chapter 2. Various forces and motions of the leg during the walk cycle are presented, and some aspects of muscle functions are discussed. Also, some of the popular techniques used in gait research are presented.

The experimental procedures used in this study are discussed in Chapter 3. Some of the problems associated with signal processing and acquisition are discussed and possible solutions are suggested.

A study of the kinematics of human gait is presented in Chapter 4. Various digital signal processing techniques are used in the conditioning and analysis of joint-angle data. The processed joint-angle signals are used in the derivation of spatial trajectories of joints using a six-link model of the lower part of the body.

In Chapter 5, the equations of motion of the lower extremity are solved to obtain muscle torques and joint forces during the swing phase. A method for averaging data corresponding to a number of walk cycles is presented. The chapter then ends with a study of energy expenditure by the leg muscles of normal subjects and hemiplegic patients.

Processing of electromyographic signals is studied in Chapter 6. Aspects of linear-system's theory are discussed and used in evaluating the various EMG processing strategies. Transfer-function modeling of the locomotor system is presented in this chapter, and the models are used to predict forces and torques during the stance phase.

Chapter 7 includes some concluding remarks concerning the work presented in earlier chapters. The major difficulties encountered during this work are discussed, and possible solutions are suggested.

CHAPTER 2

HUMAN GAIT: MECHANISMS AND METHODS OF STUDY

2.1 Introduction

Walking from one place to another on two legs seems to be a simple act. Actually, it is the product of many complex interactions between the forces generated within the body and several forces acting upon it. These interactions must be coordinated in such a way as to produce a particular pattern of movement referred to as "gait". Human gait is accomplished by means of an extremely complex control system which automatically integrates changing conditions in the force-motion-position picture at a large number of joints within the body, and the changing pattern of external gravitational forces. Then it modulates the set of internal forces and motions to produce a "normal gait".

In this thesis, our attention is devoted mainly to the role of the three major determinants of gait, namely, the kinematics, kinetics and muscles of the lower part of the body. The analysis is limited to one plane, that is the plane of progression.

This chapter has been written for the benefit of the reader who is not familiar with the various aspects of human

gait. We hope that by understanding some of the complex events that take place during gait, the reader would be able to appreciate some of the motivations behind this work.

The following sections describe some of the events that take place, in the plane of progression, during human gait.

2.2 Terminology

The lower limb is divided into three major segments. The uppermost, which is built around the femur and extends from the hip joint to the knee joint, is the thigh. The second segment, from the knee to the ankle, is technically called the "leg". Since this term is used in everyday language for the entire lower limb, most researchers find a distinct advantage in using the term "shank". The third major subdivision of the limb is the foot.

In this thesis, the term shank is used whenever we deal with the kinetics or the kinematics of the lower extremity. However, when reference is made to the anatomical aspects of the lower limb, we use the term "leg" rather than "shank". The term "shank" is usually used by biomechanical engineers, while anatomists prefer to use the term "leg" instead.

Locomotion is achieved by coordinating the movements of the three segments of the lower limb in space. Our

concern in this thesis is to study movements of the lower extremities in the plane of progression. The possible movements of the segments relative to each other in this plane are depicted in Figure 2.1. The figure shows that movements of the thigh are reflected as rotations at the hip joint, and therefore are termed "hip flexion" and "hip extension". Movements of the shank relative to the thigh are defined as "knee flexion" and "knee hyperextension". Movements of the foot are termed "ankle dorsiflexion" and "ankle plantarflexion". The arrows in the figure indicate the directions of movement of the various segments of the lower limb.

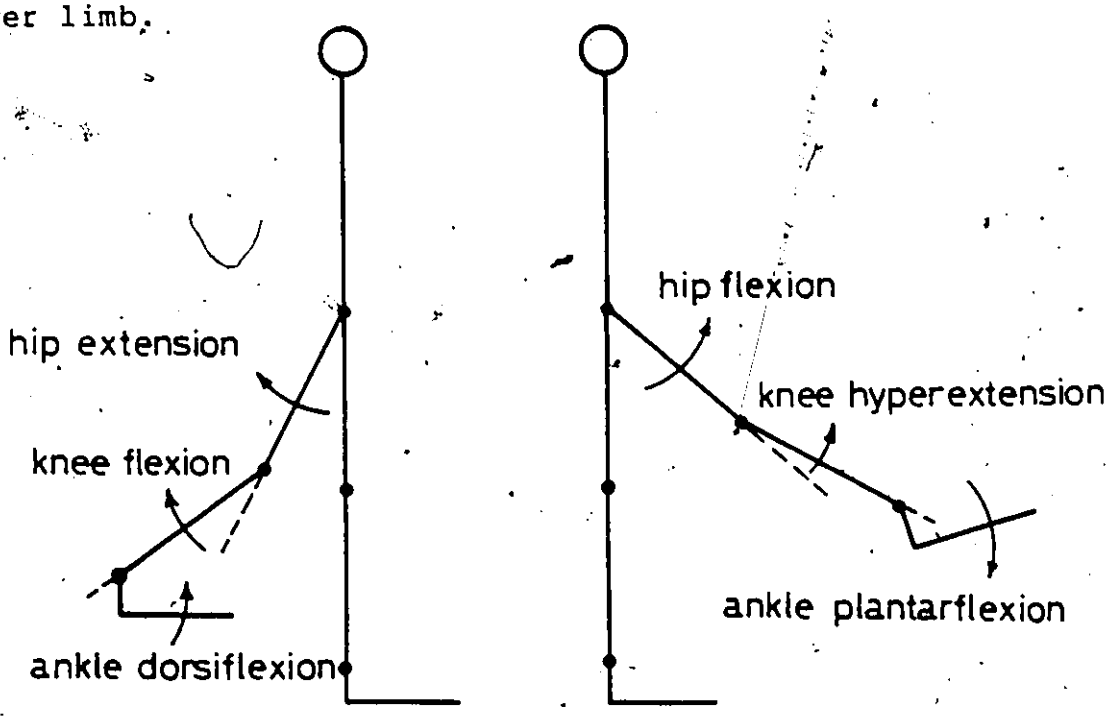

Figure 2.1

Direction of flexion and extension

2.3 Muscles and Electromyography

Muscles play a major role in human locomotion. Not only do muscles move the limb segments in a highly coordinated manner, they also produce forces that help to prevent the body from collapsing under the influence of externally applied forces. The intricate control of the coordinated contraction of various muscles of the body is performed and supervised by the central nervous system.

In this section we are going to discuss briefly some of the main functional characteristics of muscles. In-depth studies of the anatomical, physiological and functional characteristics of muscles can be found in the textbooks by Hollinshead (1976), Katz (1966) and Basmajian (1974) respectively.

2.3.1 Muscle Contraction

The basic structural unit of contraction in the muscle is the muscle fiber. It can be described as a fine thread which has a length of up to 30 cm. and a diameter that can range between 10 and 100 microns. The muscle fiber is capable of contraction to about 57% of its resting length.

When observing the intact muscle during contraction, one would be tempted to think that all the fibers are in some sort of a continuous smooth contraction. In fact, this

is not true, instead the fibers are contracting in a twitch-like pattern and the smooth contraction is a result of summation of all the asynchronous fiber twitches.

The muscle fiber rarely, if ever, acts individually. Instead, small groups of fibers contract at the same moment. Each of these groups is supplied by the terminal branches of one nerve fiber or axon whose cell body lies in the anterior horn of the spinal cord. The nerve cell body, the axon and all the muscle fibers that it activates constitute the "motor unit". The motor unit is the smallest subdivision of the muscle that can undergo a conscious contraction.

The central nervous system controls the muscle activity by sending streams of electrical impulses to the various motor units. When the amplitude of an impulse exceeds a certain threshold, an electrochemical process is triggered. This process results in the activation of muscle fibers in the motor unit, and each fiber undergoes a single twitch of contraction. The threshold of activation varies from one motor unit to the other. Control of the muscle activity is achieved by one of two mechanisms:

(1) At lower force levels, the "recruitment mechanism" is the dominant mechanism in increasing the force level. For very low force levels, only the motor units with lower thresholds of activation are recruited. As the force level increases, motor units with higher

thresholds are recruited as needed.

(2) At high force levels, when all the motor units in the muscle have already been recruited, the "frequency mechanism" takes over. Force level is increased by increasing the frequency of activation of the motor units.

2.3.2 Electromyographic Signals

When the nerve innervates the muscle fibers in a motor unit, a wave of contraction spreads along the fibers resulting in a brief twitch followed by a rapid and complete relaxation. If one places a pair of electrodes along the muscle fiber and observes the amplified electrical activity that accompanies the fiber twitch, certain potential changes will be noticed. These changes are called the "action potential".

The action potential is the result of a spread of a wave of depolarization along the muscle fibers. In the resting state, the voltage across the fiber membrane is about 90 mV with a negative polarity inside the fiber and positive outside. As soon as the fiber is innervated by an incoming impulse from the nerve, the polarity reverses and the change spreads along the fiber. The aggregate potential changes produced by all the muscle fibers in one or more

motor units is called "the electromyographic signal" or "EMG".

The local activity of a limited number of muscle fibers can be monitored by inserting needle or fine-wire electrodes into the muscle. These types of electrodes permit the monitoring of individual action potential trains from one or more muscle fibers.

When EMG signals are monitored by placing electrodes on the muscle surface, an interference pattern is observed. This interference pattern is the result of spatial and temporal summation of action potentials from motor units in the vicinity of the electrodes. Since every contraction of muscle fibers in a motor unit is accompanied by an action potential, EMG signals carry some information concerning the muscle tension. However, the recording electrodes can monitor the activity of a limited number of motor units. Therefore, EMG signals differ from the corresponding smooth tension profiles in that they have the nature of random signals with a bandwidth that extends from zero to a few hundred Hz.

In order to use the EMG signal as a measure of muscle tension, some processing of the signal is needed. The most popular method of processing is to pass the signal through a full-wave rectifier and then smooth the output by a low-pass filter. The resulting signal usually resembles the

corresponding tension profile.

2.3.3 Muscles of the Lower Limb

The musculature of the lower limb includes many muscles that perform various functions, including flexion, extension, adduction, abduction, external rotation, and internal rotation of various segments of the limb. Figure 2.2 shows the anatomical structure of the segments of the lower limb.

Since we are only interested in motion of the lower limb in the plane of progression, only the muscles responsible for motion of the limb segments in this plane are presented. The major muscles of the lower limb, classified according to location, are:

(1) Muscles crossing the front of the hip joint (Figure 2.2a): these are the psoas major and iliacus muscles. These two muscles blend together as they go to a common insertion and have a common action. They are often regarded as one muscle called the iliopsoas muscle. The iliopsoas muscle performs the function of flexing the hip.

(2) Anterior muscles of the thigh (Figure 2.2a): the quadriceps group is the most important group in this category. It consists of the rectus femoris, vastus lateralis, vastus medialis, and vastus intermedius

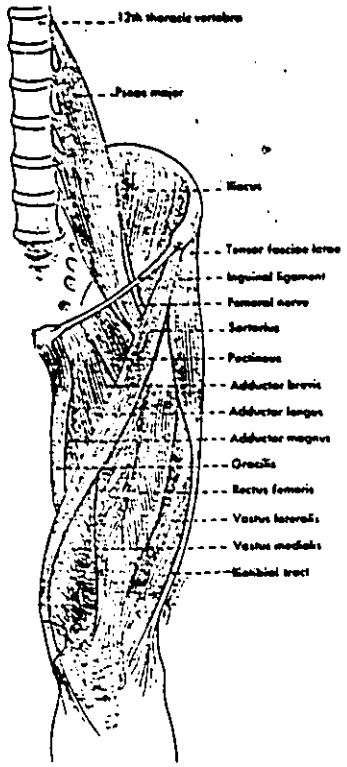

(a) Muscles crossing the front of the hip joint

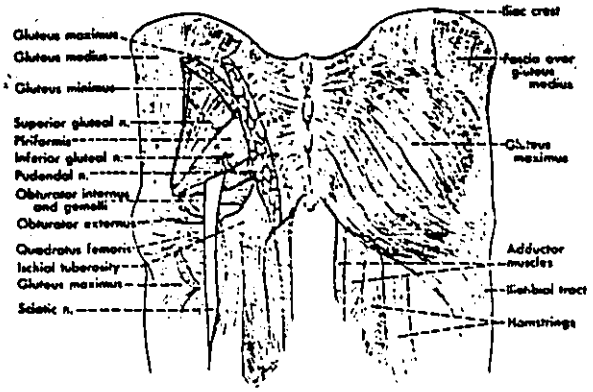

(b) Muscles of the buttock

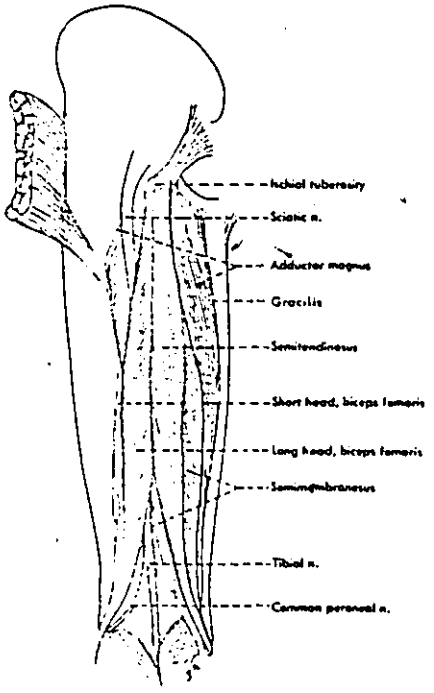

(c) Posterior muscles of the thigh

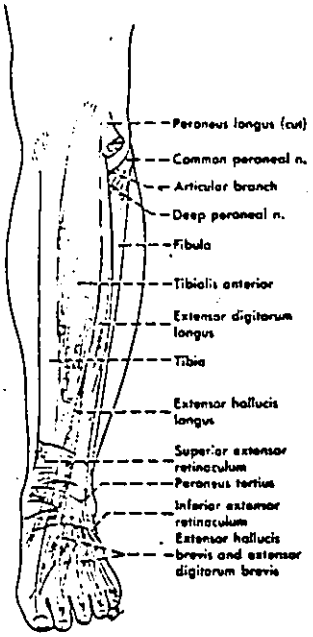

(e) Anterior leg muscles

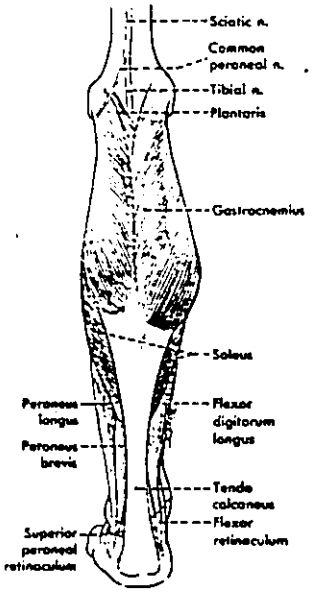

(d) Posterior leg muscles

Figure 2.2
Muscles of the lower extremity
(Hollinshead, 1976)

muscles. The group performs the function of knee extension. In addition, the rectus femoris muscle is also a hip flexor.

(3) Muscles of the buttock (Figure 2.2b): the major muscles that belong to this category are the three gluteal muscles. These are the gluteus maximus, gluteus medius, and gluteus minimus muscles. The gluteus maximus is the only muscle in this group that moves the thigh in the plane of progression. This muscle serves as a powerful extensor of the hip.

(4) Posterior muscles of the thigh (Figure 2.2c): this group of muscles is known as the hamstrings. The group consists of the semitendinosus, semimembranosus and biceps femoris muscles. The first two muscles are both hip extensors and knee flexors. The biceps femoris consists of two heads. The long head is also a hip extensor and knee flexor, while the short head is only a knee flexor.

(5) Posterior muscles of the leg (Figure 2.2d): in this category, the gastrocnemius, soleus, and plantaris muscles play the dominant role in plantarflexing the ankle.

(6) Anterior muscles of the leg (Figure 2.2e): of all the muscles that belong to this category, the tibialis anterior is the most important ankle

dorsiflexor. All the other muscles of the anterior aspect of the leg are either less powerful ankle dorsiflexors, or control motion of the toes.

2.4 Biomechanics of Gait(Peizer and Wright, 1971)

2.4.1 Kinematics of Gait

Human gait is a cyclic process that is based on the repetition of a basic "walk cycle". The walk cycle consists of two main phases, namely, stance and swing phases. The cycle starts when the heel-strike on one leg takes place, and ends when the heel-strike on the same leg occurs. Figure 2.3 depicts the various events that take place during each of the two phases of the walk cycle. The stance phase begins at the heel-strike on one leg and ends at toe-off on the same leg. The swing phase begins where the stance phase ends and represents the period between toe-off on one foot and heel-strike on the same foot.

Stance is characterized by six key events. It begins at the instant the heel touches the floor (heel-strike). Shortly thereafter, the sole makes contact with the ground (foot-flat). Next, the body weight is swung directly over the supporting extremity and continues to rotate over the foot (mid-stance). As the body mass above the ankle continues to rotate forward, the heel lifts off the ground (heel-off). Shortly after this, the body is propelled

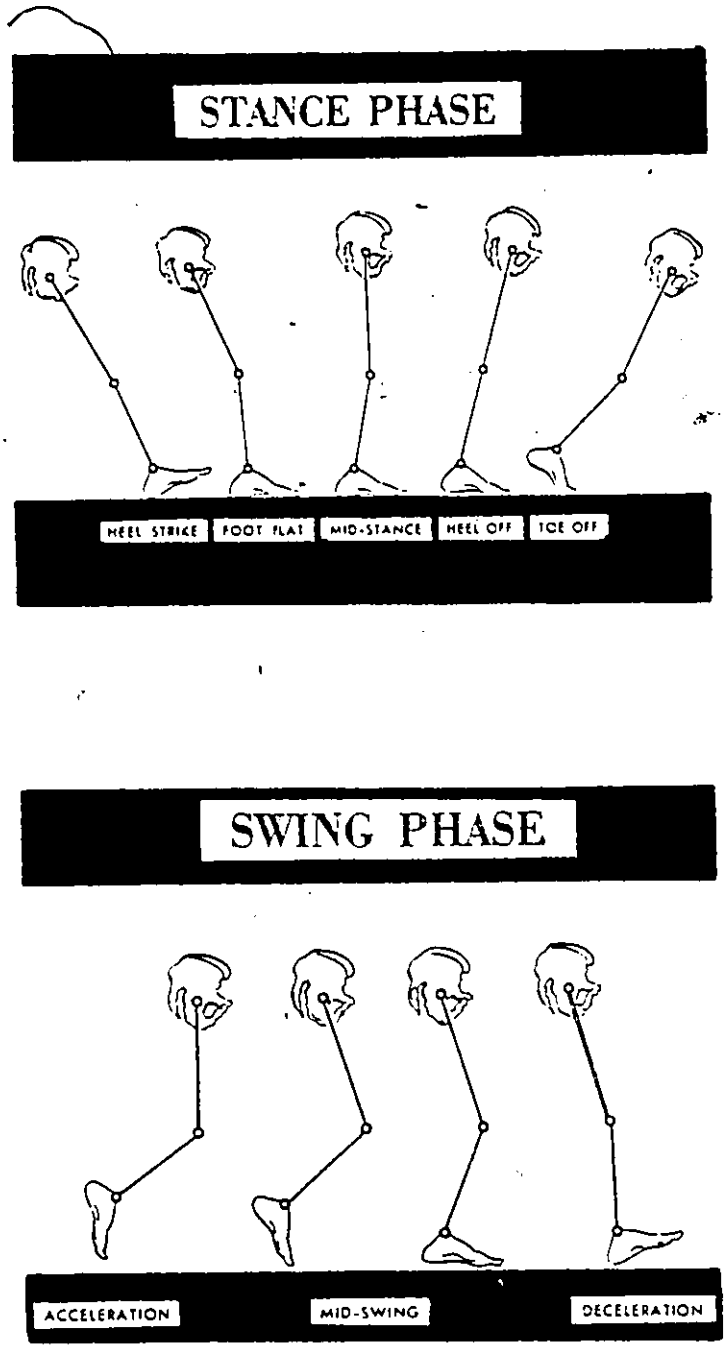

Figure 2.3
Phases of the walk cycle
(Peizer and Wright, 1971)

forward by the forceful action of the calf muscles (push-off). The push-off phase terminates when the entire foot rises from the ground (toe-off).

Swing phase consists of three main events. It starts when the foot lifts off the ground. At this point, the leg is accelerated forward in order to catch up and pass the body. When the swinging leg has caught up and passes directly beneath the body, it is said to be in "mid-swing". A period of deceleration begins after mid-swing when the forward motion of the leg is restrained to control the position and velocity of the foot immediately before heel-strike.

As we alternate from stance to swing on each leg there is a period when both feet are in contact with the ground simultaneously. This period is called "double-support" and it occurs between push-off and toe-off on one foot and heel-strike and foot-flat on the other. Duration of the double-support period is inversely proportional to the speed of walking. Absence of double-support indicates that the person is running rather than walking.

At ordinary speeds, a single leg is in stance for approximately 60% of the cycle and in swing for approximately 40%. Double-support occupies about 25% of the walk cycle time and, of course, includes a portion of the stance phase time for each leg.

2.4.2 Kinetics of Gait

Motion of the joints of each segment of the body results from the interaction of internal forces produced by the muscles and external forces represented principally by the influence of gravity and inertia on the body. In the standing position, the center of gravity (CG) of the body is anterior to the hip joint, tending to flex it, anterior to the knee joint, tending to extend it, and anterior to the ankle joint, tending to dorsiflex it. Therefore, the process of standing is a result of the combined action of the plantarflexors of the ankle and the extensors of the hip. To begin walking, we relax the plantarflexors of one leg, allowing the body to fall forward on that side, and swing the other leg forward at the hip.

Figure 2.4 shows the variations of the ankle angle during the various phases of the walk cycle, along with the ankle moment that is responsible for these variations. After the heel strikes the ground, increasing amounts of body weight are being transmitted to the ground, and reaction forces pushing back against the heel create a moment that tends to plantarflex the ankle. Just before the sole touches the ground (foot-flat), the peak plantarflexion moment is reached at approximately 10% of the cycle. This is immediately followed by the peak plantarflexion angle of the ankle (approximately 15-20 degrees). The ground

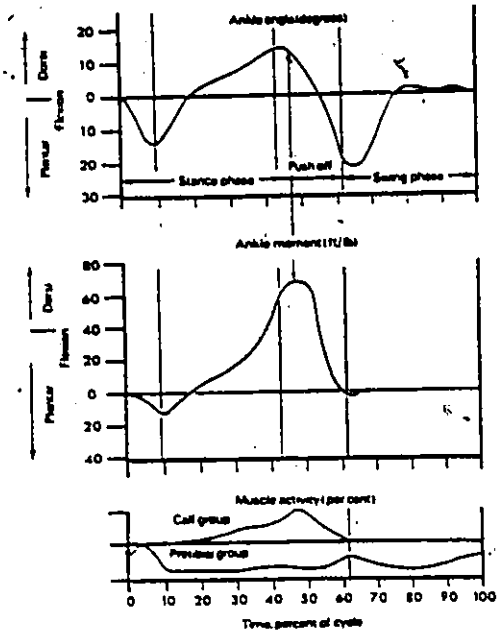

Figure 2.4
Kinematics and kinetics of the ankle joint
(Peizer and Wright, 1971)

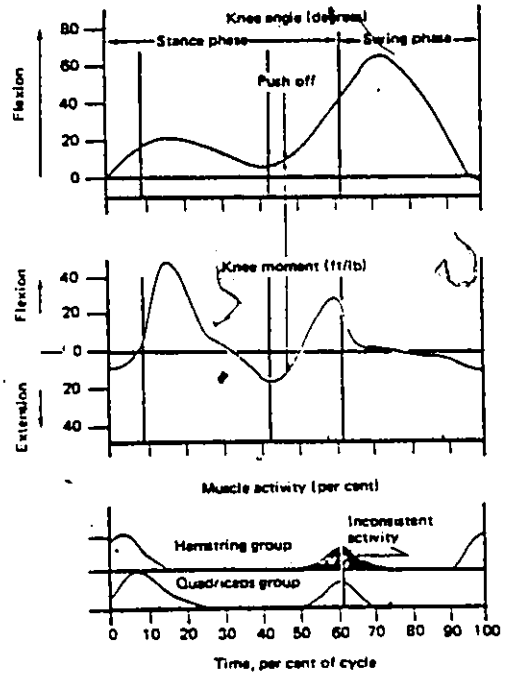

Figure 2.5
Kinematics and kinetics of the knee joint
(Peizer and Wright, 1971)

reaction force causes motion about the ankle at a rate governed by the dorsiflexor muscles of the ankle which absorb this force by stretching and allowing the ankle to move into plantarflexion.

With the foot flat, the mass of the body rotates forward about the ankle, changing the direction of ankle motion from plantar- to dorsiflexion. As both the swinging leg and the body CG move forward, a large moment is generated about the ankle joint tending to dorsiflex it. The peak of this moment is reached very shortly after heel-off when the CG is well in front of the ankle joint and the full body weight is being carried on the ball of the foot. Just before heel-off, the ankle joint moves from maximum plantarflexion to maximum dorsiflexion at a rate governed by the gastrocnemius and soleus muscles.

At the instant of toe-off the ankle is in approximately 15 degrees of plantarflexion. During the swing phase the foot returns to an approximately neutral position and remains in that position until the next heel-strike.

As shown in Figure 2.5, the normal motions and forces acting about the knee joint also demonstrate a characteristic pattern. After heel-strike, with the heel in contact with the ground and increasing amounts of body weight being applied through the leg, the ground reaction line passes behind the knee joint creating a large flexion moment. The

quadriceps muscles resist that moment, and by stretching they permit the knee to flex to approximately 20 degrees in early stance.

The flexion moment diminishes rapidly after foot-flat, as the mass of the body rotates forward, reducing the distance between the knee joint and the line of the ground-reaction force. The instant of mid-stance is indicated by zero moment about the knee after which an extension moment is generated and the knee joint becomes fully extended. At the time of heel-off, the knee begins to flex again under the influence of a moment that increases as the knee joint moves anterior to the ground reaction line.

During swing, forcible hip flexion accelerates the knee center forward. Due to their inertia, the shank and foot tend to lag behind the accelerating knee center, producing flexion about the knee which reaches approximately 65 degrees, and then the knee begins to extend, reaching full extension at the time of the next heel-strike.

The characteristic pattern of normal hip motion is shown in Figure 2.6. As body weight is applied just after heel-strike, the line of ground reaction force passes just anterior to the hip joint, creating a flexion moment at the hip that reaches a maximum just before foot-flat. As the mass of the body rotates over the ankle and knee joints, between foot-flat and mid-stance, the ground reaction force

passes through and then behind the hip joint; the hip moment is zero when the reaction line passes through the hip joint. An extension moment about the hip is generated shortly after foot-flat and gradually increases to a maximum between heel-off and toe-off, which coincides with push-off.

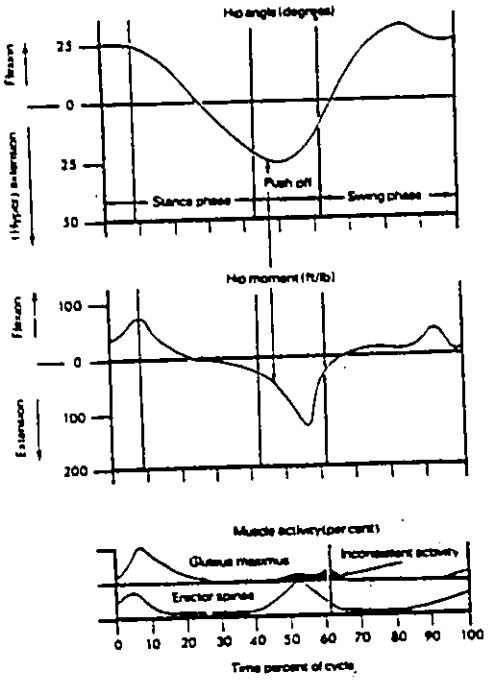

Figure 2.6
Kinematics and kinetics of the hip joint
(Peizer and Wright, 1971)

During all the movements at the three joints, muscles crossing these joints play an important role in generating moments that oppose the externally applied moments or initiate movements of the limb segments. Figure 2.7 shows

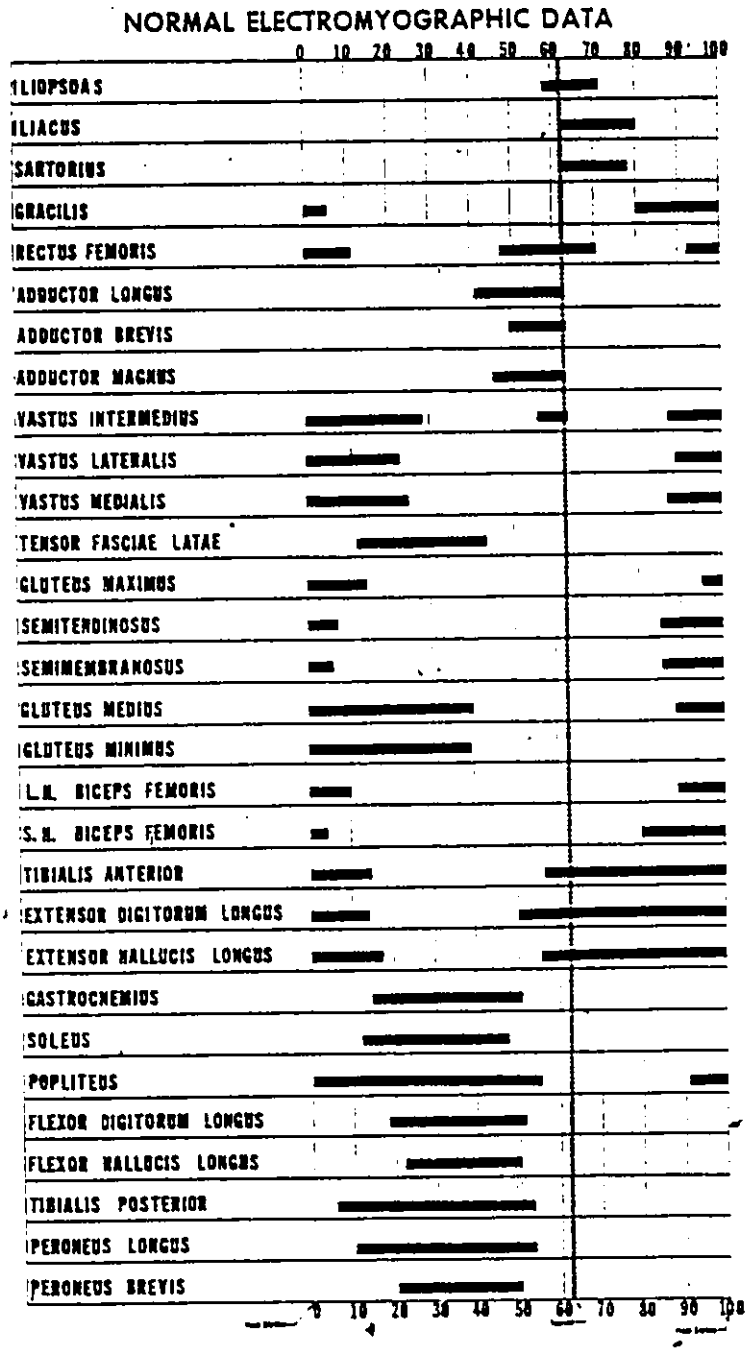

Figure 2.7
Phasic activity of muscles during the walk cycle
(Shriner's Hospital for Crippled Children, San Fran.)

the intervals during which the various leg muscles are active. The figure clearly indicates that there is strong correlation between the phasic activities of the various muscles and the moments generated at the joints. For example, the gastrocnemius and soleus muscles are only active in the interval between about 15% and 50% of the walk cycle. It is during this period that the ankle dorsiflexion moment reaches a maximum, and these two plantarflexor muscles are called upon to oppose this externally applied moment.

2.5 Techniques of Acquiring Human Gait Data

There are many techniques used by researchers to monitor the various events that take place during human gait. The techniques vary in complexity depending on the variables to be monitored. This section describes the most popular techniques used in human gait research.

2.5.1 Temporal Data

In order to measure the times spent by the subject in the various phases of the walk cycle, switches attached to the underside of the subject's shoes are usually used to identify the start and end of each of the different periods in the walk cycle. By placing a switch at the subject's heel and another at the toes, we can identify all the events

of the walk cycle. Closure of only the heel switch indicates "heel-only"; closure of both the heel and toe switches indicates "foot-flat"; closure of only the toe switch indicates "toe-only". When both switches are open, the extremity is in swing.

Footswitch data is usually recorded using a chart recorder or fed directly to a computer. Temporal data is usually used to compute important gait parameters such as stance-to-swing ratio and cadence. These parameters are helpful in assessing the recovery of patients suffering from various pathological problems. The same temporal information can be obtained using any of the camera systems described in the following section.

2.5.2 Kinematic Data

There exists a variety of systems that can be used to record the trajectories of various extremities of the body. These trajectories are important in comparative studies of normal and pathological gaits. In addition, knowledge of the absolute trajectories in space is essential in any study of the kinetics of gait.

The stroboscopic flash-photography system (Kasvand et al., 1976) is one of the many systems used to record the spatial trajectories. This system utilizes an interrupted light to obtain multiple exposures on a single film frame.

The subject wears a special black "cat-suit" with bright markings on the joints and the limb segments. The photograph obtained using this system is a "stick-figure diagram" that indicates the sequential actions of a particular motion in space. One of the disadvantages of this system is that, other than the interrupted light, the system has to be used in complete darkness. This is usually a hazardous procedure, particularly when patients are involved. In addition, the task of digitizing the photographs is a very tedious and laborious one.

Motion pictures, when taken of a moving body and a timer simultaneously, serve as a satisfactory record of absolute motion. Associated equipment project the film, frame by frame, to reduce the photographic sequence to trajectories of the points of interest. Again, time-consuming data reduction is the major problem of this technique. However, this task can be somewhat simplified by using a Vanguard motion analyzer (Sutherland and Hagy, 1972).

Kasvand and Milner (1972) were able to simplify the task of data reduction associated with the use of motion pictures by using a flying spot scanner. Motion pictures are taken of the subject when he walks against a background marked with gray codes. These codes are used to indicate the distance of the subject from a fixed origin. Each joint

is identified by a black circle on a white background. Trajectories of the joints in space are obtained using a flying spot scanner interfaced to a computer. The scanner reads the black circles on the joints and the gray codes in the background and feeds the information to the computer which finds the absolute trajectories. This technique facilitates data reduction with minimum operator intervention.

Television cameras are used by some researchers to monitor human motion. Winter et al. (1972) recorded the data on video tapes and then digitized the tapes, frame by frame, for further computer analysis. Cheng et al. (1975) proposed a simple computer-television interface system for gait analysis. Brugger and Milner (1977) developed a computer-aided tracking system. They used a charge-coupled-device (CCD) image sensor interfaced to a computer. They used small light bulbs to identify the various joints.

All the above-mentioned camera systems enable us to record the absolute trajectories of limb segments in space. On the other hand, relative angular variations between limb segments can be measured by electrogoniometers. The simplest form of an electrogoniometer is a potentiometer attached to two bars. The bars are fastened to the limb segments about the joint, and the relative angle between the

two bars is obtained by measuring the potentiometer voltage and multiplying it by a calibration constant. The calibration constant relates the potentiometer voltage to the actual angle between the two bars. The disadvantage of goniometer systems is that they only measure relative angles between limb segments, and therefore they are not usually used to monitor the absolute spatial trajectories of limbs.

2.5.3 Kinetic Data

In order to find the forces acting at the various joints, external forces acting on the body segments during gait should be known. In particular, ground-reaction forces acting on the foot during stance should be measured before the kinetics of the limb segments can be analyzed.

Ground-reaction forces are usually measured by force plates (Paul, 1965). These consist of strain gauges mounted in a special arrangement on plates that are either built into the floor or above it. The components of the reaction force are measured by the strain gauges. This system is always used in conjunction with a camera system in order to determine the point of application of the reaction force on the foot. Force-plate systems are usually used to measure the reaction forces on one foot during a single step of the subject's walk. If the subject steps on the force plate with both feet simultaneously, it becomes very difficult to

identify the force acting on each foot.

CHAPTER 3

EXPERIMENTAL SETUP AND PROCEDURES

3.1 Introduction

In order to study human gait, a large number of variables have to be monitored. Among these are the trajectories of both the upper and lower extremities. These trajectories are usually used in comparative studies of normal and pathological gaits (Murray and Clarkson, 1966 and Milner et al., 1973). In addition, studies of the kinetics of gait require knowledge of the trajectories, velocities, and accelerations of the centers of gravity of various limb segments. Also, floor-reaction forces, acting on the foot during the stance phase, play an important role in determining the forces and moments acting at the different joints. These reaction forces can be measured using a force plate (Elftman, 1939a).

Any gait study would not be complete unless the forces produced by various muscles are taken into account. However, there is no practical technique that can be used to measure these forces directly. An alternative approach is to monitor the electromyographic (EMG) activities of the muscles and then try to relate these activities to the

muscle forces.

The enormity of the number of variables discussed above makes it impractical to design an experiment to study all the aspects of human gait simultaneously. For this reason, a limited number of variables are considered in this study. Only the role of the lower extremities during gait is studied. In addition, only the components of motion, of segments of the lower limb, in the plane of progression are considered. In all the experiments performed for this study, three different sets of variables were monitored:

(1) Kinematic variables: Electrogoniometers were used to measure the relative angular variations of joints of the lower extremities. Hip, knee, and ankle angles were measured for each extremity. Altogether, six channels were used to acquire the kinematic measurements.

(2) Timing variables: Various phases of the walk cycle were identified using switches attached to the subject's shoes. Two footswitch channels were used during each experiment.

(3) Electromyographic signals: EMG signals from some of the major muscle groups of the lower extremity were recorded. Only eight muscle groups of one extremity were monitored.

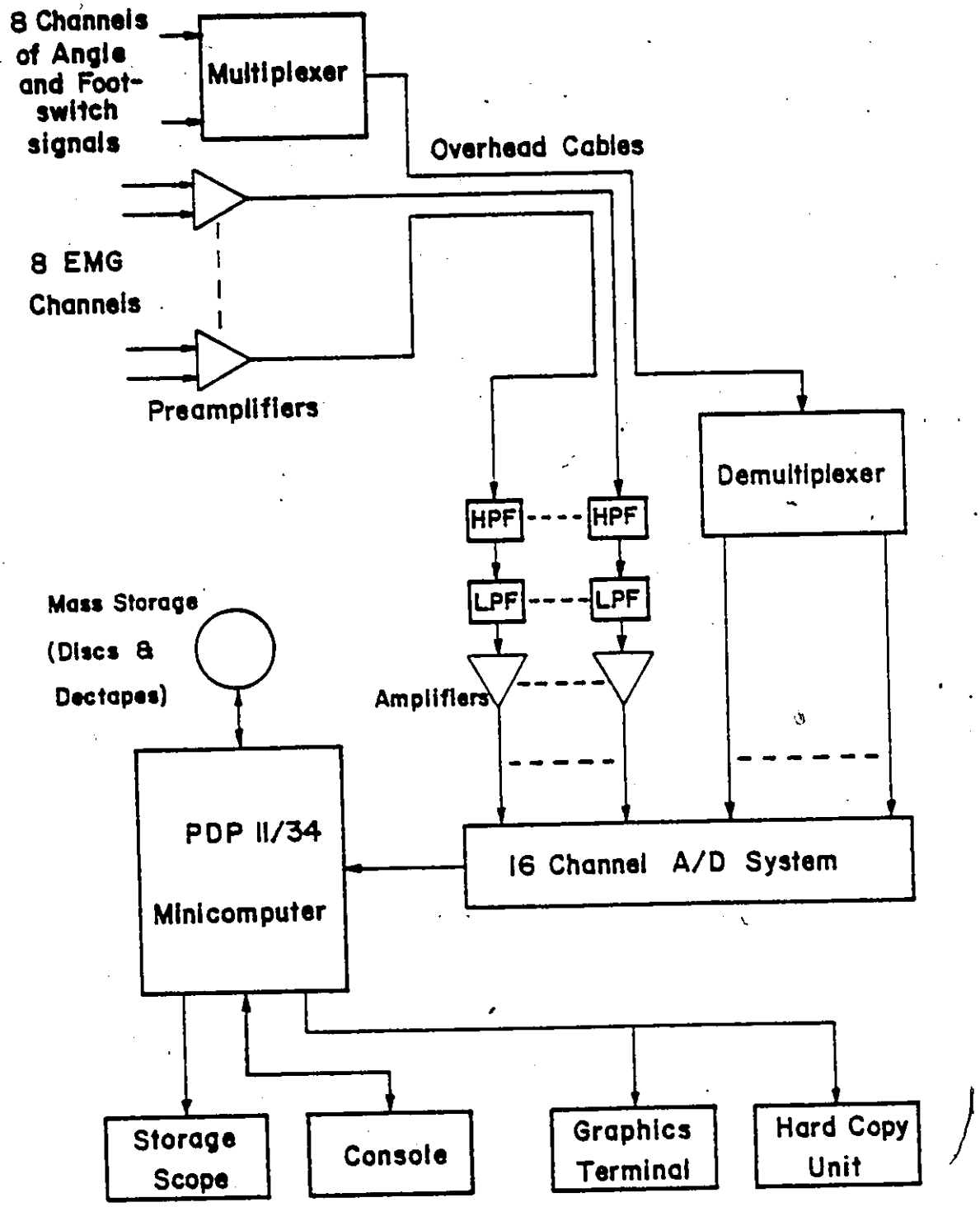

Figure 3.1
Signal acquisition and processing system

Figure 3.1 shows a block diagram of the signal acquisition and processing system used in this study. A detailed description of the different blocks is given in this chapter.

3.2 Experimental Procedures

The experiments were conducted by asking the subject to walk along a straight line in a walkway about eight meters long. One of the important parameters of gait is the speed of walking (Milner et al., 1971). Every effort was made to ensure that the subject maintained a constant speed during each run. For this purpose, a metronome was used to produce beats at a preselected rate. Before each experiment, the subject was asked to practice walking at a given speed by pacing his steps to the beats of the metronome. Data acquisition was not started until the subject was able to walk at the selected speed without any difficulty.

The average speed of walking was measured by placing two modulated light sources, 4 meters apart, on one side of the walkway and two reflectors on the other side. When the subject crossed the first beam of light a timer was started. Interruption of the second beam of light stopped the timer, and the elapsed time interval was read via an LED display. Once the time taken by the subject to walk the 4 meters distance was known, an estimate of the average speed was

calculated. If the measured average speed differed by more than 10% from the desired speed, the run was rejected and the experiment was repeated.

Signals from the measuring instruments and transducers were fed to the computer via a set of multiconductor coaxial cables. These cables were also used to connect the DC power supplies to the instruments. The cables were supported overhead by runners on a tension cable. One end of each cable was connected to the computer, and the other end was connected to a connector block that was fastened to a waist band worn by the subject during the experiment.

3.3 Acquisition of Electromyographic Signals

Due to the low levels of EMG signals (about 0.5 mV peak to peak), several stages of signal processing and conditioning were needed. Details of the various stages of EMG signal processing are given in the following subsections.

3.3.1 Recording Electrodes

The choice of the type of recording electrodes was influenced by several practical factors. Surface electrodes were chosen because of their ease of placement, and because they usually monitor the aggregate activity of muscles, as opposed to indwelling fine-wire electrodes which can only

detect the activity of a small number of muscle fibers. In addition, the pain that results from insertion of indwelling electrodes could affect the subject's gait. However, the disadvantage of using surface electrodes is that only the activity of superficial muscles can be monitored.

Figure 3.2 shows a kit of surface electrodes of the type used in our experiments. This is a Becton-Dickinson disposable electrode kit that consists of 4 silver-silver-chloride electrodes 1 cm in diameter, electrode paste, and an alcohol swab.

Figure 3.2
Surface electrodes for EMG signals

To place the electrodes, the skin was first prepared by rubbing it with the alcohol swab to remove any greasy residues. Th electrode paste was applied to the surface of the electrodes which were then attached to the skin by means of adhesive collars. The purpose of using an electrode paste was to minimize the skin-to-electrode impedance. This is an important consideration because of the low signal levels. A high source impedance could result in an attenuation of the signals, which decreases the signal-to-noise ratio.

One pair of electrodes was used for each muscle of interest. In addition, one ground reference electrode was used in each experiment.

The choice of the muscles to be monitored was affected by two factors:

(1) The muscle had to be superficial so that its activity could be monitored by surface electrodes.

(2) The muscle had to be responsible for moving the limb segments in the plane of progression (sagittal plane).

Eight muscles of the lower extremity were chosen for this study, these were:

(1) Anterior muscles of the thigh: Three muscles that belong to the quadriceps group were chosen, these

were the rectus femoris, the vastus lateralis, and the vastus medialis muscles. These are three of the major extensors of the knee joint. In addition, the rectus femoris is also a hip flexor.

(2) Posterior muscles of the thigh: The short and long heads of the biceps femoris were considered as one source. Also, due to the difficulty in separating EMG signals from the semitendinosus and semimembranosus muscles, they were treated as one muscle. All these muscles are extensors of the hip joint and flexors of the knee joint, except the short head of the biceps femoris which is only a flexor of the knee joint.

(3) Leg muscles: Three of the major leg muscles were chosen, these were the gastrocnemius which is a flexor of the knee joint and a powerful plantarflexor of the ankle joint, the soleus which is also a plantarflexor of the ankle joint, and the tibialis anterior which is the strongest dorsiflexor of the ankle joint.

For each muscle, the two electrodes were placed along the muscle length and were separated by a distance of 4 cm (center to center). Electrodes were placed at the bellies of muscles in an attempt to monitor the activity of as many muscle fibers as possible. The only exceptions were the

cases of muscles with two heads, or two muscles that were to be monitored with the same electrodes; in these cases the electrodes were placed between the muscles in order to pick up an interference pattern from the two sources.

3.3.2 Preamplification of EMG Signals

Electromyographic signals were fed to preamplifiers attached to the subject as close as possible to the electrodes. This stage of preamplification was used to minimize interference from the 60 Hz mains and from other sources. For this purpose, miniature differential amplifiers molded in clear resin (Figure 3.3) were used. Electrode leads were cut to a length of about 4 centimeters and connected to the amplifiers via spiral springs. Outputs of the amplifiers were connected to the connector block by light-weight coaxial cables. These cables were also used to connect the ±15 volt supplies required by the amplifiers. Figure 3.4 shows the circuit diagram of the preamplifiers, and Table 3.1 summarizes their electrical characteristics.

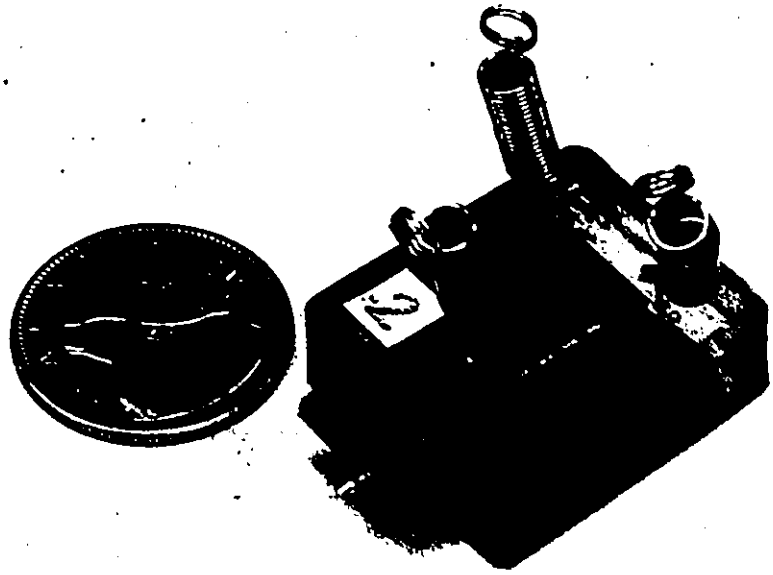

Figure 3.3
Miniature EMG preamplifier

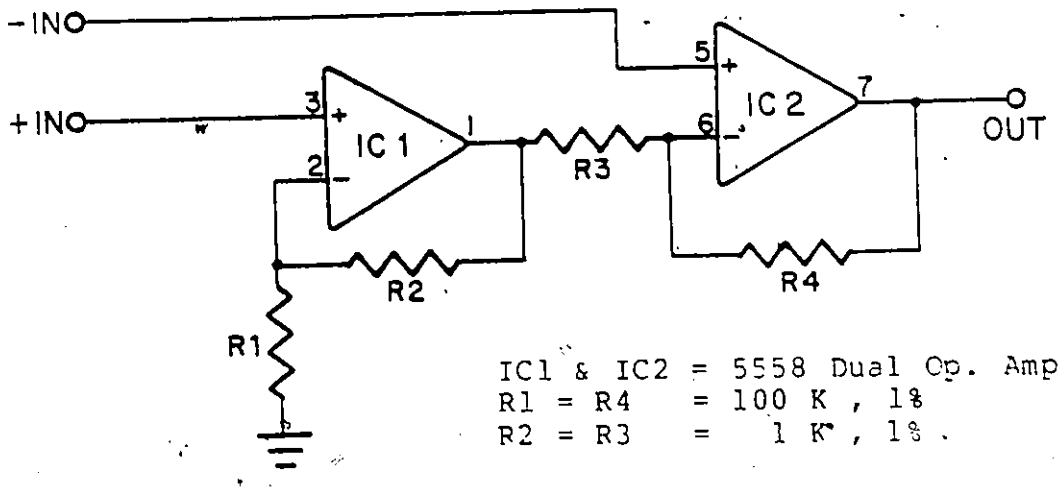

Figure 3.4
Circuit diagram of EMG preamplifier

Common mode gain	= -38 dB
Difference mode gain	= 40 dB
Common mode rejection ratio	= 78 dB
Input impedance	= 1.2 MΩ
Output impedance	= 15 Ω
Upper 3 dB point	= 20 KHz
Gain x bandwidth product	= 2×10^6 Hz

Table 3.1

Characteristics of the preamplifier

3.3.3 Analog Processing of EMG Signals

If not properly processed, EMG signals can be degraded by several sources of noise. Among these sources are:

(1) Motion artifacts: These artifacts result from motion of the cables during the experiment, and also from motion of the skin relative to the muscles. Motion artifacts are regarded as noise of very small bandwidth (0 to 7 or 8 Hz).

(2) Undersampling: According to Nyquist's theory,

sampling of a continuous signal should be performed at a rate equal to, or higher than, twice the highest frequency component in the signal. Sampling at lower than this rate results in the frequency components above half the sampling rate being folded over onto the lower frequency band, distorting the signal in that band. This phenomenon is called "aliasing".

Study of the spectral content of EMG signals, recorded by surface electrodes (Abdel-Azim, 1975), shows that most of the signal power lies in the range from 10 to 200 Hz. This means that high-pass filtering at 10 Hz can be used to filter out motion artifacts without causing a significant loss in useful signal power. In addition, if EMG signals were passed through low-pass filters with cutoff at 200 Hz, the signals could be sampled at any frequency equal to or higher than 400 Hz without being aliased.

To filter out motion artifacts, high-pass filters were used for all the EMG channels. These were fourth order Butterworth high-pass filters with a 10 Hz cutoff frequency and -24 dB/octave roll-off. Figure 3.5 shows the circuit diagram and component values of the filters used.

Aliasing of EMG signals, sampled at 500 Hz, was reduced by using low-pass filters designed and constructed by the author. The design was based on the monographs given by Hilburn and Johnson (1973). These filters were also of

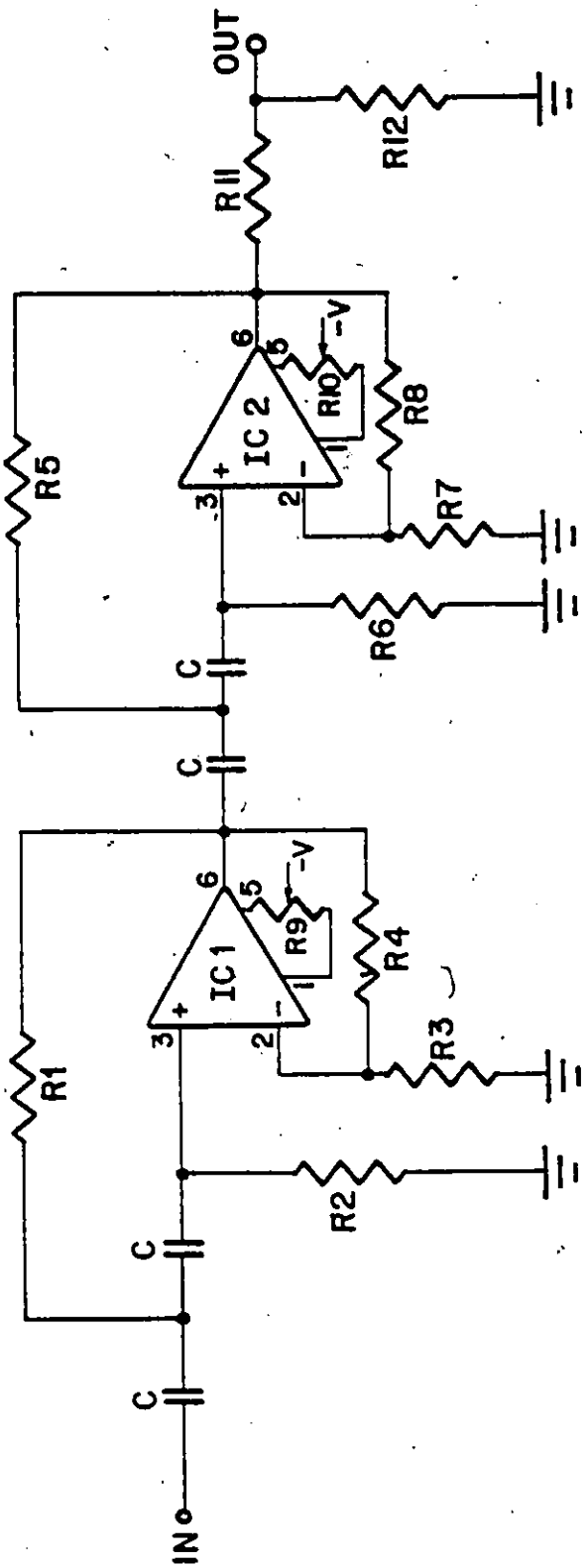

R1 = 16.2 KΩ, 1%
R2 = 19.1 KΩ, 1%
R3,R4 = 38.3 KΩ, 1%
R5 = 23.2 KΩ, 1%
R6 = 13.3 KΩ, 1%
R7,R8 = 27.4 KΩ, 1%

R9,R10 = 10 KΩ trim pot.
R11 = 1 KΩ, 5%
R12 = .33 KΩ, 5%
C = 1 μF
IC1,IC2 = LM741CN

Figure 3.5
Circuit diagram of EMG high-pass filter

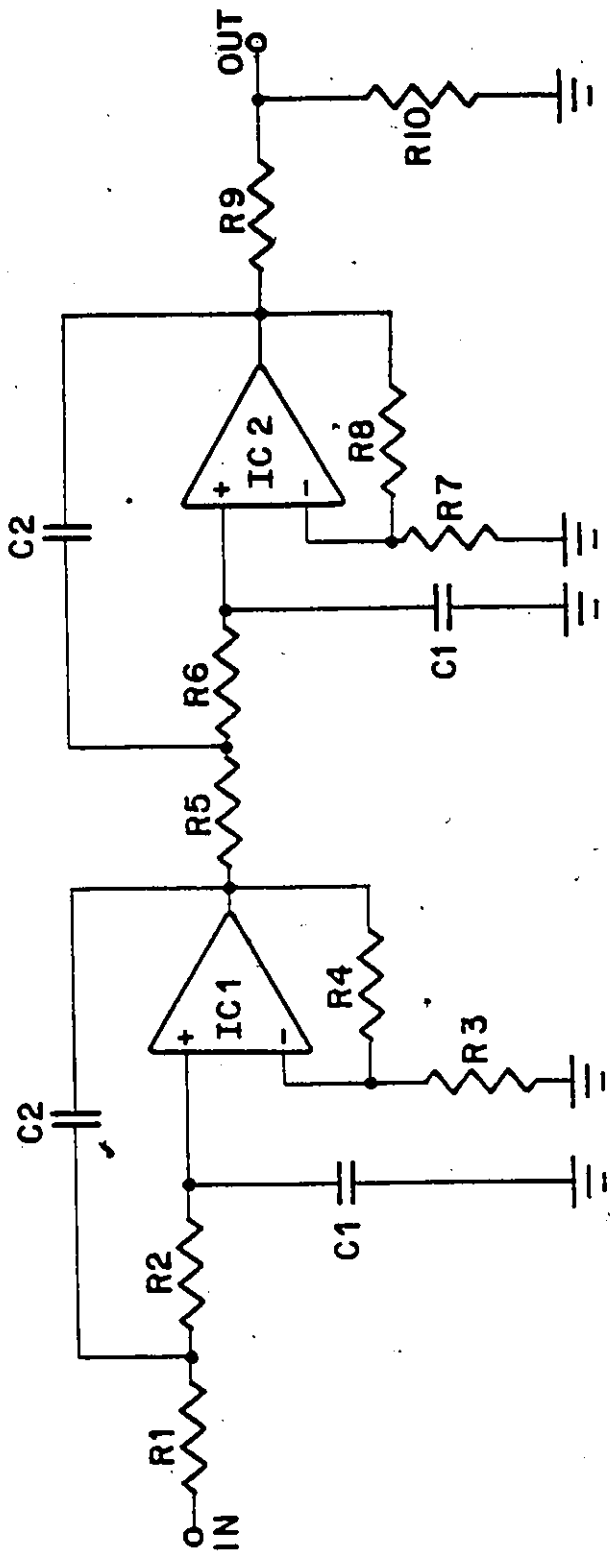

R1 = 5.6 KΩ, 1%
R2 = 3.3 KΩ, 1%
R3,R4 = 18 KΩ, 1%
R5 = 2.2 KΩ, 1%
R6 = 8.2 KΩ, 1%
R7,R8 = 22 KΩ, 1%

R9 = 1 KΩ, 5%
R10 = .33 KΩ, 5%
C1,C2 = .22 μF
IC1,IC2 = 1/2 LM1458

Figure 3.6
Circuit diagram of EMG low-pass filter

the fourth order Butterworth type with a 3 dB frequency equal to 200 Hz (Figure 3.6).

Sampling of the signals was performed using 12-bit analog-to-digital (A/D) converters that had a maximum input of ±5 volts and an error of ± 1/2 the least significant bit. For higher accuracy in the conversion of EMG signals, the levels of these signals had to be increased to values close to - but not higher than - the ±5 volts maximum inputs of the A/D converters. To achieve this, amplifiers with selectable gain settings of 1, 2, 5, 10, or 20 were used to amplify EMG signals at the computer site.

3.4 Acquisition of Kinematic Data

The advantages and disadvantages of the various strategies used in monitoring human gait were discussed in Chapter 2. One of the disadvantages of electrogoniometers is that they only measure relative angles between segments of the lower extremities. However, goniometers were used in our study because of their low cost and ease of use. In Chapter 4, we will present a technique that can be used to derive absolute linear displacements of the limbs from relative angular trajectories.

The electrogoniometers used in this study were developed at the Biomedical Engineering Department, Chedoke Rehabilitation Centre, after a design of Lamoreux (1971).

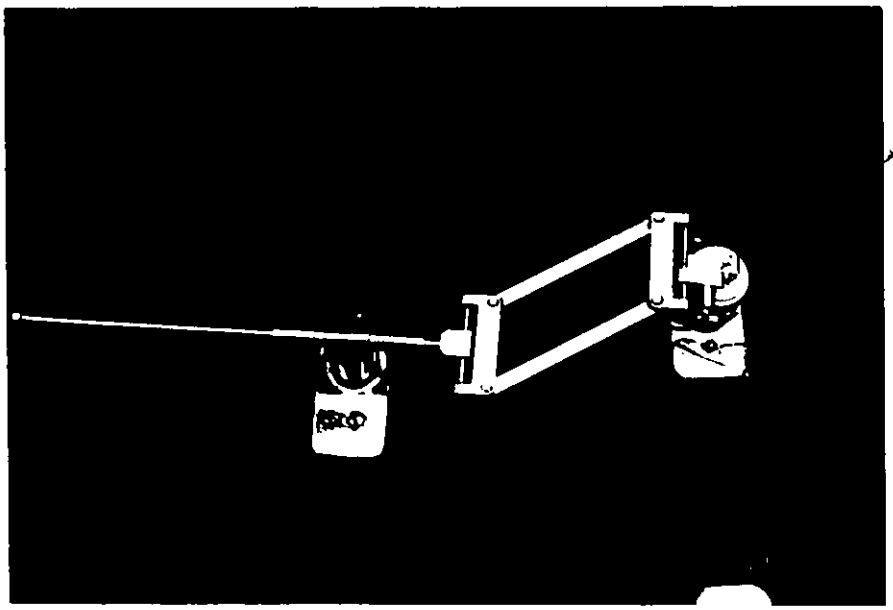

Figure 3.7
Self-aligning electrogoniometer

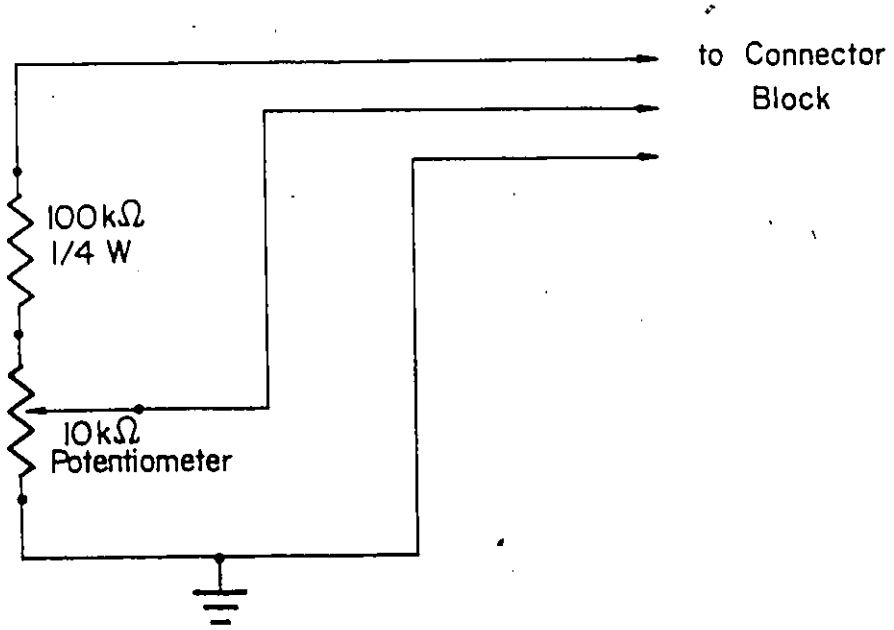

Figure 3.8
Circuit diagram of electrogoniometer

These goniometers differ from other goniometer systems (Trnkoczy and Bajd, 1975) in that they are the self-aligning type. They consist of a precision one-turn linear potentiometer attached to a parallelogram linkage (Figure 3.7). This special design allows the measurement of angles in one plane while compensating for motions in other planes. The goniometers are secured to the appropriate limbs with the aid of elastic velcro straps. A series resistor is connected to the potentiometer and a +15 volts supply is applied via the connector block (Figure 3.8).

Because of the self-aligning property of the goniometers, precision of measurements do not depend on accurate alignment with any anatomic joints. It is important, however, to make sure that the goniometer linkages and potentiometer are mounted such that they lie in the plane of progression (sagittal plane).

The hip goniometer was mounted such that the potentiometer was located just above the bony prominence of the greater trochanter. The upper strap was attached around the pelvis and the lower strap around the thigh (Figure 3.9(a)). The two straps of the knee goniometer were attached to the thigh and leg just above and below the knee joint (Figure 3.9(b)). The ankle goniometer has only one strap that was attached to the leg just above the ankle

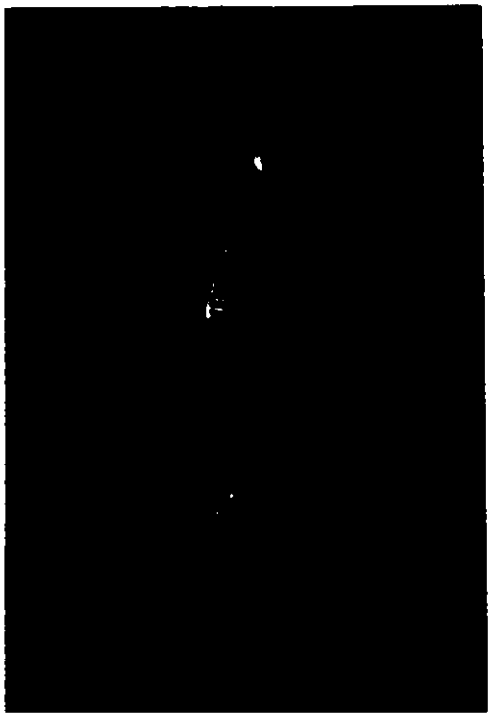

(a) Hip goniometer

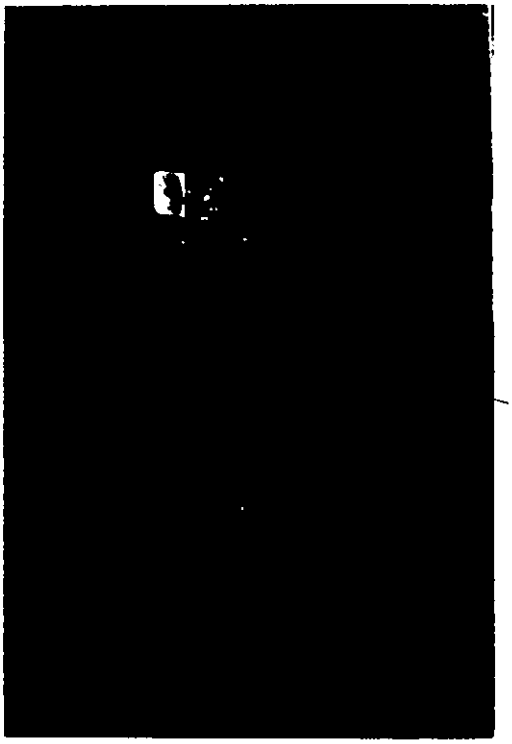

(b) Knee goniometer

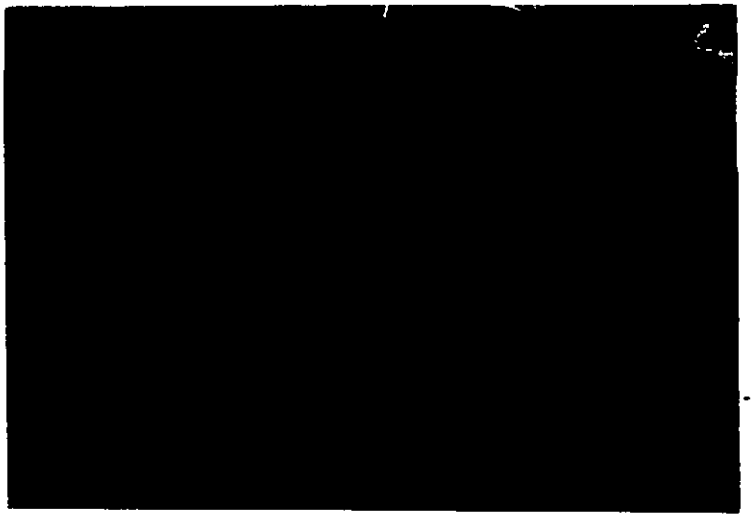

(c) Ankle goniometer

Figure 3.9
Placement of electrogoniometers

joint. The other end was fitted inside the subject's shoe (Figure 3.9(c)).

Before the angles could be measured, calibration of all the goniometers had to be performed. It is the calibration step that determines the accuracy of measurements. The calibration procedure can best be explained after the "anatomical" zero positions of various joints have been defined:

(1) The hip joint is said to be in a zero angular position when the thigh and trunk form a straight line. Flexion of the hip results in a positive hip angle, and extension results in a negative angle.

(2) The knee joint is said to be in a zero angular position when the femur and tibia form a straight line. Flexion of the knee results in a positive knee angle, while hyperextension results in a negative angle.

(3) The ankle joint is said to be in a zero angular position when the shank assumes a position perpendicular to the floor. A positive ankle angle results from ankle dorsiflexion, and a negative angle results from plantarflexion. It is important, however, to account for the slight plantarflexion of the ankle that is attributed to the subject's footwear. The heel height of the subject's shoe results

in a bias in the calibration. This bias should be measured and subtracted from the ankle angle measurements.

To perform the calibration, the goniometers were connected to the computer and the appropriate joint was placed in the zero anatomical position; assume that the joint angle in this position is γ_1 and that the goniometer output voltage is v_1. The joint was then flexed to an arbitrary angle γ_2, with the corresponding goniometer voltage v_2. Assuming a linear relationship between the joint angles and goniometer voltages, a slope s and an intercept γ_0 were calculated from the following relations:

$$s = (\gamma_2 - \gamma_1)/(v_2 - v_1) \tag{3.1}$$

and

$$\gamma_0 = \gamma_1 - s \times v_1 \tag{3.2}$$

These values were stored by the computer for later use in the computation of joint angles. During the experiment, if a joint angle γ was to be computed, the goniometer voltage v was measured and the angle was obtained using the following linear equation:

$$\gamma = \gamma_0 + sv \tag{3.3}$$

In order to test the adequacy of a linear fit, a quadratic fit of 3 calibration angles and voltages was performed. It was found, however, that the differences

between angles computed from a linear fit and those obtained from a quadratic fit were less than 2%. These differences were considered negligible and were hardly worth the effort of using an extra calibration angle for each joint.

3.4.1 Multiplexing of Kinematic Data

When this work started, only 8 signal channels were available. However, due to system expansion, 8 new channels became available. The connection of the new channels to the connector block required a set of coaxial cables similar to that used for the original channels. It was found, however, that the extra weight of the new cables made the total weight large enough to affect the subject's gait. To avoid this problem, the author decided to multiplex the new channels using a multiplexer circuit mounted inside the connector block, and then demultiplex these channels at the computer site. This resulted in a considerable reduction in the required number of cables, and the weight of all the cables was hardly felt by the subject.

The multiplexer-demultiplexer system (Figure 3.10), developed by Perritt and Milner (1976), was used in our study to multiplex the kinematic data. This system consists of an 8 channel analog multiplexer controlled by an 80 KHz clock. Control of the sampling sequence of the channels is achieved by applying the clock signal to a decade counter

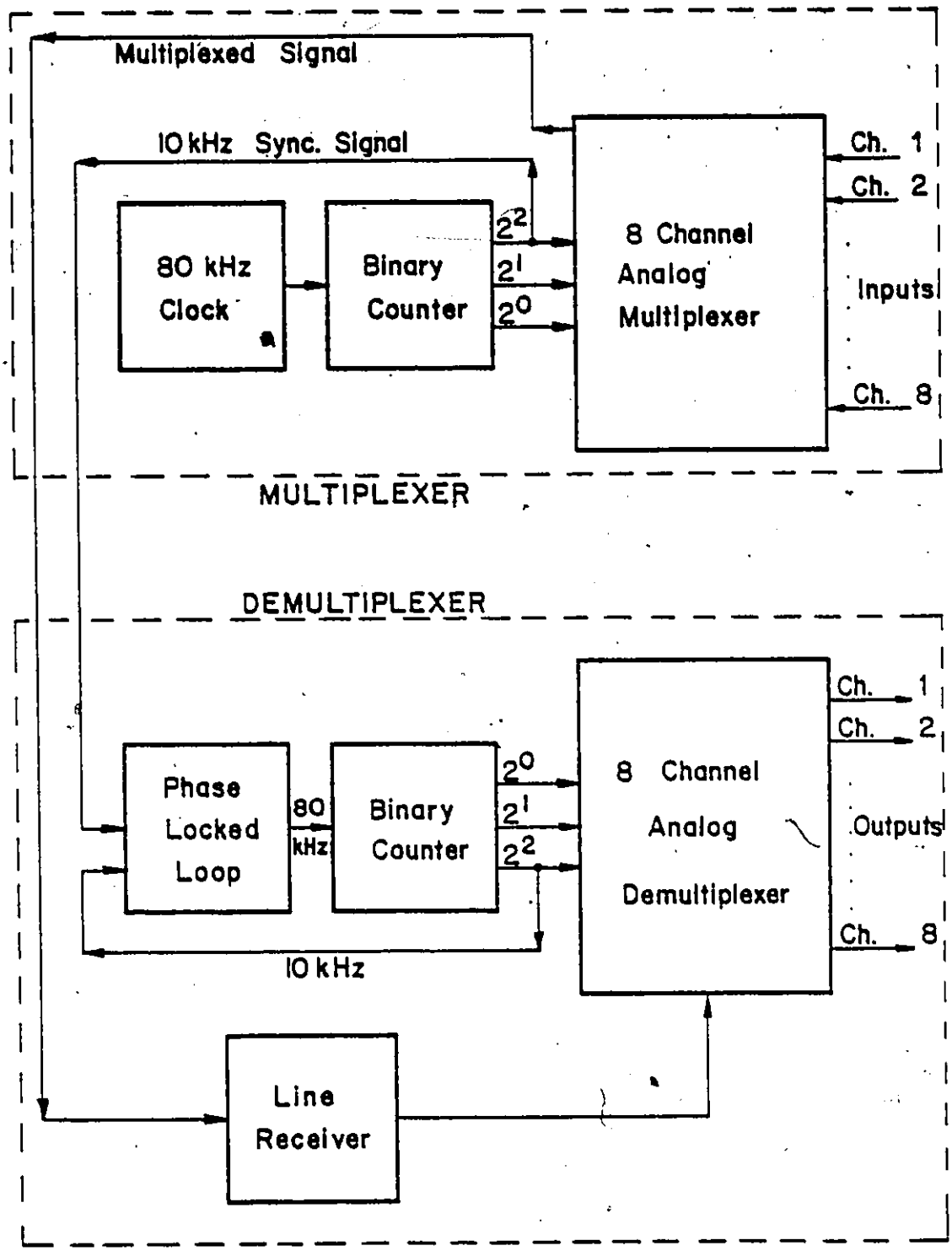

Figure 3.10
Multiplexer-demultiplexer system

whose ÷2, ÷4 and ÷8 outputs are used to form a 3 bit address word which can be used to select any channel from 0 to 7. The multiplexed signal and the ÷8 output of the counter (10 KHz) are connected via the overhead cables to the demultiplexer system at the computer site. The 10 KHz signal is used as a synchronization signal by the demultiplexer. This sync. signal is fed to a phase locked loop (PLL) which produces an 80 KHz signal. This signal is divided by 8 using a decade counter, and the output is fed back to the PLL. The PLL serves the function of locking the 10 KHz signal of the demultiplexer to the sync. signal generated by the multiplexer. An analog demultiplexer, addressed by the binary counter, is used to demultiplex the signals.

The sync. logic of the demultiplexer system was quite complicated because the PLL circuit used (NE 565) could only lock two signals 90 degrees out-of-phase. However, because of the availability of a new PLL integrated circuit (CD 4046) that allows the locking of signals in-phase, the author was able to redesign the demultiplexer system. The sync. logic of the new system became much simpler than that of the original system, and the number of parts was greatly reduced. A detailed description of the system, along with circuit diagrams and printed circuit board layouts can be obtained from the Biomedical Engineering Department, Chedoke

Rehabilitation Centre, Hamilton, Ontario.

3.4.2 Analog Processing of Kinematic Data

Since the bandwidth of angle measurements is quite small (0 to 7 Hz), low-pass filters with cutoff frequency of 25 Hz were used. In fact, this filtering process was included to remove the glitches that resulted from the multiplexer switching. Since the clock rate of the multiplexer was 80 KHz, the effective sampling rate for each of the eight channels was 10 KHz. This means that a filter cutoff at a frequency much higher than 25 Hz could have been equally appropriate. It was decided, however, to use the 25 Hz cutoff to reduce any 60 Hz interference.

A second order Butterworth circuit was used for the construction of the low-pass filters. This circuit is identical to one stage of the filters used for EMG (Figure 3.6), with the following substitution of component values:

R1 = 12 KΩ R2 = 15 KΩ

R3 = 33 KΩ R4 = 150 KΩ

C1 = 0.63 μF C2 = 0.22 μF

IC1 = LM741CN

3.5 Footswitch Signals

In order to acquire information regarding the time intervals between various phases of the walk cycle, small contact switches were attached to the underside of the subject's shoes. A set of 4 footswitches were used for each foot. One switch was attached at the heel, and the other three were attached near the toes. A resistor network (Figure 3.11) was used in such a manner that closure of the heel switch produced a 1/3 of a volt, and closure of any of the toe switches produced 2/3 of a volt. The purpose of using three toe switches was to improve reliability via some redundancy. This is important because gait patterns differ from one subject to the other, and this could result in the point of toe contact being different for different subjects.

To place the footswitches, the subject's footwear was inspected for wear marks and the switches were placed at these marks and secured in place by masking tape. Figure 3.12 shows a typical footswitch pattern. The various events of this pattern are explained as follows:

(1) As the swing phase ends, the heel strikes the floor and the onset of stance is marked by closure of the heel switch (heel-strike), and the voltage changes from 0 to 1/3 volt.

(2) As the foot rotates quickly about the heel, the toes come in contact with the floor. This results in the

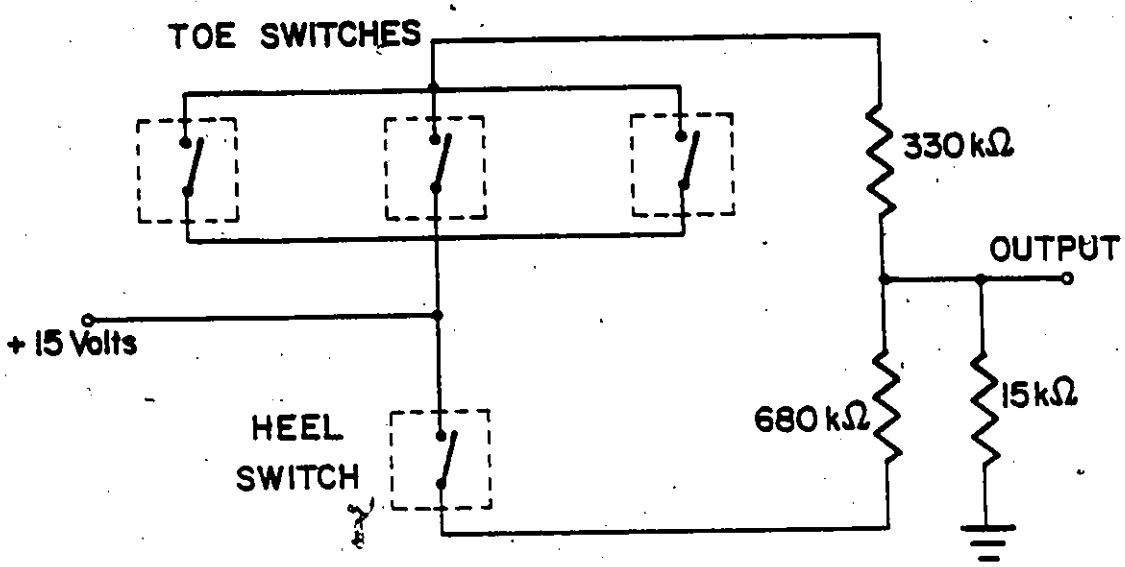

Figure 3.11
Circuit diagram of footswitches

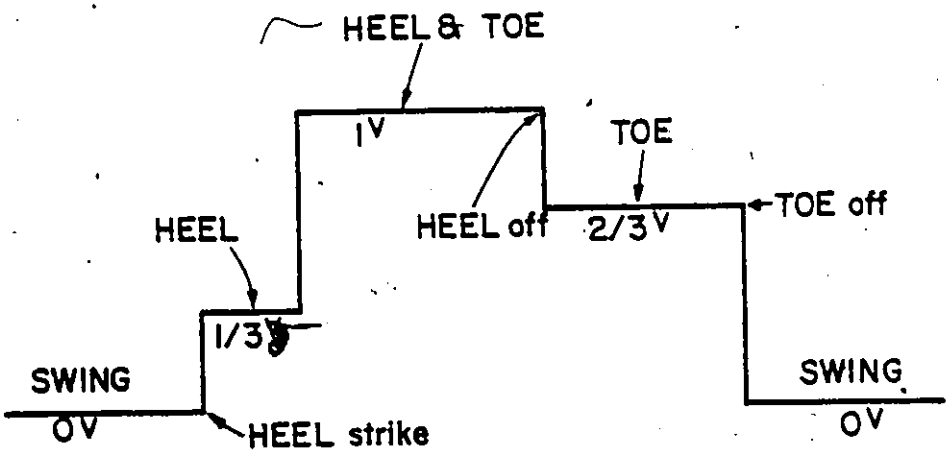

Figure 3.12
Footswitch signal

closure of one or more of the toe switches, and the voltage level rises to 1 volt. This marks the start of the "foot-flat" period where both the heel and toes are in contact with the floor.

(3) As the ball of the foot becomes a pivot point about which the heel starts to rotate, the foot-flat period is terminated. At this point the heel switch opens, reducing the voltage to 2/3 volt, and marking the start of the "toe-only" period.

(4) As the foot is lifted from the floor, the toe switches open and the swing period starts.

Although footswitch patterns provide important information about the subject's gait, interpretation of these patterns should be accompanied with caution. In some cases, even with normal subjects, the stance phase starts when both the heel and toes strike the floor simultaneously, which results in the absence of the 1/3 volt level. Also, in some pathological gaits, the subjects drag their toes during the swing phase. This results in an intermittent 2/3 volt level during the swing phase, instead of the expected steady 0 volt level.

3.6 Computer Interface

3.6.1 Laboratory Peripheral Interface

Conversion of the signals to digital information was achieved using the Digital Equipment's Laboratory Peripheral Interface System (LPS). This system included the following facilities:

(1) 16 channels of 12-bit analog-to-digital (A/D) converters with conversion time of 20 μs.

(2) A programmable real-time clock (LPSKW) that was used to select the sampling rates of the signals.

(3) A schmitt trigger input that allowed the remote starting and termination of data acquisition.

(4) 2 digital-to-analog (D/A) converter channels that were used to control a storage scope for display purposes.

3.6.2 The Computer System

A PDP 11/34 minicomputer system was used during this study. Permanent storage was facilitated by two RK05 disk drives and two Dectape drives. Graphics were obtained using a Tektronix 4006 graphics terminal with a hard copy unit.

An extensive software package was written by the author. This package included routines for the real-time signal acquisition, in addition to routines for data analysis and digital signal processing. These routines were

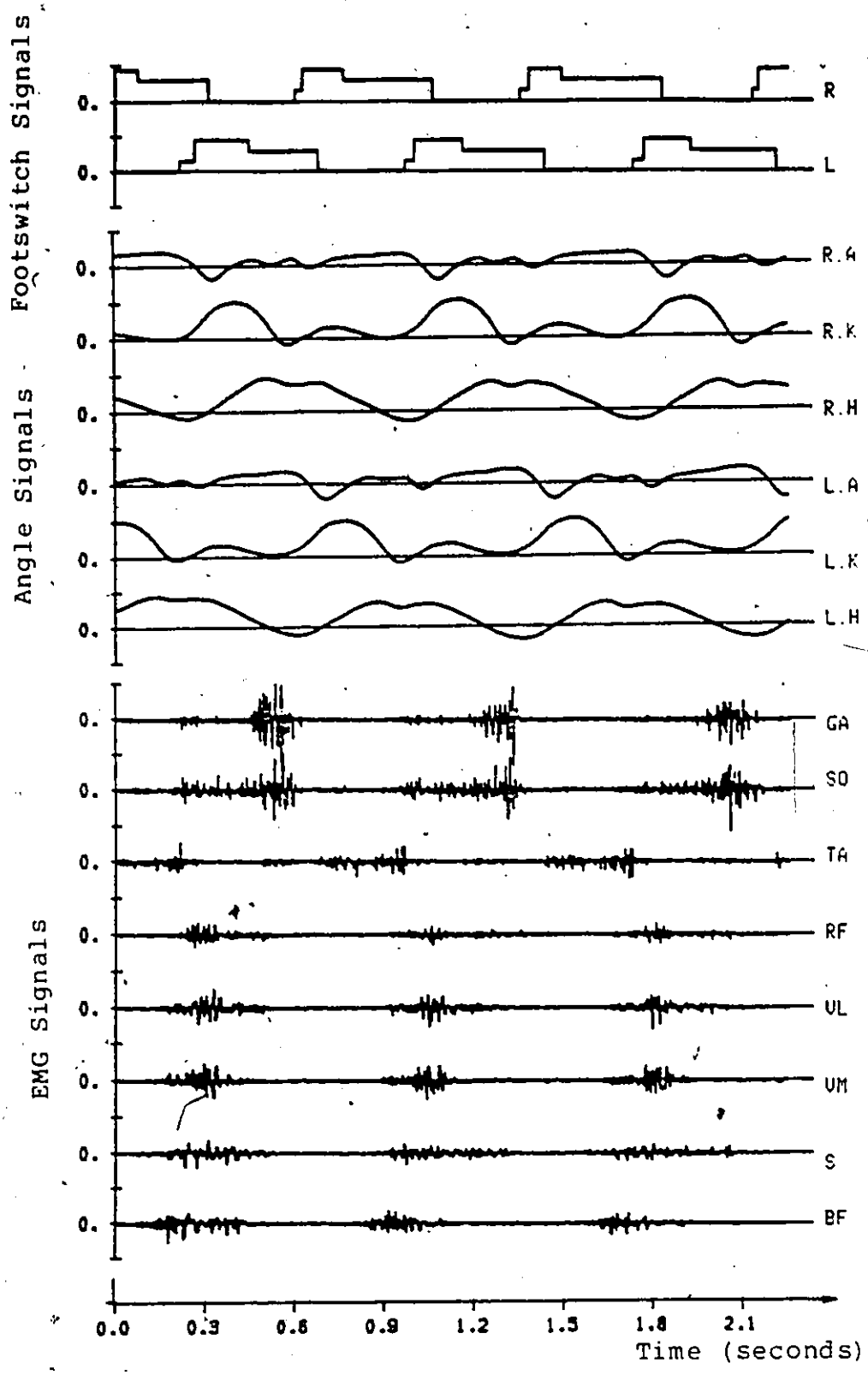

Figure 3.13
Signals from a sample experimental run

(L: Left, R: Right, A:ankle, K: knee, H: Hip,
GA: Gastrocnemius, SO: Soleus, TA: Tibialis Anterior,
RF: Rectus Femoris, VL: Vastus Lateralis, VM: Vastus
Medialis, S: Semitendinosus, BF: Biceps Femoris)
Scales: Footswitch signals, 1.5 V/div
Angles, 80 degrees/div
EMG signals, .5 mV/div

written in both Fortran IV and assembly languages under the control of an RT11 software system. This software system had the disadvantage of being able to access a maximum of 28 kilowords of memory. This was a severe limitation because it limited the sampling rate and the sampling interval of the signals.

After loading the acquisition program into memory, the amount of usable memory was reduced to about 22 kilowords. This meant that sampling of 16 channels at 500 Hz resulted in a sampling interval of about 3 seconds. This interval was just enough to accommodate two complete walk cycles of normal gait at an average speed.

Figure 3.13 shows the signals collected from 16 channels including 2 footswitch channels, 6 goniometer channels and 8 EMG channels. These signals were collected during an experiment on a 30 year old normal male subject.

CHAPTER 4

PROCESSING AND ANALYSIS OF KINEMATIC MEASUREMENTS

4.1 Introduction

In order to derive the equations of motion of different limb segments, knowledge of the kinematics of each segment is needed. In addition to angular displacements, absolute linear displacements of the centers of gravity of the segments must be measured. Once these variables have been determined, forces and moments acting at various joints can be calculated.

Earlier in this thesis, the various methods of monitoring the kinematics of gait were discussed. It was emphasized that different photographic and video methods allow measurement of the trajectories of various landmarks of the body in space; the angular displacements of the limbs can then be derived from these trajectories. On the other hand, electrogoniometers can only measure relative angular displacements between segments of the lower extremities. This has limited the use of electrogoniometric measurements to the study of angle-angle diagrams (Grieve, 1968), and the measurement of step length (Bajd et al., 1974).

Electrogoniometers are relatively easy to use,

inexpensive, and can be interfaced directly to a computer. These advantages have prompted the author to investigate methods that can be used to derive as much information from goniometric measurements as possible. Later in this chapter, a technique that can be used to derive absolute linear displacements from relative angular trajectories is presented and its accuracy is discussed.

In the following section it will be shown that angle measurements cannot be used in their raw form. Digital signal processing is required in order to reduce measurement noise that contaminates the signals.

4.2 Filtering of Angle Data

Although every effort was made to minimize measurement noise, the signals were contaminated by several sources of noise. The following are among the sources of noise that affected the angle signals:

(1) Noise that is attributed to the uncertainty in the least significant bit in the binary values of the signals. This type of noise results from the process of analog-to-digital conversion, and is referred to as "quantization noise".

(2) Noise that is attributed to components in electronic circuits such as resistors and integrated circuits.

Both of the above-mentioned types of noise have the

nature of white noise, that is a flat power spectrum. For most applications these sources of noise can be neglected because the noise power is usually very small compared to the signal power. However, when the signals are to be differentiated, the resulting derivatives are often severely contaminated by noise. This phenomenon results due to the tendency of the differentiation process to preferentially amplify high frequency noise relative to lower frequency signals. Figure 4.1 shows the raw hip angle measurements and the resulting contaminated derivative (angular velocity). To overcome this problem, low-pass filtering of angle data was needed. The cutoff frequency of the filter could only be determined after the power spectra of angle data have been studied.

4.2.1 Spectral Content of Angle Data

To study the spectral content of angle data, the Fast Fourier Transform algorithm (FFT), suggested by Cooley and Tukey (1965), was used to compute the Discrete Fourier Transform coefficients of angle signals. The procedure presented by Welch (1967) was used to compute the power spectral densities (PSD) of the signals.

Signals from ten experiments on normals and hemiplegic patients, walking at speeds ranging from 0.5 to

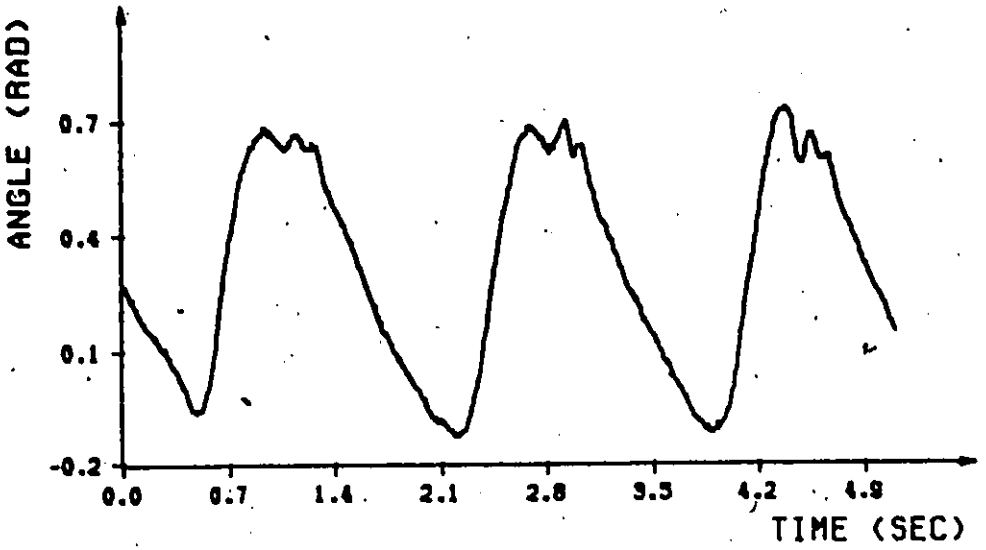

(a) Hip-angle signal

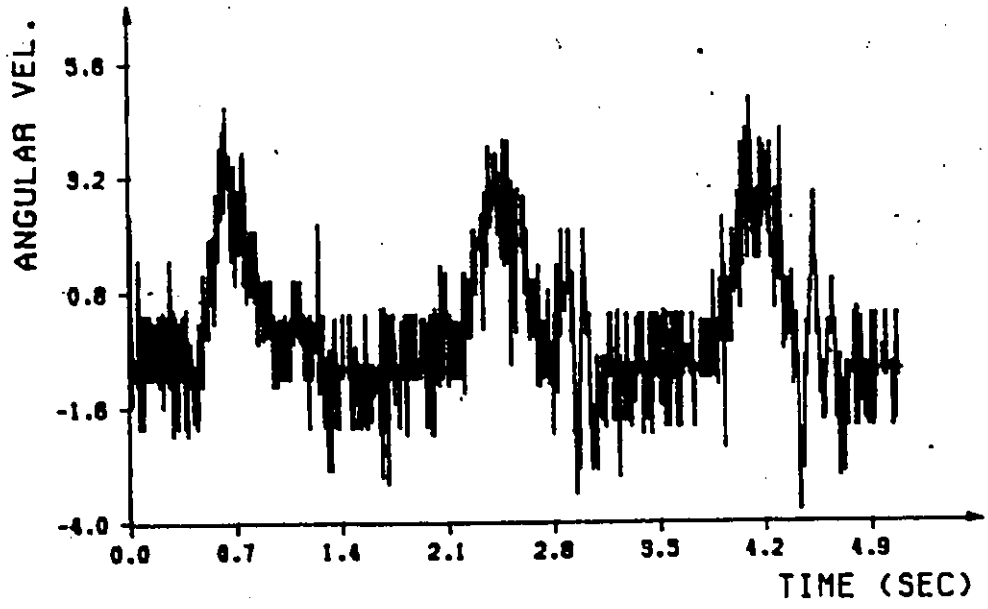

(b) Noisy derivative

Figure 4.1
Effect of noise on the derivative
of hip-angle signal

1.5 m/s, were used to study frequency spectra of hip, knee, and ankle angles. Figure 4.2 shows typical power spectra of the three angle signals. The figure shows the power coefficients at various frequencies expressed as percentages of the total signal power.

An arbitrary frequency band, from 0 to 8 Hz, was chosen for this analysis. The total power in that band was computed as a percentage of the total signal power. This quantity, call it the normalized power, was determined for all the signals. It was found that the normalized power was never less than 99.4% for the hip angle, 98.7% for the knee angle, and 97.3% for the ankle angle. These results suggested that low-pass filtering at a 3 dB frequency of 8 Hz or higher could be used without significant loss in the signal power. Therefore, we decided to use a digital low-pass filter with cutoff frequency of 10 Hz.

4.2.2 Design of a Digital Low-Pass Filter

There are several techniques that can be used to design a digital filter, and they vary in complexity depending on how stringent the requirements on the filter response are. A simple method, described by Rader and Gold (1967) to design a digital filter using a transformation of a known continuous filter function, was utilized in this work. This method makes use of the well-established design

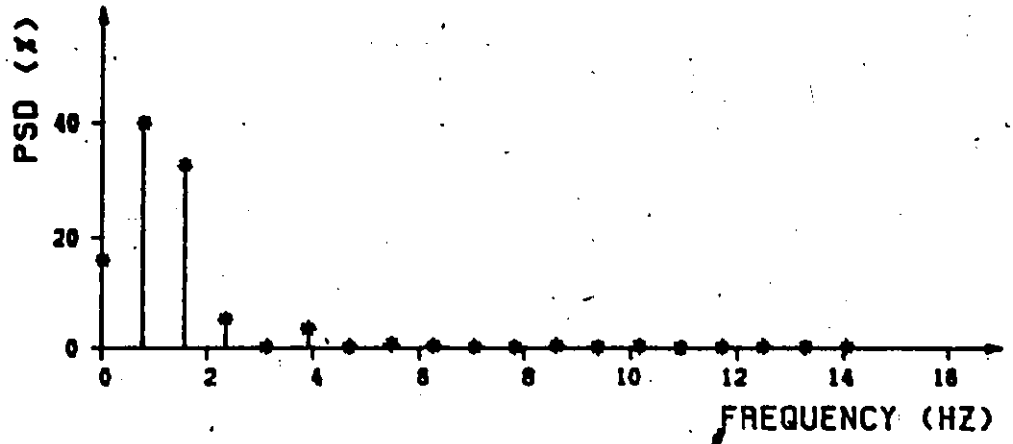

(a) Hip-angle spectral density

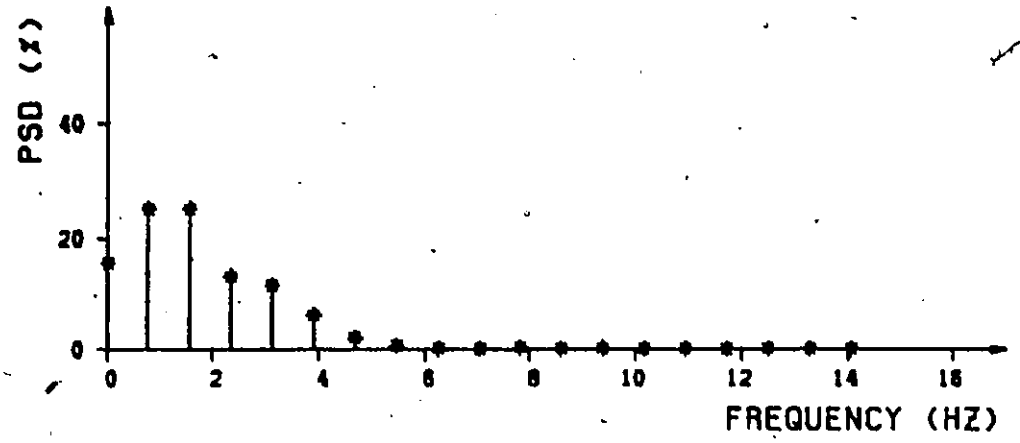

(b) Knee-angle spectral density

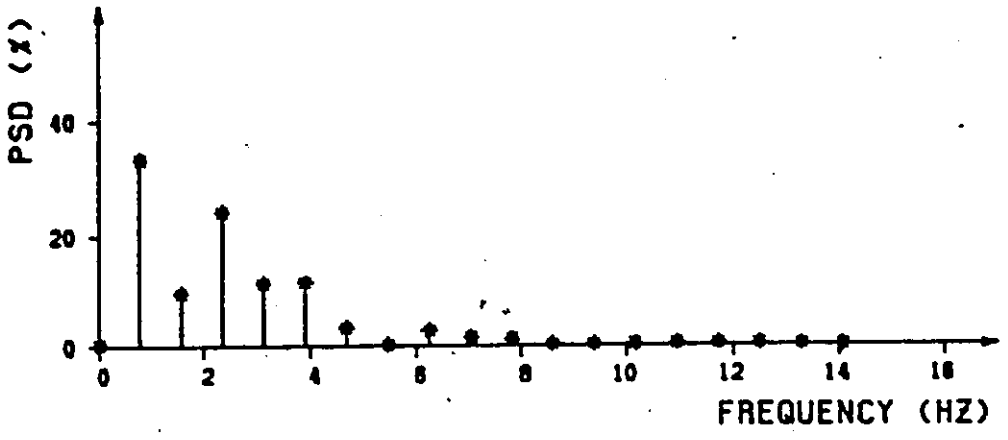

(c) Ankle-angle spectral density

Figure 4.2
Power spectral densities of angle signals

techniques of analog filters by applying a bilinear transformation to the analog filter function

$$s \rightarrow \frac{z-1}{z+1} \tag{4.1}$$

This transformation maps the jω axis in the s-plane onto the unit circle in the z-plane, and the left half of the s-plane onto the inside of the unit circle. This ensures that the resulting digital filter is realizable and stable. If H(s) and H'(z) are the analog and digital filter functions, respectively, then $H(\omega_A)$ and $H'(\omega_D)$ will take on the same values for

$$\omega_A = \tan(\omega_D T/2) \tag{4.2}$$

where ω_A and ω_D are the analog and digital frequencies, and T is the sampling period of the signal.

For the purpose of reducing high frequency noise in the angle data, a second order Butterworth filter was considered adequate. The normalized transfer function of this filter is

$$H(s_n) = \frac{1}{s_n^2 + \sqrt{2}\, s_n + 1} \tag{4.3}$$

where s_n is the normalized frequency = s/ω_c, and $\omega_c = 2\pi f_c$ where f_c is the cutoff frequency.

Now, for a digital filter with 3 dB point at 10 Hz

and signal sampling rate of 500 Hz, we have

$$\omega_D = 2\pi \times 10$$

and $$\omega_A = \tan(2\pi \times 10/2 \times 500) = 0.063$$

hence $$H(s) = \frac{0.004}{s^2 + 0.0895s + 0.004}$$

Applying the bilinear transformation, we get:

$$Y(z)[1-1.823z^{-1}+0.837z^{-2}] = 0.0036\ U(z)[1+2z^{-1}+z^{-2}] \qquad (4.4)$$

where U(z) and Y(z) are the z-transforms of the input and output signals of the filter, respectively. The recursive filter equation is obtained by applying the inverse z-transform to the above equation:

$$y(nT) = 0.0036\ u(nT) + 0.0072\ u(nT-T) + 0.0036\ u(nT-2T) + 1.823\ y(nT-T) - 0.837\ y(nT-2T) \qquad (4.5)$$

The above equation was implemented in the form of a computer program and used to filter the angle data. Due to the phase lag introduced by the filter, a second pass of the data through the filter was performed in the reverse direction of time, i.e. the last point first(Winter et al., 1974). This resulted in the reduction of the cutoff frequency to about 8 Hz. Figure 4.3 shows the amplitude and phase responses of the filtering operation.

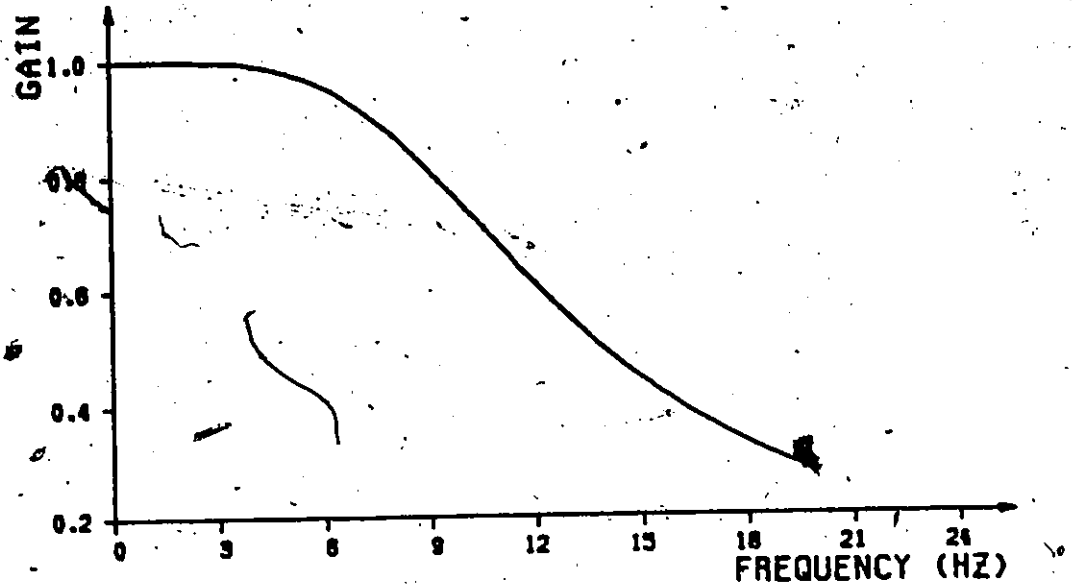

(a) Amplitude response

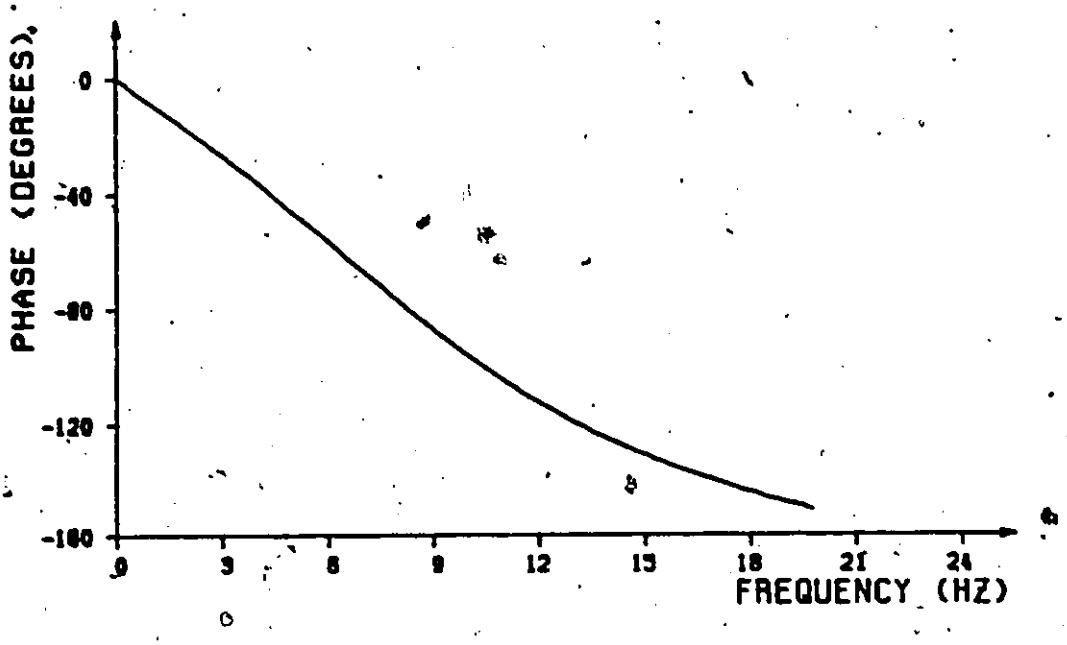

(b) Phase response

Figure 4.3
Response of the digital low-pass filter

4.3 Numerical Differentiation of Signals

In the study of the kinetics of gait, described in Chapters 5 and 6, angular and linear accelerations of limbs were needed. These were computed by numerically differentiating angular and linear trajectories twice, using the method described by Hilderbrand (1956). In this method, a Lagrangian interpolation polynomial of degree 4 is fitted to 5 successive, equally spaced, points of the signal. An approximate estimate of the derivative at time t is then obtained by evaluating the derivative of the polynomial at time t.

Given a uniformly sampled signal y_i, $i = 1, 2, \ldots, n$ with a sampling period T, the derivatives are given by z_i, $i = 1,2,\ldots,n$, where

$$z_i = \begin{cases} (-25y_1+48y_2-36y_3+16y_4-3y_5)/12T & i=1 \\ (-3y_1-10y_2+18y_3-6y_4+y_5)/12T & i=2 \\ (y_{i-2}-8y_{i-1}+8y_{i+1}-y_{i+2})/12T & i=3, \ldots, n-2 \\ (-y_{n-4}+6y_{n-3}-18y_{n-2}+10y_{n-1}+3y_n)/12T & i=n-1 \\ (3y_{n-4}-16y_{n-3}+36y_{n-2}-48y_{n-1}+25y_n)/12T & i=n \end{cases} \quad (4.7)$$

The above equations were used to compute angular and linear velocities and accelerations of various limb segments. Figure 4.4 shows the filtered hip angle and its

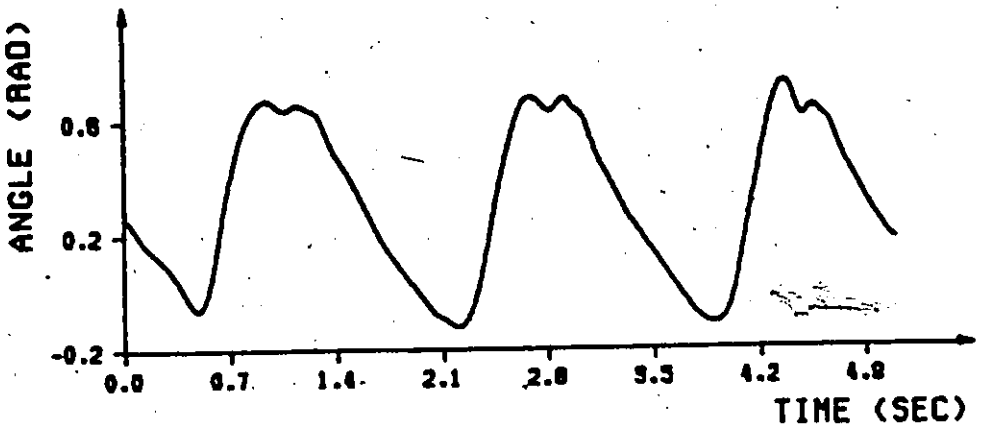

(a) Filtered hip-angle signal

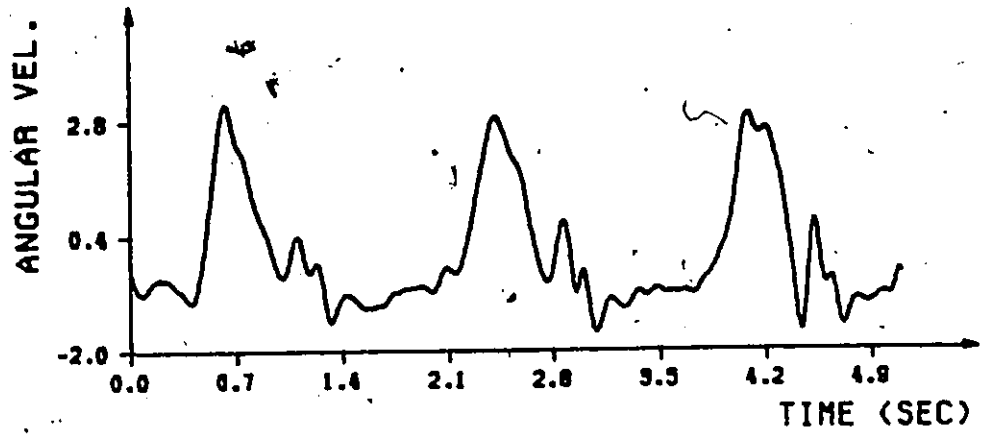

(b) Angular velocity

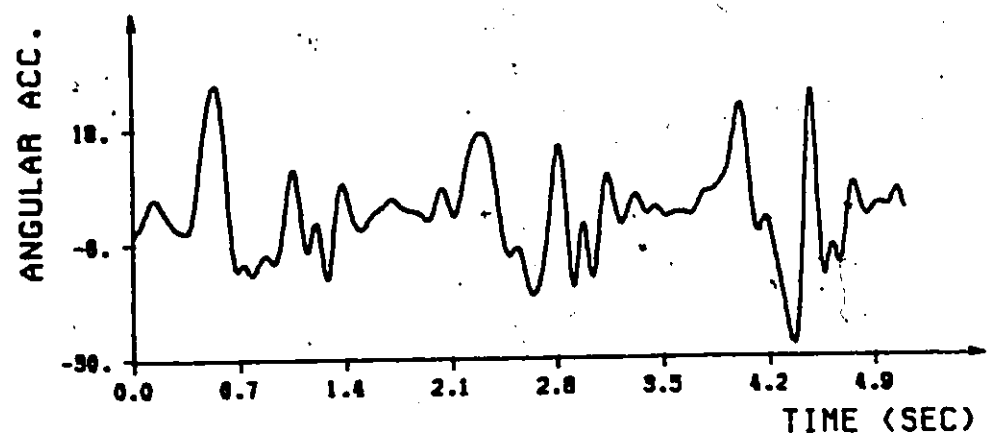

(c) Angular acceleration

Figure 4.4
Derivatives of the filtered hip-angle signal

first and second derivatives (angular velocity and acceleration).

4.4 Extraction of Linear Measurements from Angle Data

4.4.1 Definition of Planes of Motion

Locomotion results from displacement of various limbs and joints in highly complex and coordinated movements in space. In order to describe these movements, researchers have adopted a coordinate system defined as follows (Figure 4.5):

x-axis: is an axis parallel to the floor and points in the direction of progression.

y-axis: is a vertical axis pointing away from the floor.

z-axis: is the axis completing the right-handed set of axes.

Associated with these axes, a set of planes is defined as:

Sagittal Plane: is the plane that divides the body into right and left halves (x-y plane)

Frontal Plane: is the plane that divides the body into front and back portions (y-z plane)

Horizontal Plane: is the plane that divides the body into upper and lower portions (x-z plane).

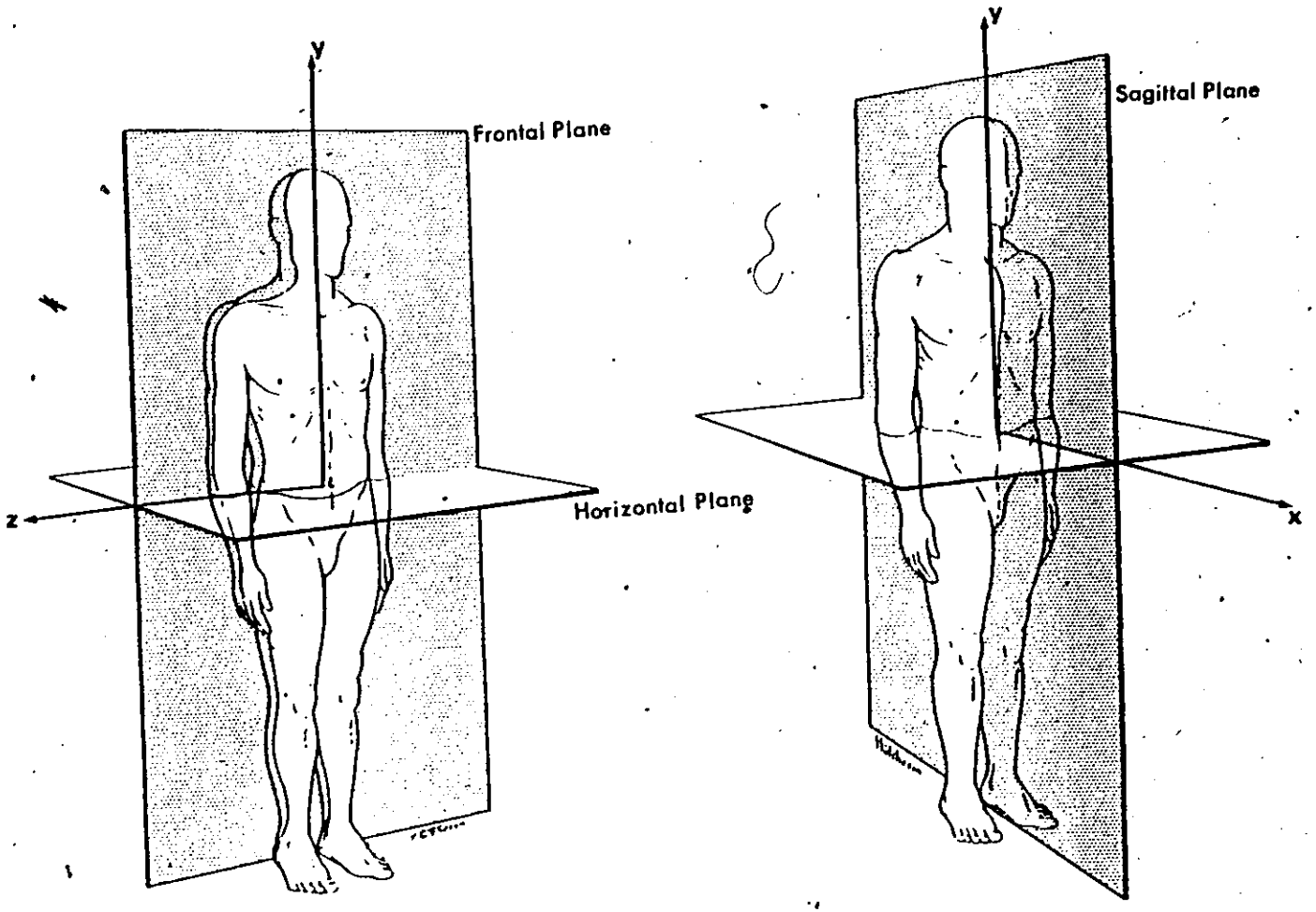

Figure 4.5
Coordinate system of the human body

In this work the above-mentioned coordinate system was used, but instead of having the origin at the center of gravity of the body, the origin was considered to be fixed in space and the body moved relative to that origin. Since the largest joint displacements occur in the sagittal plane, models developed in this thesis were confined to that plane. The effects of joint motion in the other planes are discussed in the following section.

4.4.2 Link Model of the Lower Body

The objective of this study is to develop a simple model that represents the lower body in the sagittal plane. However, motion of joints in other planes can affect the accuracy of results obtained using such a model.

Consider an imaginary line connecting the two hip joints. During gait, this line rotates in both the frontal and horizontal planes. Angular rotations of the hip line are usually very small during free-speed walking, and tend to increase with speed (Murray et al., 1966b). Rotation of the hip line in the horizontal plane results in a relative horizontal displacement between the two hip joints in the sagittal plane, while rotation in the frontal plane is reflected as a relative vertical displacement. Experimental studies by several investigators, including Murray (1967), and Lamoreux (1971), show that hip line rotations can be up

to 10 degrees in the horizontal plane and 4 degrees in the frontal plane. These correspond, for an average subject, to x and y relative displacements of about 4 cm and 2 cm between the two hip joints in the sagittal plane. These displacements are neglected in this analysis and it will be shown later that errors introduced by neglecting hip line rotations are relatively small. This assumption amounts to considering the hip line to be perpendicular to the sagittal plane during various phases of the walk cycle. In other words, we can look at the two hip joints as one point in the sagittal plane.

It was mentioned earlier that angles measured using goniometers are relative angles between limb segments. For this study, however, we need to determine angles of the segments relative to axes fixed in space. In Figure 4.6 a simple model of the body is presented. This model represents the trunk, thigh, shank, and foot as straight lines connected at the joints. The angles θ, ϕ and α represent hip, knee, and ankle angles, respectively. From the figure, it is clear that if the trunk assumes an angle of ρ degrees with a vertical line (y-axis), then the angle between the thigh and the y-axis is equal to $(\theta-\rho)$. Accordingly, the angles that the shank and foot assume with respect to the y-axis are $(\phi-\theta+\rho)$, and $(\alpha-\phi+\theta-\rho)$, respectively. For most normal subjects, the angle ρ is very

small and can be neglected. However, in some pathological cases, such as patients with hip pain, the angle ρ can be as large as 20 degrees (Murray, 1967). This means that if we need to estimate absolute angles of limb segments relative to the y-axis, we first have to determine the angle ρ.

A simple method of estimating the angle ρ can be derived by considering the lower extremity during the "foot-flat" period (Figure 4.6). During this period, the foot is constrained in a horizontal position by the floor. This results in the angle ρ being dependent on the three angles θ, ϕ, and α:

$$\rho = \alpha + \theta - \phi \qquad (4.7)$$

An average value of the angle ρ can be estimated during the "foot-flat" period using the above relation. The word "average" is used because the angle ρ does not remain constant during the walk cycle. However, changes in ρ are so small that we can replace the changes with a constant value.

The above discussion can be summarized in the following two assumptions concerning a model of the lower extremities:

(1) Displacements of the two hip joints relative to each other are negligible, and the two lower extremities

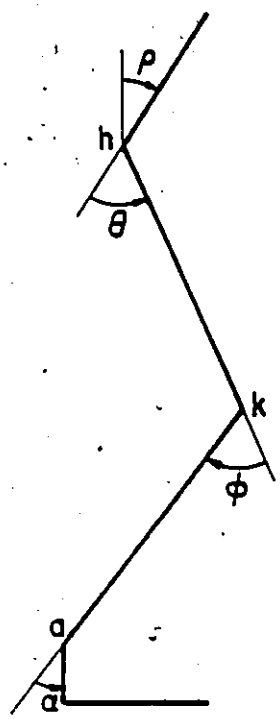

Figure 4.6
The lower extremity during foot-flat period

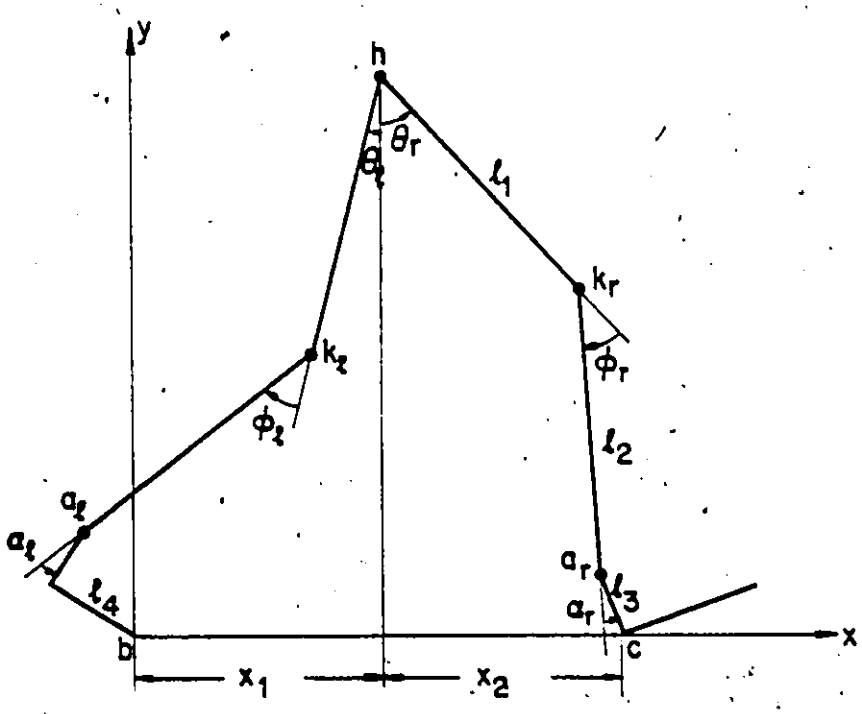

Figure 4.7
The lower extremity during double-support period

are considered to be connected by a single joint, referred to as the hip joint.

(2) Angular displacements relative to axes fixed in space can be determined from relative joint angles, provided that changes in the trunk angle relative to a vertical axis are negligible.

Based on the above assumptions, Figure 4.7 shows a six-link model representing the lower part of the body. To simplify the analysis, the angle ρ has been set to zero. However, in the actual computer simulations the angle ρ was calculated using equation (4.7) and used to compute absolute angles of the segments relative to the y-axis. In the model under consideration, each extremity is represented by three links connected at the joints. The lengths ℓ_1, ℓ_2, ℓ_3, and ℓ_4 are defined as follows:

ℓ_1 is the distance between the hip and knee joints.

ℓ_2 is the distance between the knee and ankle joints.

ℓ_3 is the height of the ankle joint measured from the bottom of the foot.

ℓ_4 is the distance between the heel and the ball of the foot.

The subscripts ℓ and r refer to the left and right extremities respectively. The hip, knee, ankle, heel, and ball of the foot are designated by the letters, h, k, a, c,

and b, respectively.

4.4.3 Spatial Trajectories of Joints

Having developed a link model of the lower extremities, we can now derive the spatial trajectories of various joints. The approach developed here relies on the fact that, at any point in time during gait, there is at least one point of either foot in contact with the floor. In other words, there is always a point, fixed with respect to our coordinate system, to which we can reference other points of the extremities. First, spatial trajectories of the hip joint are derived, and then trajectories of the rest of the joints can easily be obtained.

Figure 4.7 shows the link model in an arbitrary starting position at time t_0. This position is chosen such that the right extremity has just started its stance phase (heel-strike). The origin of the coordinate system is arbitrarily chosen at the ball of the left foot. Careful interpretation of the joint angles shown in Figure 4.7 is important. Recalling the definitions of the signs of joint angles in Chapter 3, we notice that all the angles shown in the figure are positive except the left hip angle, which is negative (hip extension). This point should be kept in mind when deriving the spatial trajectories.

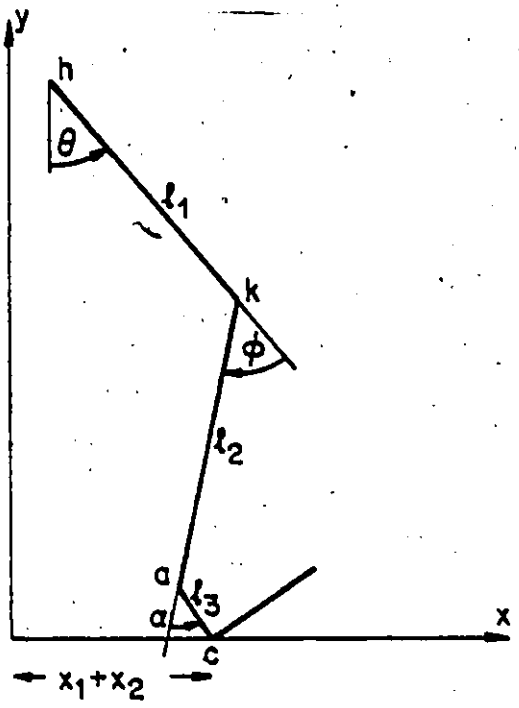

(a) Heel-only

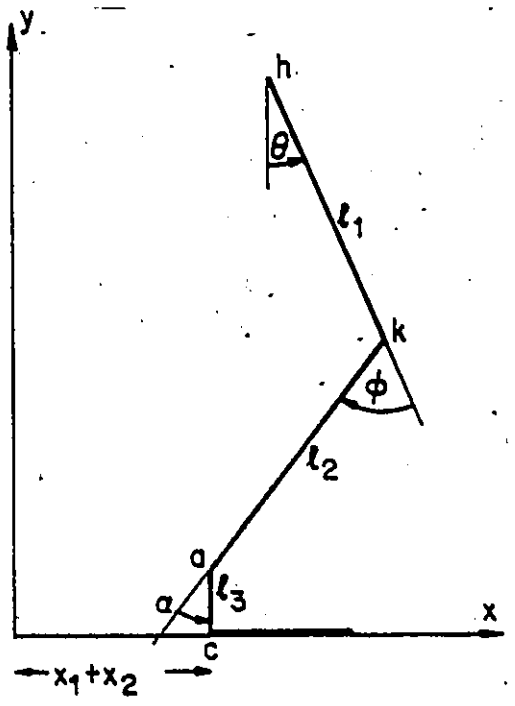

(b) Foot-flat

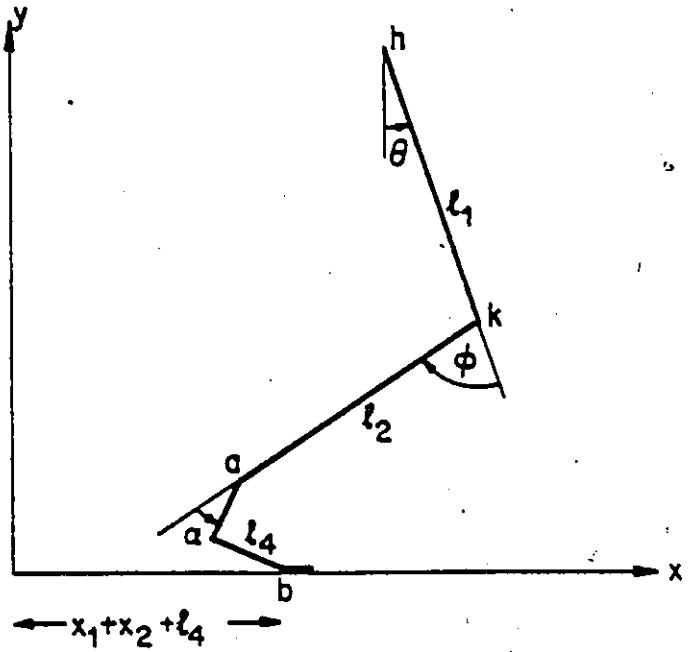

(c) Toe-only

Figure 4.8
The lower extrtemity
during various periods of the stance phase

At time t_0, the distances x_1 and x_2 are given by:

$$x_1 = -\ell_1\sin(\theta_\ell)-\ell_2\sin(\theta_\ell-\phi_\ell)-\ell_3\sin(\theta_\ell-\phi_\ell+\alpha_\ell)$$
$$-\ell_4\cos(\theta_\ell-\phi_\ell+\alpha_\ell) \qquad (4.8)$$

$$x_2 = \ell_1\sin(\theta_r)+\ell_2\sin(\theta_r-\phi_r)+\ell_3\sin(\theta_r-\phi_r+\alpha_r)$$

and the hip horizontal displacement is given by:

$$x_h(t_0) = x_1 \qquad (4.9)$$

If t_1 denotes the starting time of the right "foot-flat" period, then from Figure 4.8(a), the hip coordinates during the "heel-only" period ($t_0 \leq t < t_1$) are:

$$x_h(t) = x_1+x_2-[\ell_1\sin(\theta_r)+\ell_2\sin(\theta_r-\phi_r)$$
$$+\ell_3\sin(\theta_r-\phi_r+\alpha_r)] \qquad (4.10)$$

$$y_h(t) = \ell_1\cos(\theta_r)+\ell_2\cos(\theta_r-\phi_r)+\ell_3\cos(\theta_r-\phi_r+\alpha_r)$$

At time t_1, the right "foot-flat" period starts and lasts until "heel-off" occurs at time t_2 (Figure 4.8(b)). During this period ($t_1 \leq t < t_2$), the hip coordinates are given by:

$$x_h(t) = x_1+x_2 -[(\ell_1\sin(\theta_r)+\ell_2\sin(\theta_r-\phi_r)] \qquad (4.11)$$

$$y_h(t) = \ell_1\cos(\theta_r)+\ell_2\cos(\theta_r-\phi_r)+\ell_3$$

If t_3 denotes the end of the "toe-only" period of the right

foot (Figure 4.8(c)), coordinates of the hip joint during the "foot-flat" period ($t_2 \leq t < t_3$) are given by:

$$\begin{aligned} x_h(t) &= x_1+x_2+\ell_4-[(\ell_1\sin(\theta_r)+\ell_2\sin(\theta_r-\phi_r) \\ &\quad +\ell_3\sin(\theta_r-\phi_r+\alpha_r)+ \ell_4\cos(\theta_r-\phi_r+\alpha_r)] \\ y_h(t) &= \ell_1\cos(\theta_r)+\ell_2\cos(\theta_r-\phi_r)+\ell_3\cos(\theta_r-\phi_r+\alpha_r) \\ &\quad -\ell_4\sin(\theta_r-\phi_r+\alpha_r) \end{aligned} \tag{4.12}$$

At time t_3, the lower extremities assume a position similar to that assumed at t_0 (Figure 4.7), with the two extremities interchanged. Computation of the hip coordinates continues using the same equations with the subscripts r and ℓ interchanged. The process is repeated until the end of the run.

Once the hip trajectories have been computed, the knee, ankle, and heel trajectories are easily derived using the following equations:

$$\left.\begin{aligned} x_k &= x_h+\ell_1\sin(\theta) \\ y_k &= y_h\ \ell_1\cos(\theta) \end{aligned}\right\} \text{ knee coordinates} \tag{4.13}$$

and

$$\left.\begin{aligned} x_a &= x_k+\ell_2\sin(\theta-\phi) \\ y_a &= y_k-\ell_2\cos(\theta-\phi) \end{aligned}\right\} \text{ ankle coordinates} \tag{4.14}$$

and

$$\left.\begin{aligned} x_c &= x_a + \ell_3 \sin(\theta - \phi + \alpha) \\ y_c &= y_a - \ell_3 \cos(\theta - \phi + \alpha) \end{aligned}\right\} \text{ heel coordinates} \qquad (4.15)$$

In the above equations, the subscripts r and ℓ have been omitted because these relations apply equally to both of the lower extremities. Also, the time variable t has been omitted in most of the equations for simplicity. However, it should be understood that all the angles and coordinates are functions of time.

The procedure outlined above was implemented in the form of a computer program, which was used to compute trajectories of various joints. Figure 4.9 shows a stick-figure diagram, obtained using this program, of a normal subject walking at a speed of 1 meter per second. The arrows in the figure indicate onsets of heel-strike of the left lower extremity. Intervals between stick figures are 0.05 seconds. In addition to reconstructing the stick-figure diagrams representing the subject's walk, the program also computed step and stride lengths.

Figure 4.10 shows the hip, knee, ankle, and heel horizontal and vertical trajectories as function of time. Notice that the x-displacements in Figure 4.10(a) were offset from each other for the sake of clarity. The actual starting points are 0.5 m for the hip, 0.496 m for the knee, 0.187 m for the ankle, and 0.154 m for the heel.

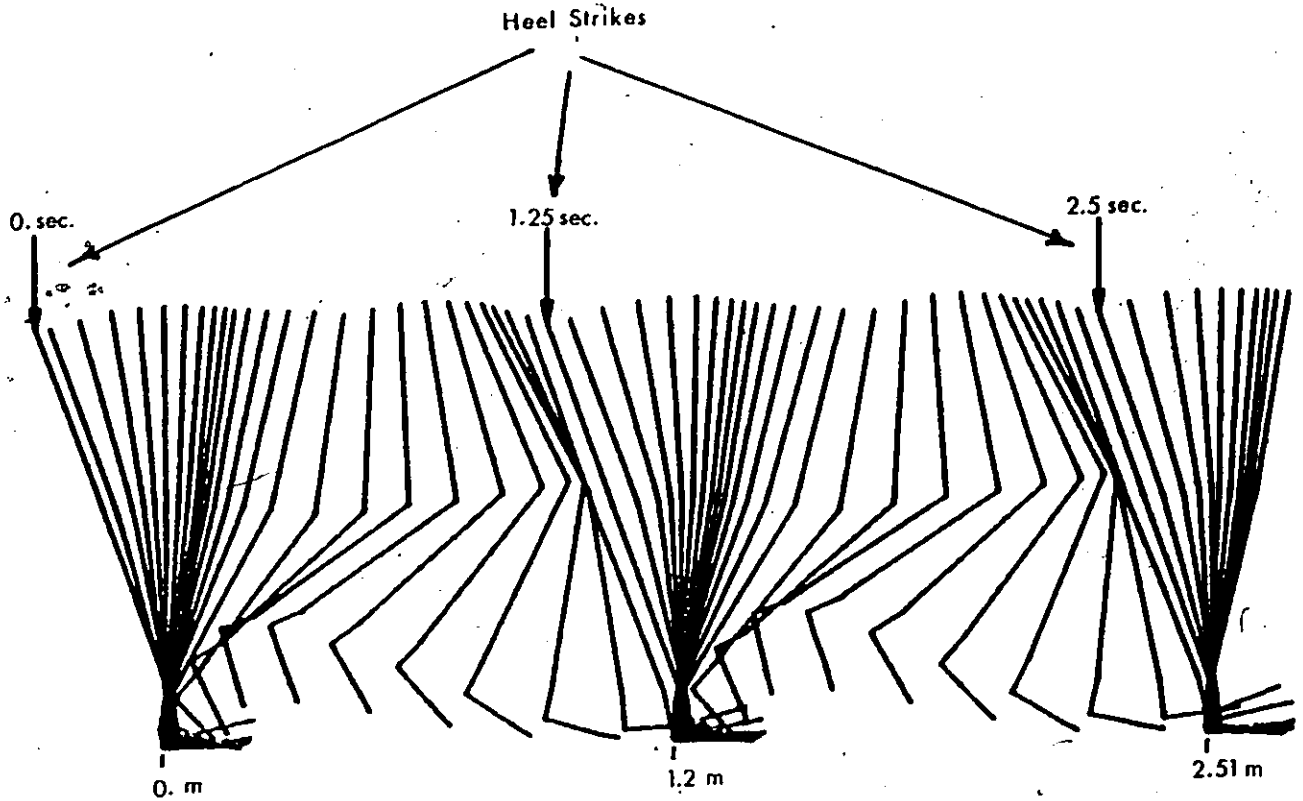

Figure 4.9
Stick-figure diagram obtained from goniometric measurements

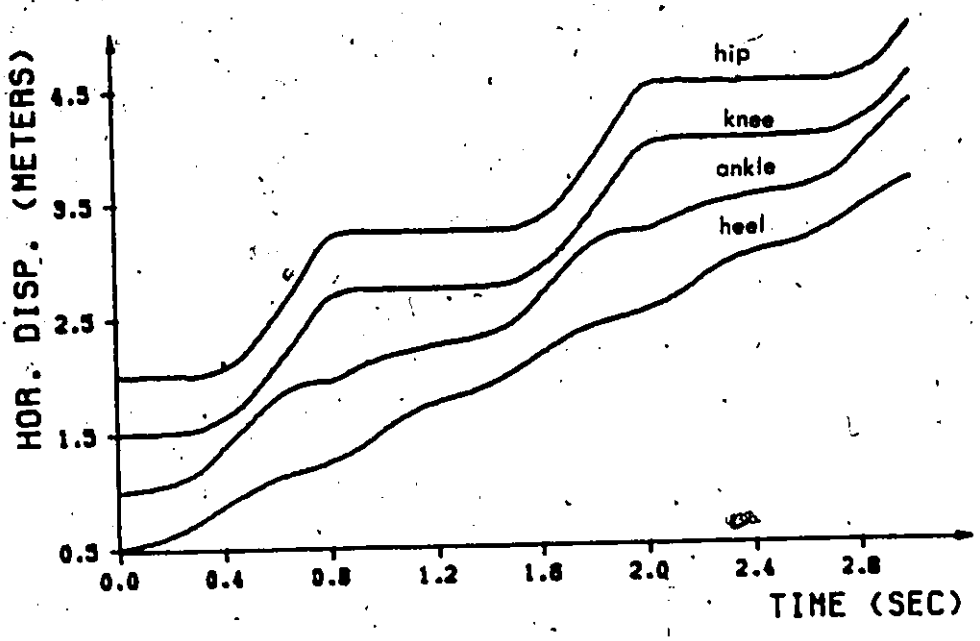

(a) Horizontal trajectories

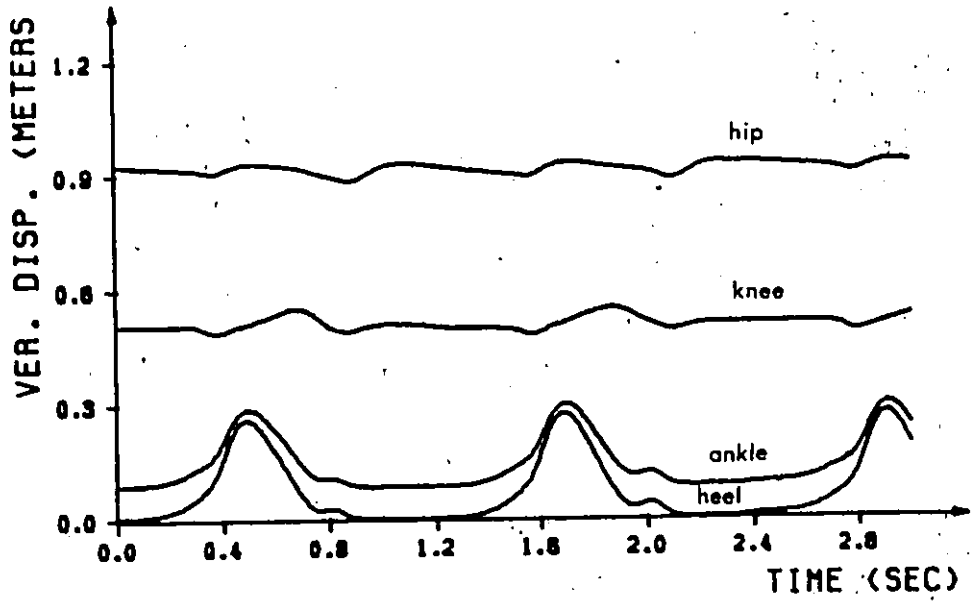

(b) Vertical trajectories

Figure 4.10
Spatial trajectories of joints
of the lower extremity

Once all the trajectories have been computed, velocities and accelerations of the joints can be obtained by differentiation with respect to time. In fact, we are more interested in accelerations of the centers of gravity of the limb segments. These can be obtained by locating the centers of gravity relative to the nearest joints and computing the trajectories in a manner similar to that previously discussed. Accelerations can then be found by differentiating twice the trajectories with respect to time.

4.4.4 Accuracy of Spatial Trajectory Computations

In addition to measurement errors, the simplifying assumptions used in our model resulted in errors in the trajectory computations. In order to assess our technique, these errors had to be estimated. Comparison of the computed trajectories with those measured using an optical system, such as T.V. cameras, would have been an ideal method of assessment of our technique. However, no optical system was available for this study to carry out the comparison. A simpler procedure had to be developed to test some of the results obtained using the proposed model.

When the link model was derived, rotations of the hip line in both the frontal and horizontal planes were neglected. Neglecting hip line rotation in the horizontal plane results in errors in the computations of the

horizontal trajectories of joints. In addition, neglecting hip line rotation in the frontal plane results in errors in the computations of the vertical trajectories.

Comparison of computed and measured step lengths was used in this study to assess the accuracy of the computed horizontal trajectories. Measurements of successive step lengths were performed by attaching small pieces of foam to the heels of the subject's shoes. These pieces of foam were immersed in black ink and the subject walked on the floor after overlaying it with large sheets of paper. Distances along the walkway between successive heel imprints of the two extremities were measured and taken as successive step lengths. Experiments were conducted on 3 subjects and each experiment consisted of 5 runs. A sampling rate of 100 Hz was used during this set of experiments, and that rate enabled us to collect data corresponding to 4 to 6 walk cycles in each run.

Table 4.1 summarizes the results of comparison of computed and measured step lengths. There are 15 entries in the table corresponding to the 15 runs. For each run, the step with the largest computation error is included. Also, the average step length and average error are included for each run. These results show that, as far as step length computations are concerned, our proposed technique results in less than 7% error.

Subject No.	Run No.	S_m cm.	S_c cm.	ϵ %	$\bar{S}_m$ cm.	$\bar{S}_c$ cm.	$\bar{\epsilon}$ %
1	1	72.9	70.1	3.8	73.6	71.0	3.5
	2	73.4	70.0	4.6	72.5	69.5	4.1
	3	77.3	74.1	4.1	76.7	73.6	4.0
	4	71.9	68.6	4.6	73.9	71.0	3.9
	5	73.3	70.4	3.9	73.8	71.1	3.7
2	1	81.9	77.6	5.3	80.0	76.3	4.6
	2	79.6	74.7	6.2	80.2	76.1	5.1
	3	78.6	74.7	4.9	80.4	77.1	4.1
	4	82.3	78.5	4.6	81.6	78.5	3.8
	5	79.7	75.6	5.2	82.1	78.2	4.7
3	1	68.3	65.8	3.6	70.2	68.2	2.8
	2	69.6	66.7	4.2	71.3	69.2	3.0
	3	70.7	67.7	4.2	72.4	69.8	3.6
	4	67.9	65.0	4.2	69.6	67.1	3.6
	5	68.5	66.0	3.7	68.9	66.9	2.9

Table 4.1

Comparison of measured and computed step lengths

S_m = measured step length

S_c = computed step length

ϵ = error

$\bar{S}_m$ = average measured step length

$\bar{S}_c$ = average computed step length

$\bar{\epsilon}$ = average error

Another test of accuracy of our technique was performed by considering the "double-support" period. During this period, both feet are in contact with the floor and the hip height can be estimated using the position of either extremity. For example, the hip height in Figure 4.7 can be estimated using either of the following two equations:

$$y_h = \ell_1\cos(\theta_r)+\ell_2\cos(\theta_r-\phi_r)+\ell_3\cos(\theta_r-\phi_r+\alpha_r) \tag{4.16}$$

or

$$y_h = \ell_1\cos(\theta_\ell)+\ell_2\cos(\theta_\ell-\phi_\ell)+\ell_3\cos(\theta_\ell-\phi_\ell+\alpha_\ell) -\ell_4\sin(\theta_\ell-\phi_\ell+\alpha_\ell) \tag{4.17}$$

Discrepancy in hip heights obtained using the two equations indicates inaccuracy of the model. In our experiments, the largest discrepancy was found to be less than 3 cm (less than 4% of the average hip height).

Although only partial tests of accuracy were performed, results of these tests indicated that, for practical applications, our model was quite adequate. In a clinical setting, 10% errors or even higher can usually be tolerated.

CHAPTER 5

ENERGY EXPENDITURE AS A MEANS OF ASSESSING HUMAN GAIT

5.1 Introduction

Quantitative techniques for the assessment of human gait are needed in order to gain better understanding of the human locomotor system, and to be able to assess the stages of recovery of patients suffering from various pathological problems. Many techniques have been used by researchers and clinicians to assess human gait. Most of the methods of assessment rely on the fact that normal gait exhibits almost stereotyped patterns of movements. By studying normal gait, researchers can define standard sets of parameters that can be used to assess the performance of patients.

One of the simplest procedures of assessment is carried out by considering the temporal information in the walk cycles. In other words, by measuring the time intervals spent by the subject in the stance and swing phases and computing the ratio of these intervals, we arrive at a parameter that is one of the most basic and important parameters of gait (stance-to-swing ratio). The stance-to-swing ratio of normals is usually about 1.5, and it varies for abnormal gaits depending on the pathology type.

Kljajic and Trnkoczy (1978) derived a method of assessment based on the speed of walking, cadence, and energy consumption. They defined a performance criterion based on these variables and used it to assess functional electro-stimulation of hemiplegic patients.

Several investigators used angle-angle diagrams for the assessment of gait (Grieve, 1969 and Milner et al., 1973). This method is based on plotting the time histories of both the hip angle and the ankle angle versus the time history of the knee angle. The resulting plots usually exhibit stereotyped patterns for normals that differ dramatically from those of pathological gaits. However, the process of assessing these diagrams is usually carried out in a qualitative manner. Hershler (1977) proposed the first attempt at the quantification of angle-angle diagrams by dividing the perimeter of the patterns by the square-root of their areas and using the resulting ratios in the assessment of gait.

Measurements of joint and muscle forces were used by several researchers, including Seireg and Arvikar (1973, 1975) and Paul (1967, 1971), to study the performance of the lower extremities during gait. The study of joint forces is usually directed towards the design of prostheses and orthoses and sometimes to the evaluation of the maximum loads that can be borne by the bones and muscles.

In this chapter, we present an analysis of the kinetics of the lower extremities and then develop a criterion for the assessment of gait, based on energy expenditure by the leg muscles.

5.2 Kinetics of the Lower Extremities During the Swing Phase

Muscles of the lower extremities play an important role in human locomotion. Not only do muscles act as prime movers of limbs, but they also function as "brakes" that decelerate the limbs near the end of the swing phase to reduce the impact of the extremities with the floor. Almost every procedure that is used to assess human gait can be looked at as a technique for assessment of muscle function. For example, assessment of angle-angle diagrams is an indirect method of studying the harmony between muscles acting at various joints. Therefore, it seems logical to assume that studying muscle forces can yield, at least, as much information about the subject's gait as other methods of assessment.

Muscle actions manifest themselves in the form of torques that either tend to rotate the limb segments about the joints or oppose externally applied torques. To determine the muscle torques, dynamics of the lower extremities have to be studied. The link model presented in

Chapter 4 is used in this analysis, with the additional assumption that the joints between the limb segments act as "hairpin" frictionless joints.

Several types of forces act on the lower extremities, these are:

(1) Gravitational forces: these are forces that result from the weights of various limb segments. Gravitational forces act at the centers of gravity of the segments.

(2) Muscular forces: these are forces that result from contraction of muscles. Because muscles traverse one or more joints, they develop forces on more than one limb segment at the same time. When a muscle has its origin on one segment and insertion on another, any force +F developed at the origin is accompanied by a force -F at the insertion. These forces result in reaction forces, -F and +F, respectively, that act at the joint connecting the two segments. Therefore, each limb segment is effectively subjected to a couple consisting of the two forces +F and -F, and this couple is referred to as "Muscle torque". Muscle torques do not appear in the equations of motion unless each limb segment is analyzed separately.

(3) Floor-reactions forces: these are reaction forces

produced by the floor on the feet during the stance phase. The magnitudes, directions and lines of action of these forces change during the stance phase.

(4) Inertial forces: these are forces that result from the motion of limb segments. The problem of dynamics of a body experiencing linear translation can be reduced to a problem in statics, using d'Alembert's principle, by introducing a force $-m\underline{a}$, where $\underline{a}$ is the acceleration vector of the center of gravity and m is the mass of the body. This force is in equilibrium with the other forces acting on the body and is called "the reversed effective force". Similarly, rotational motion of a body can be represented by a "reversed effective moment" equal to $I\ddot{\underline{\gamma}}$, where I is the moment of inertia of the body about the line passing through the center of gravity of the body and perpendicular to the plane of motion, and $\ddot{\underline{\gamma}}$ is the angular acceleration vector.

Figure 5.1 shows the free-body diagrams of the segments of the lower extremity. Centers of gravity of the thigh, shank and foot are denoted by t, s, and f respectively. Forces and moments shown in the figure are defined as follows:

W_t, W_s and W_f = weights of the thigh, shank, and foot, respectively.

U_i, i=1,2,3 = total muscle torques at the hip, knee, and ankle joints, respectively.

I_i, i=1,2,3 = moments of inertia of the thigh, shank, and foot about their respective centers of gravity.

$\ddot{\theta}$, $\ddot{\beta}$ and $\ddot{\psi}$ = angular accelerations of the thigh, shank, and foot, respectively, where $\beta = \phi-\theta$, and $\psi = \alpha+\theta-\phi$, where θ, ϕ, and α are the hip, knee, and ankle angles.

$\ddot{x}_i$, $\ddot{y}_i$, i=1,2,3 = horizontal and vertical components of the accelerations of the centers of gravity of the thigh, shank, and foot.

g = gravitational constant.

F_{xi}, F_{yi}, i=1,2,3 = horizontal and vertical components of the reaction forces acting at the joints.

d_1 = distance between the center of gravity of the thigh and the hip joint.

d_2 = distance between the center of gravity of the shank and the knee joint.

d_3 = distance between the heel and the center of gravity of the foot.

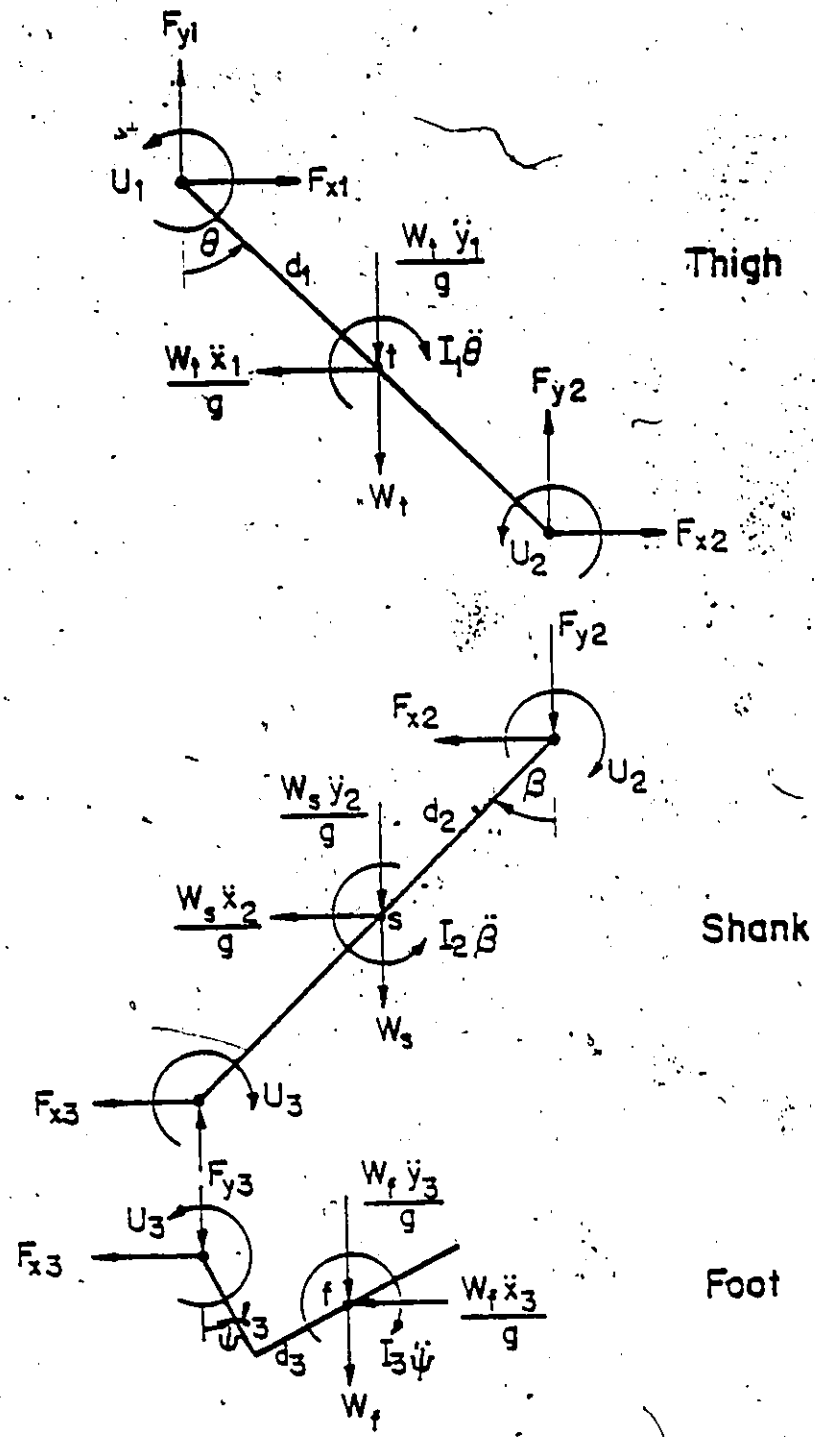

Figure 5.1
Free-body diagrams of segments of the lower extremity during the swing phase

The analysis is carried out for the swing phase only, therefore, there are no floor-reaction forces acting on the foot. Inspection of the figure shows that there are 6 unknown forces and 3 unknown moments. These forces and moments can be determined using the 9 equations of equilibrium of the three limb segments. However, if the extremities were considered in the stance phase, floor-reaction forces would increase the number of unknown forces and the problem could not be solved. In Chapter 6, we shall present a technique that makes use of the EMG activities of the muscles to determine the floor-reaction forces during the stance phase.

Considering the equilibrium of the foot, we obtain the following equations that result from resolving the forces in the x and y directions and taking moments about the center of gravity, respectively:

$$F_{x3} = -\frac{W_f}{g}\ddot{x}_3 \tag{5.1}$$

$$F_{y3} = -W_f - \frac{W_f}{g}\ddot{x}_3 \tag{5.2}$$

$$U_3 = I_3\ddot{\psi} - F_{x3}(\ell_3\cos\psi - d_3\sin\psi) - F_{y3}(\ell_3\sin\psi + d_3\cos\psi) \tag{5.3}$$

Similar analysis of the shank results in the

following equations:

$$F_{x2} = F_{x3} - \frac{W_s}{g} \ddot{x}_2 \tag{5.4}$$

$$F_{y2} = F_{y3} - W_s - \frac{W_s}{g} \ddot{y}_2 \tag{5.5}$$

$$U_3 = I_2\ddot{\beta} - U_3 + F_{x2}d_2\cos\beta - F_{y2}d_2\sin\beta + F_{x3}(\ell_2 - d_2)\cos\beta - F_{y3}(\ell_2 - d_2)\sin\beta \tag{5.6}$$

and for the thigh, we have:

$$F_{x1} = - F_{x2} + \frac{W_t}{g} \ddot{x}_1 \tag{5.7}$$

$$F_{y1} = - F_{y2} + W_t + \frac{W_t}{g} \ddot{y}_1 \tag{5.8}$$

$$U_1 = I_1\ddot{\theta} - U_2 + F_{x1}d_1\cos\theta + F_{y1}d_1\sin\theta - F_{x2}(\ell_1 - d_1)\cos\theta - F_{y2}(\ell_1 - d_1)\sin\theta \tag{5.9}$$

where ℓ_1, ℓ_2, and ℓ_3 are the link lengths defined in Chapter 4.

In order to determine the muscle torques during the swing phase, the above equations should be solved simultaneously. However, before the solution can be carried out, we must know the dimensions of the limb segments, locations of the centers of gravity, moments of inertia, and the weights of various segments.

5.3 Anthropometric Data

Exact determination of the weights of various limb segments is not possible, and this presents a problem that has always faced researchers in the field of human locomotion. According to Plagenhoef (1971), Braune and Fischer were the first to present a significant work on the subject in 1889, based on their dissection of four cadavers. It was not until 1955 that more comprehensive work, based on the dissection of eight cadavers, was presented by Dempster. In his work, Dempster related the weights of various limb segments to the total body weight. In addition, he related lengths of the various segments of the body to the height of the subject. Moreover, Dempster determined the radii of gyration and the locations of the centers of gravity as percentages of segment lengths. Less accurate measurements, on 35 living males and 76 living females, were performed by Plagenhoef (1971).

Some of the results obtained by Dempster are shown in Table 5.1. The table gives the weights of the thigh, shank, and foot as percentages of the total body weight, and the segment lengths as percentages of the total body height. Table 5.2 gives the radii of gyration with respect to the centers of gravity of the segments, and the locations of the centers of gravity relative to known landmarks of the lower extremity.

Limb segment	Weight	Length
Thigh	$W_t = 0.102\ W$	$\ell_1 = 0.248\ H$
Shank	$W_s = 0.470\ W$	$\ell_2 = 0.249\ H$
Foot	$W_f = 0.145\ W$	$\ell_3 = 0.049\ H$
		$\ell_4 = 0.163\ H$

Table 5.1

Weights and lengths of the leg segments (ℓ_4 is the distance measured between the heel and the ball of the foot; W is the total body weight; H is the total height)

Limb segment	Location of CG	Radius of gyration
Thigh	$d_1 = 0.433\ \ell_1$	$k_1 = 0.323\ \ell_1$
Shank	$d_2 = 0.433\ \ell_2$	$k_2 = 0.302\ \ell_2$
Foot	$d_3 = 0.5\ \ell_4$	$k_3 = 0.475\ \ell_4$

Table 5.2

Radii of gyration and locations of the centers of gravity of the leg segments

Using the values listed in Tables 5.1 and 5.2, moments of inertia were computed using the following relation:

$$I_i = (W_i/g)\ (k_i)^2 \qquad (5.10)$$

where I_i is the moment of inertia of the i'th segment about its center of gravity. The moments of inertia of the thigh, shank, and foot were computed in terms of the total body weight W, in kilograms, and the total body height H, in meters. These values are listed in Table 5.3.

Limb Segment	Moment of Inertia (in kg.m)
Thigh	$67 \times 10^{-6}\ WH^2$
Shank	$27 \times 10^{-6}\ WH^2$
Foot	$9 \times 10^{-6}\ WH^2$

Table 5.3

Moments of inertia of the leg segments

Having determined all the parameters required for the solution of equations (5.1) through (5.9), the muscle

torques at the various joints were computed numerically using these equations. The program computed all the forces and muscle torques as values normalized to the body weight in kilograms. The program required to following variables as inputs:

(1) The height of the subject.

(2) The angular variations, angular velocities and angular accelerations of the hip, knee, and ankle joints.

(3) The linear displacements, velocities, and accelerations of the joints and the centers of gravity of the leg segments.

All the computations were carried out for an average walk cycle. The averaging procedure used in the analysis is described in the following section.

5.4 Averaging of Walk Cycles

The aim of this work is to present the clinician with a simple quantitative technique for the assessment of human gait. The number of parameters used in the assessment should be as small as possible. For a realistic assessment we cannot extract the parameters from the data of one cycle of the subject's walk, because the gait of any person changes slightly from one stride to the next. On the other

hand, straightforward averaging of the data corresponding to successive strides is not possible, because the duration of each stride is usually different from the durations of the other strides. Hershler (1977) was able to average data from several walk cycles by selecting only those cycles with durations that were within 40 ms of each other. He then uniformly deleted or added samples to the data of each cycle, such that the resulting cycles would have the same number of samples, and then averaged the walk cycles. The drawback of this technique is that it restricts the analysis to only those walk cycles that are very close in duration to each other, and this results in the exclusion of a large number of cycles of the subject's walk.

A new approach, developed by the author, was used to average the data from all the cycles of the subject's walk. This was achieved by defining a "normalized" walk cycle that retained all the information in the original cycle. The number of samples in the normalized cycle was arbitrarily chosen to be 100. The normalization was achieved by resampling the original cycle at a new sampling rate, determined by the number of samples in the original cycle, such that the resulting number of samples would always be 100. The sampling was performed by applying a moving window of variable length and weighting coefficients. If we denote the original signal by $u(m)$, $m=1,2,\ldots,n$, and the normalized

signal by y(j), j=1,2,...,100, the normalization procedure can be described by the following equations:

$$y(j) = \sum_{i=k(j)}^{\ell(j)} a_i \, u(i)/r \qquad (5.11)$$

where

$$r = \text{sum of the weighting coefficients of the window} = n/100 \qquad (5.12)$$

$$\sum_{i=k(j)}^{\ell(j)} a_i = r \qquad (5.13)$$

$$a_{k(j)} + a_{\ell(j-1)} = 1 \qquad (5.14)$$

$$a_i = 1 \qquad k(j) < i < \ell(j) \qquad (5.15)$$

In the above equations the a's are the weighting coefficients of the window. The equations can best be explained by the following numerical example: suppose that a cycle of 270 samples is to be normalized; the sum of the weighting coefficients of the window is given by:

$$r = 270/100 = 2.7$$

thus the first sample of the normalized signal is:

$$y(1) = a_1(1)\, u(1) + a_2(1)\, u(2) + a_3(1)\, u(3)$$

$$= u(1) + u(2) + .7\, u(3) \qquad \left(\sum_{i=1}^{3} a_i(1) = 2.7\right)$$

Using equation (5.14) we have:

$$a_3(2) + a_3(1) = 1$$

thus

$$a_3(2) = .3$$

hence the second sample is given by:

$$y(2) = a_3(2)\ u(3) + a_4(2)\ u(4) + a_5(2)\ u(5) + a_6(2)\ u(6)$$

$$= .3\ u(3) + u(4) + u(5) + .4\ u(6) \qquad \left(\sum_{i=3}^{6} a_i(2) = 2.7\right)$$

the procedure is continued for other samples to give:

$$y(3) = .6\ u(6) + u(7) + u(8) + .1\ u(9)$$

$$y(4) = .9\ u(9) + u(10) + .8\ u(11)$$

$$y(5) = .2\ u(11) + u(12) + u(13) + .5\ u(14)$$

$$\vdots$$

etc.

If the number of samples in the original signal is an integral multiple of 100, the procedure reduces to simple averaging of neighbouring points. In order to retain the information contained in the original signal, the sampling rate of the original signal has to be much higher than the Nyquist frequency, so that the averaging procedure does not distort the information contained in the signal. This was not a problem because the angle signals were sampled at 500 Hz while most of the information was contained in the band

from 0 to 10 Hz. If the sampling period of the original signal is denoted by T, then the effective sampling period of the normalized signal becomes:

$$T' = T \times r = (Txn)/100 \qquad (5.16)$$

After normalizing each cycle in the subject's walk, an average cycle was obtained by averaging all the normalized cycles. Figure 5.2 shows the hip, knee and ankle muscle torques, computed using equations (5.1) through (5.9). The torques were first obtained for the swing phases of the whole walk. The torques during an "average swing phase" were then computed using the procedure described above. The torques computed by Elftman (1939b) were included in the figure to facilitate the comparison of our results with those obtained by other researchers.

5.5 Proposed Criterion for Assessment of Gait

So far we have dealt with forces and torques acting at the joints without reference to the effect of these forces and torques on movements of the limb segments during walking. Since the muscles of the lower extremities are the primary source of energy required for motion, then the pathology of some of the muscles could result in an abnormal gait. Therefore, it is reasonable to assume that studying the energy exchange between muscles of the leg and the leg

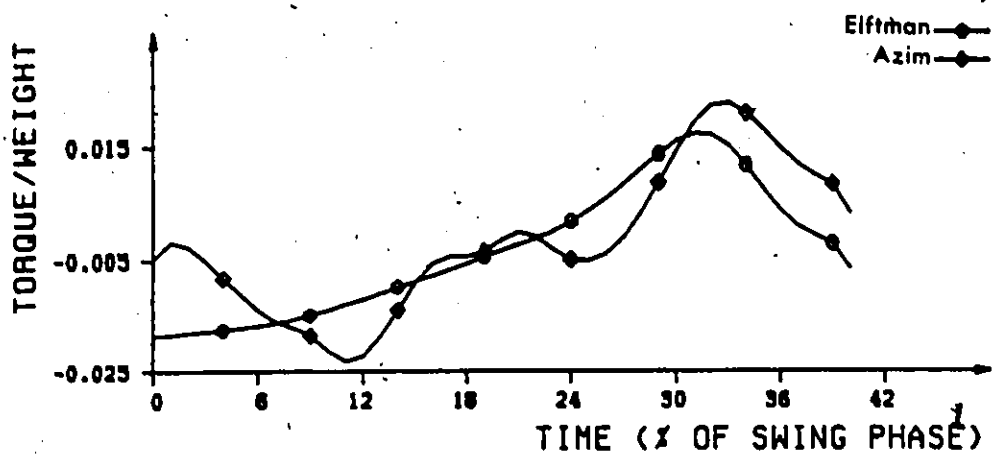

(a) Hip-joint muscle torque

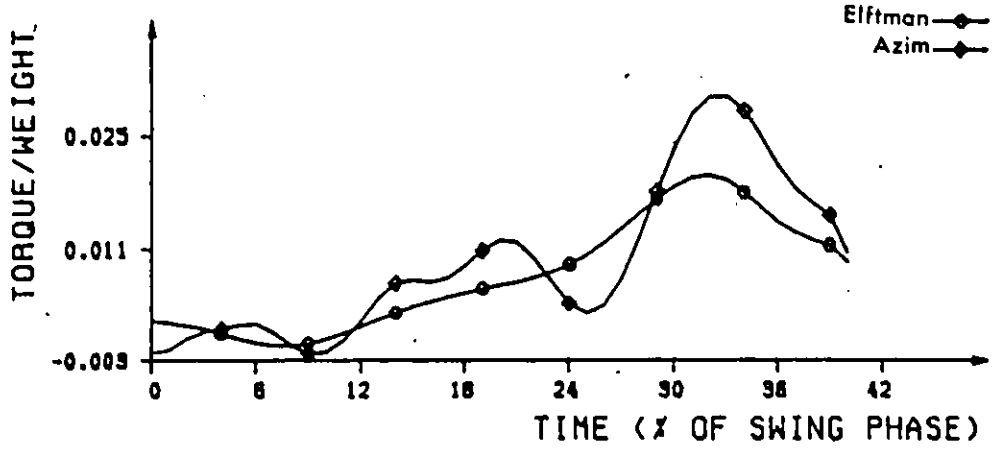

(b) Knee-joint muscle torque

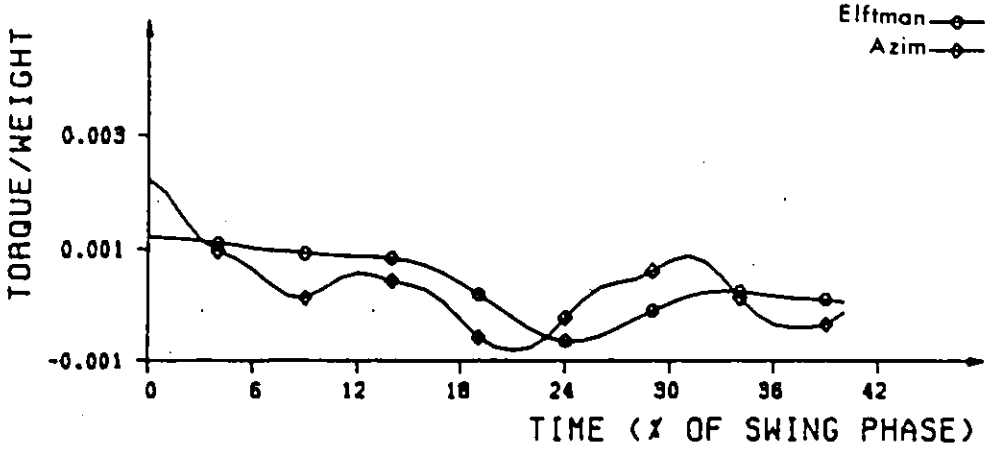

(c) Ankle-joint muscle torque

Figure 5.2
Muscle torques at the joints during the swing phase
(Torque in N.m ; Weight in Kg)

segments can give us some information about the subject's gait.

Energy exchange within segments of the lower extremities has been dealt with by several researchers, including Elftman (1939a), Beckett and Chang (1968), and Chow and Jacobson (1971). In order to explain the energy exchange between muscles of the leg and the various limb segments, we first have to derive the equations describing the power (rate of doing work) at the various joints.

Consider the torque developed by a muscle crossing the joint between two segments to be U(t). If the two segments are rotating at angular velocities of $\omega_1(t)$ and $\omega_2(t)$, then the rate of doing work on each of the two segments is given by the product of the torque acting at the joint and the angular velocity of each segment. Denoting the power by P, we have:

$$P_1(t) = U(t)\ \omega_1(t) \qquad (5.17)$$

$$P_2(t) = -\ U(t)\ \omega_2(t) \qquad (5.18)$$

where $P_1(t)$ and $P_2(t)$ are the powers on the first and second segments respectively. Notice that, although the torques acting on the two segments are equal in magnitude and have opposite signs, the rates of doing work on the two segments are different because the segments have different angular velocities. The algebraic sum of the two rates gives the

total rate of energy exchange between the muscle and the two segments, i.e.

$$P_m(t) = P_1(t) + P_2(t) \qquad (5.19)$$

where m denotes the muscle.

In practice there are usually several muscles crossing each joint, and $P_m(t)$ gives the rate of exchange of energy between all the muscles crossing the joint and the segments connected by that joint. The resulting power curve usually has positive and negative portions. The area under the positive portion of the curve gives the energy expended by the muscles, while the negative area is the energy received by the muscles. Part of the energy received by the muscles is used to stretch the muscle tissues, while the rest is passively transferred from one segment to the other by "tendon action" (Elftman, 1939b).

Figure 5.3 shows typical power curves of muscles of the hip, knee and, ankle joints. The power is given in Watts per kilogram of the subject's weight, and the time of start of swing is arbitrarily taken as zero. Figure 5.3(a) shows that at the start of swing a large amount of energy is expended by the hip muscles in order to accelerate the extremity forward, during mid-swing very little energy exchange takes place, and near the end of swing some energy

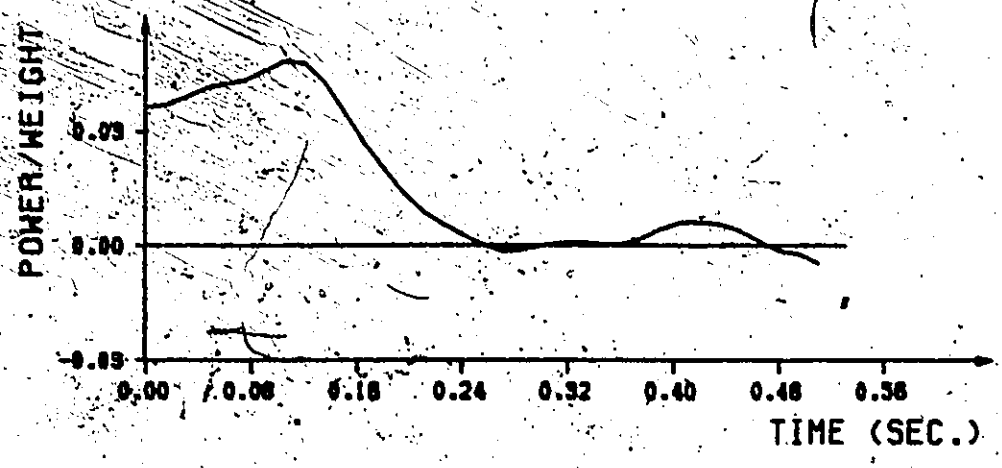

(a) Hip joint

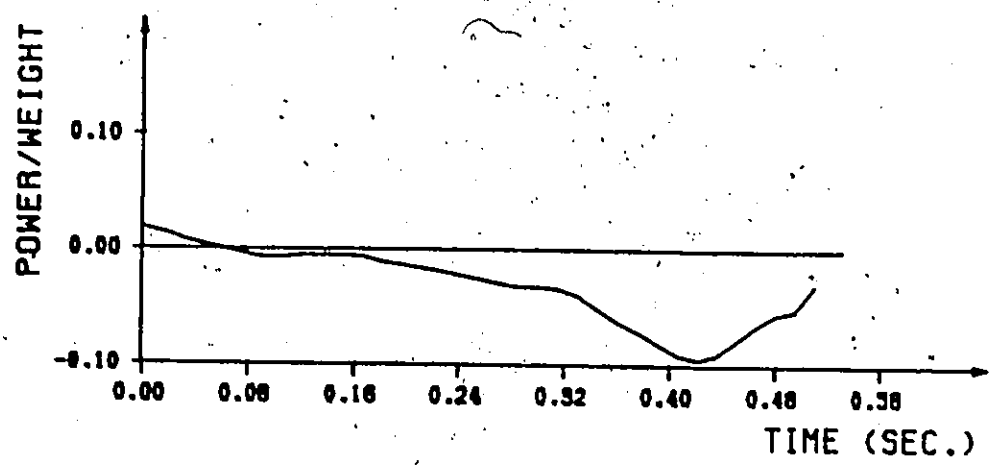

(b) Knee joint

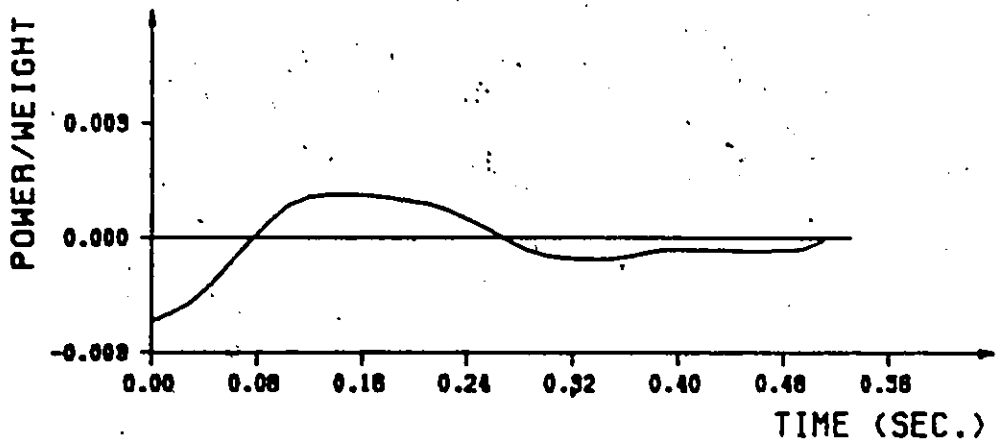

(c) Ankle joint

Figure 5.3
Rates of energy exchange between muscles of the lower extremity and the limb segments
(Power in Watts ; Weight in Kg)

is being expended in order to decelerate the limb before heel-strike takes place. Figure 5.3(b) shows that the knee muscles expend some energy at the start of swing to ensure that the extremity clears the floor, and then until the end of swing almost no energy exchange takes place as the motion becomes that of a pendulum. Figure 5.3(c) shows that the ankle muscles expend some energy during mid-swing to prevent the foot from dropping due to the effect of gravity.

The criterion that we propose for use in the assessment of gait is based on the computation of the total energy expended by the leg muscles during the swing phase for various speeds of walking. In other words, all the positive areas under the power curves of the hip, knee, and ankle joints are summed together to give a single parameter that can be used as a quantitative measure of performance of the leg muscles for a particular walking speed.

5.6 Energy Expenditure by Muscles of Normals and Hemiplegic Patients

In the preceding section, we presented the basis of a criterion for the assessment of gait, based on energy expenditure by muscles of the lower extremities during the swing phase. However, in order to use this criterion to compare the gaits of different subjects, the speed of walking has to be the same for all the subjects. Milner et

al. (1971) studied EMG signals from various leg muscles of subjects walking at various speeds; they found, with few exceptions, that the averaged-rectified EMG signals from various muscles increased linearly with the speed of walking. In addition, Bard and Ralston (1959) measured the energy expenditure of the whole body, as indicated by oxygen consumption, at various speeds of walking, and found that as the speed increased the energy expenditure also increased.

When normal subjects are studied, it is not difficult to control their speeds of walking, and thus compare their energies at the same speed. However, when patients are studied, their main concern is to walk at a speed that assures them of stability, and therefore, they usually walk at slow speeds and they do not have fine control over their speed of walking. The experimenter can only ask the patients to walk at a "fast", "medium", or "slow" speed and then they select a cadence that results in their stability.

The remainder of this chapter is dedicated to the study of the effect of the speed of walking on energy expenditure by the leg muscles of normals, and then comparing the results with those for hemiplegic patients.

5.6.1 Assessment of Normals

Several experiments were conducted by the author to study the effect of speed on muscle energy. At first, a

male subject, 31 years old, was studied. The subject walked at speeds ranging between 0.4 and 1.8 meters per second, and the kinematic variables corresponding to the various speeds of walking were recorded. The total energy expended by muscles of the leg was computed and normalized to the subject's weight. When a plot of the relation between speed and normalized energy was visually inspected, we realized that the curve could be approximated by a parabola. Therefore, we decided to plot the energy versus the square of the speed (V^2). Figure 5.4 shows the resulting plot including the linear least-squares fit of the data points. If we denote the energy per kilogram of the subject's weight (in joules/kg) by E_n, where n stands for normal, and the speed of walking (in m/s) by V, the equation of the least-squares fit is given by:

$$E_n = 0.0012 + 0.0074\ V^2 \quad \text{Joules/kg} \qquad (5.20)$$

It is clear from the above equation that the straight line does not pass through the origin. This contradicts the fact that when the speed is zero (the subject is standing still), muscles do not expend any mechanical energy. Although some muscles contract in the standing position to maintain postural stability, the muscle forces do not result in motion of the limb segments, and thus they do not work on the segments. Deviation of our experimental results from

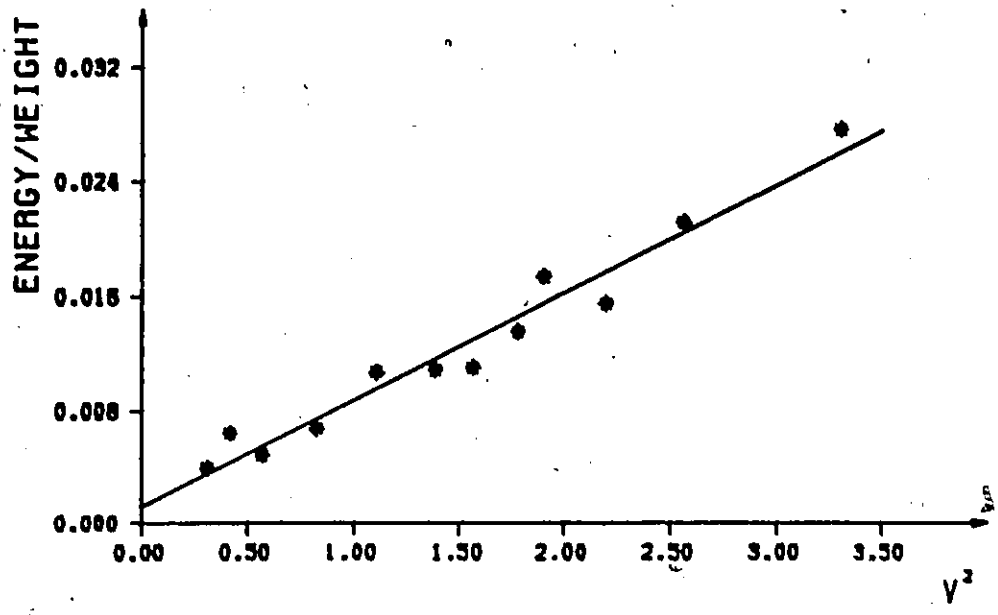

Figure 5.4
Effect of walking speed on muscle energy
(one normal subject)

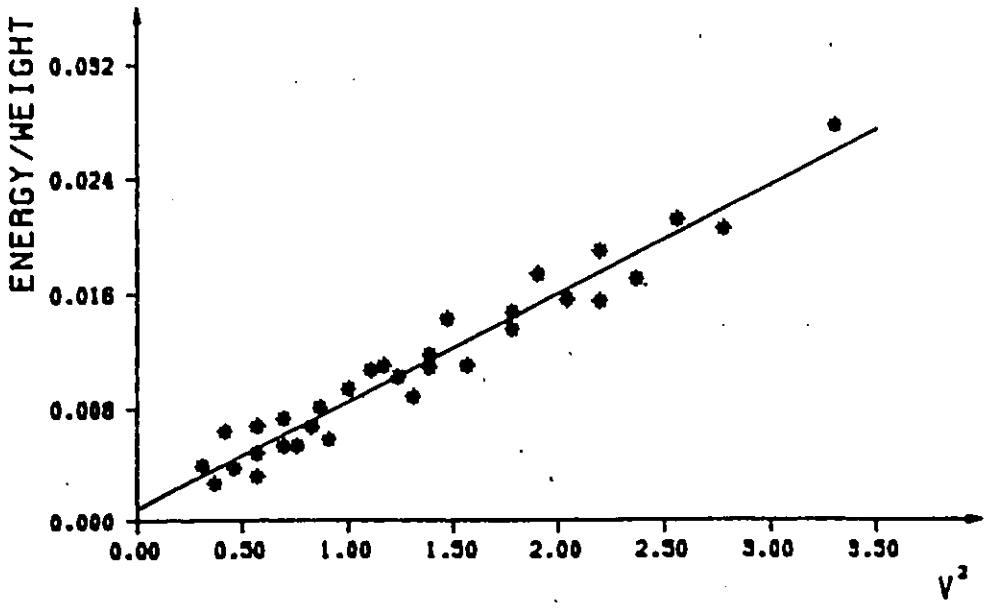

Figure 5.5
Effect of walking speed on muscle energy
(six normal subjects)
(Energy in Joules ; Weight in Kg)

the origin can be attributed either to a nonlinearity of the relation at very slow speeds, or to the measurement and computation errors, or both. Difficulty is encountered if we attempt to conduct experiments at very slow speeds because the subject's gait becomes too artificial, and he literally has to suspend his leg in the air during the swing phase in order to maintain the slow speed of walking.

In order to confirm our findings concerning the linearity of the relation between V^2 and muscle energy, five more subjects, 3 males and 2 females, were tested. Figure 5.5 shows the data for all the six subjects, together with the linear least-squares fit. Again, we notice that there is a strong linear relationship between V^2 and energy. The equation of the straight line is given by:

$$E_n = 0.0009 + 0.0076\ V^2 \quad \text{Joules/kg} \qquad (5.21)$$

The results obtained by Bard and Ralston (1959), and Corocran and Brengelmann (1970) on energy expenditure of the whole body, also show a linear relationship between the normalized energy expenditure of the body and V^2. However, they show that there is some energy expended during the standing position. Naturally, this is to be expected because the body expends energy to maintain functions other than walking.

An important remark on our results is that they show that muscle energy per kilogram of the body weight of all the subjects tested is independent of the subject. This means that equation (5.21) or Figure 5.5 can be used as a "norm" to which pathological gaits can be compared. In the following section we will present the results obtained for hemiplegic patients and compare them with those of healthy subjects.

5.6.2 Assessment of Hemiplegic Patients

Hemiplegia is a pathology that results from loss of motor control over one half of the body. In most cases, hemiplegia develops after the onset of a stroke caused by a cerebral vascular accident or thrombosis. Hemiplegics usually go through several stages of recovery of their normal motor functions. Brunnstrom (1970) observed a large number of patients and was able to classify the various levels of recovery into six distinct stages. Immediately following the acute episode, flaccidity is present and no movements of the limbs can be initiated (stage 1). As recovery begins, the basic limb synergies or some of their components start to appear. At this time spasticity begins to develop (stage 2). The next stage is characterized by some voluntary control of the movement synergies and spasticity further increases (stage 3). Then some movement

combinations that do not follow the paths of synergy are mastered, first with difficulty, then with more ease, and spasticity begins to decline (stage 4). If progress continues, more difficult combinations are learned as the basic limb synergies lose their dominance over motor acts (stage 5). With the disappearance of spasticity, individual joint movements become possible and coordination approaches normal (stage 6).

In this study, data from 17 hemiplegic patients was analyzed. Five of the patients had been previously classified as stage 6 patients, six had been classified as stage 5, and six had been classified as stage 4 patients. The analysis was carried out on three walks of each patient at different speeds. The total energy per kilogram of the subject's weight was computed for the leg of the affected side of each patient. Figure 5.6 shows the results obtained for all the patients along with the results previously obtained for normals (dashed line). The least-squares fits of the data from the three patient groups are given by:

$$E_{h6} = 0.0008 + 0.0073\ v^2 \quad \text{Joules/kg} \qquad (5.22)$$

$$E_{h5} = 0.0010 + 0.0107\ v^2 \quad \text{Joules/kg} \qquad (5.23)$$

$$E_{h4} = 0.0012 + 0.0126\ v^2 \quad \text{Joules/kg} \qquad (5.24)$$

where h stands for hemiplegic, and the numbers following the

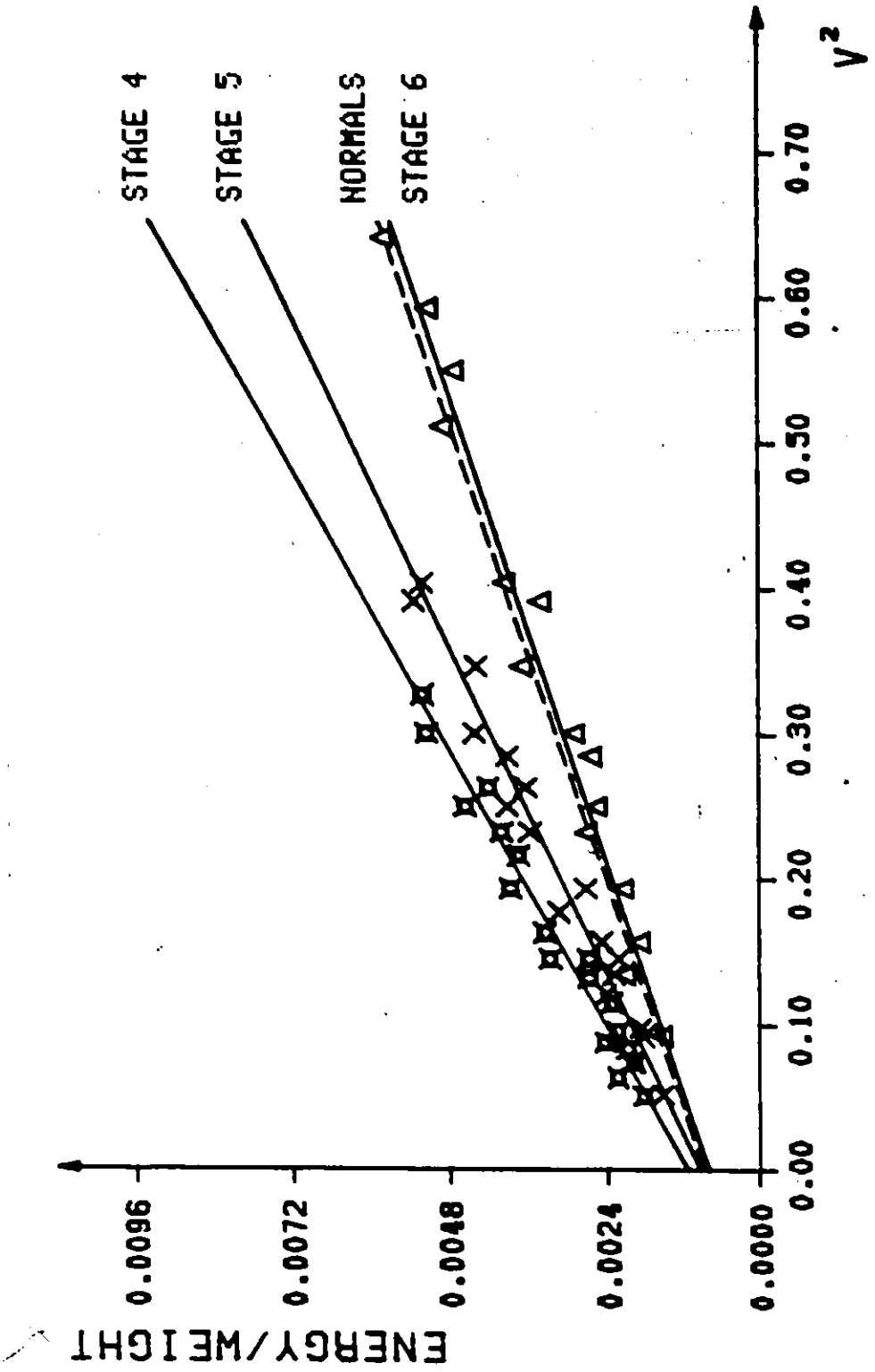

Figure 5.6
Effect of walking speed on muscle energy of hemiplegic patients

h's indicate the various recovery stages.

The results show that stage 6 patients expend about the same amount of energy as normals walking at the same speed. However, we notice that the range of speeds in hemiplegic gait is much less than that for normals. The highest speed achieved by a patient was 0.8 m/s while for normals it was 1.8 m/s. This means that although energy expenditure relationship of stage six patients is almost the same as that of normals, the patients are still unable to reach normal speeds of walking. Our results show that earlier stages of recovery (stages 5 and 4) are characterized by higher energy expenditures than normal. In addition, energy expenditure increases more rapidly as the speed of walking increases.

The decrease of energy expenditure with recovery is not surprising because normal walking is a process in which the body tries to minimize energy expenditure by coordinating the movements in such a way that locomotion is achieved in the most efficient manner. Unfortunately, patients do not have such a fine control over their movements, and thus they tend to use their muscles in a less efficient manner; they have to pay a higher price for walking by expending more energy. Consequently, patients tire more quickly and they are usually unable to walk long distances.

The inefficiency of utilization of muscles is most apparent in stage 4 patients. These patients are usually still suffering from the presence of synergy components in their movements. Synergies manifest themselves in the inability of the patient to control individual joint rotations. For example, flexor synergy of the lower extremity results in simultaneous flexion of the hip, flexion of the knee, and dorsiflexion of the ankle. During normal walking these components might not be needed simultaneously, and therefore their presence at the same time might result in an uncoordinated and inefficient gait.

Corcoran et al. (1970) studied energy consumption by the whole body for 15 hemiplegic patients and demonstrated an increase in energy consumption by the patients. However, in their work, they did not use the Brunnstrom system of classification, and therefore we were not able to compare our quantitative results of assessment with theirs.

The results shown in Figure 5.6 indicate that there is some overlap between the data points corresponding to the different stages of recovery. This overlap may be attributed, in part, to the measurement errors. In addition, the process of classifying the patients using the Brunnstrom method might be contributing to the overlap. Classification into one of six stages is usually performed in a subjective manner and is based on averaging scores

according to performance of the various extremities. The resulting average score is thus a rough measure of performance. For example, a final score of 4.5 may be set equal to 4 or 5 depending on the judgement of the physiotherapist assessing the patient.

In this chapter we have shown that energy expenditure by muscles of the leg during the swing phase can be used as a parameter for the assessment of normals and hemiplegic patients. However, before these results can be used in a clinical environment, a much larger population of normals and patients has to be studied. Once these results become available, we can start to assess normals and the various stages of recovery of patients in an objective manner.

CHAPTER 6

PROCESSING AND ANALYSIS OF ELECTROMYOGRAPHIC SIGNALS

6.1 Introduction

In Chapter 2, the underlying relationship between electomyographic (EMG) signals and muscle forces was discussed in some detail. That discussion showed that the raw EMG signal from a muscle is a poor representation of the force developed by that muscle. For example, when a smooth movement of a limb is initiated, the tension profiles of the muscles responsible for the movement are usually smooth and can be regarded as low frequency signals (less than 10 Hz). On the other hand, EMG signals from the same muscles are random signals with a much larger bandwidth (a few hundred Hz). Direct measurement of muscle forces requires the implant of force transducers at the muscle tendons. This procedure is impractical for clinical research and has rarely been used with humans. Therefore, the only alternative is to try to process EMG signals in such a manner that the processed signals bear as close a relationship to muscle forces as possible.

In this chapter, we present a new approach for evaluating EMG processors, based on the multiple-coherence

functions of the processed EMG signals as inputs to a system whose output is the total muscle torque at a particular joint. The procedure is used to arrive at the EMG processing strategy that results in a system that approximates a hypothetical linear system.

The optimal EMG processing strategy, arrived at using the above-mentioned procedure, is used to process EMG signals from a number of muscles of different subjects walking at various speeds. The linearized system consisting of processed EMG signals as inputs and muscle torque at the joint as output is analyzed during the swing phase, and a transfer-function model is derived for each joint.

During the stance phase, muscle torques at the joints cannot be computed because of the presence of unknown floor-reaction forces. A novel technique, developed by the author, is used to compute both the muscle torques and the floor-reaction forces during the stance phase. This technique makes use of the transfer-function models derived for the swing phase, and assumes that these models are also valid for the stance phase. The known processed EMG signals for the stance phase are fed to the appropriate transfer-function models, and the outputs of these models (muscle torques) are computed. Once the muscle torques during the stance phase have been estimated, the problem of computing the floor-reaction forces is reduced to a simple problem in

the dynamic equilibrium of the lower extremity.

6.2 Evaluation of EMG Processors Using Multiple-Coherence Functions

6.2.1 Commonly Used EMG Processors

Most investigators in the area of EMG signal processing have confined their studies of the relationship between processed EMG signals and muscle forces to the special case of isometric muscle contraction (contraction under constant load). Crosby (1978) processed surface EMG signals from the human triceps muscle by full-wave rectifying the signals, and then passing the rectified signals through a low-pass filter. He then modeled the relationship between the processed signals and the isometric muscle force, and found that the relationship could be represented by an overdamped second-order system.

Kreifeldt and Sumner (1974) performed a comparison between EMG processing strategies based on the signal-to-noise ratio (S/N) characteristics of the processed signals. They considered several signal analysis techniques, including half-wave rectification, full-wave rectification, and general power-laws. They found that when the square-root of the EMG signals was followed by a smoothing filter, the resulting processed signals possessed superior S/N characteristics as compared to other processors; however,

they did not attempt to relate the processed signals to muscle forces.

One of the few studies of EMG processors for signals obtained during non-isometric muscle contraction was that of Miller and Seireg (1976). They used a bicycle ergometer to study the dynamic behaviour of the intact skeletal muscle, and compared the profiles of the processed signals to the dynamic force profiles. They found that essentially the same results were obtained when processing the signals using either the rectifier-averager, or the root-mean square (RMS) obtained from power spectra of the signals, or the analog RMS.

In order to relate EMG signals to the dynamic muscle behaviour during gait, results obtained for muscles under isometric contraction may not be valid. Muscles of the lower limb experience various types of contraction during gait. The type of contraction may differ from one muscle to the other, and may also change for the same muscle during the course of the walk cycle. For this reason, reexamination of EMG processing strategies, as related to human gait, is needed.

The purpose of this investigation is to assess the suitability of various EMG processors for gait analysis. A new approach for the evaluation of EMG processing strategies is presented in this chapter. The approach is

based on the analysis of a system whose inputs are the processed EMG signals from muscles crossing a joint, and whose output is the total muscle torque at that joint.

An attempt is made to find the processing strategy that renders a system as close to linearity as possible. The EMG processor arrived at using this approach might not be the optimal processor for a particular muscle or a particular speed of walking. An attempt to find an optimal processor for each muscle and each walking speed would be highly impractical. On the other hand, a single processing strategy that results in a system with an overall improved linearity would be highly desirable and convenient to use.

Assessment of linearity of the locomotor system is carried out by computing the multiple-coherence functions for the multiple-input single-output joint systems. The following section includes a brief discussion of the input-output relations of linear systems and a definition of the multiple coherence function.

5.2.2 Input-Output Relations of Linear Systems

In this section, various input-output and spectral relations of linear systems are given without proofs. The interested reader can find more details about the subject in any reference that deals with linear systems theory; in particular, the books by Bendat and Piersol (1971) and Otnes

and Enochson (1972) are recommended.

Consider the multiple-input single-output linear system shown in Figure 6.1. The system consists of q inputs $x_i(t)$, i=1,2,...,q, and a single output y(t). The output may be considered as the superposition of the q outputs $y_i(t)$, i=1,2,...,q. That is

$$y(t) = \sum_{i=1}^{q} y_i(t) \tag{6.1}$$

where $y_i(t)$ is defined as the part of the output that is

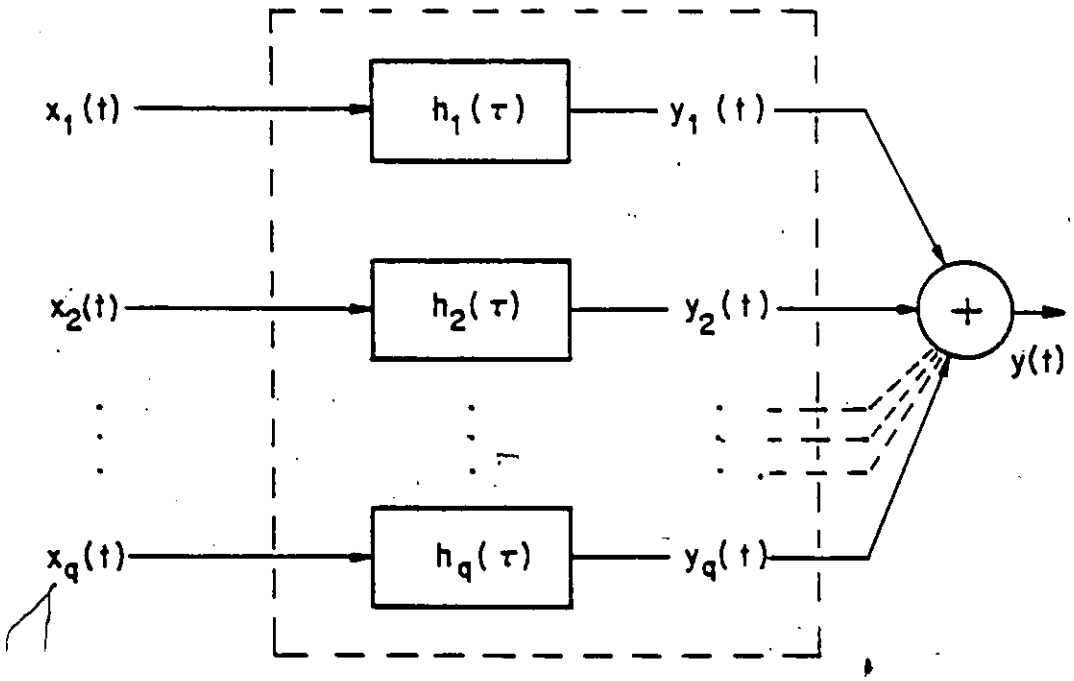

Figure 6.1
Multiple-input linear system

produced by the i'th input when all the other inputs are zero.

Each output $y_i(t)$ may be obtained by convolving the weighting function $h_i(t)$ with the corresponding input $x_i(t)$, i.e.

$$y_i(t) = \int_0^\infty h_i(\tau)x_i(t-\tau)d\tau \qquad (y_i(0) = 0) \tag{6.2}$$

The power spectral density of the output is given by

$$S_{yy}(f) = \sum_{i=1}^{q} \sum_{j=1}^{q} H_i^*(f)H_j(f)S_{ij}(f) \tag{6.3}$$

where $H_i(f)$ is the Fourier transform of $h_i(t)$, and $H_i^*(f)$ is the complex conjugate of $H_i(f)$; $S_{ij}(f)$ is the cross-spectral density function between the two inputs $x_i(t)$ and $x_j(t)$; $S_{ij}(f)$ is obtained by applying the Fourier transform to the cross-correlation function $R_{ij}(\tau)$:

$$S_{ij}(f) = \int_{-\infty}^{\infty} R_{ij}(\tau)\, e^{-j2\pi f\tau}\, d\tau \tag{6.4}$$

where

$$S_{ij}(f) = S_{ji}^*(f) \tag{6.5}$$

The cross-spectral density between the output $y(t)$

and the input $x_i(t)$ is given by

$$S_{yi}(f) = \sum_{i=1}^{q} H_j^*(f) S_{ji}(f) \tag{6.6}$$

also

$$S_{yi}(f) = S_{iy}^*(f) \tag{6.7}$$

The multiple-coherence function between the output and the inputs is defined by

$$\gamma_{yx}^2 = \frac{\sum_{i=1}^{q} H_i(f) S_{yi}(f)}{S_{yy}(f)} \tag{6.8}$$

It is clear from equations (6.3) and (6.6) that the numerator of equation (6.8) is equal to $S_{yy}^*(f)$. Since $S_{yy}(f)$ is a real-valued function, then $S_{yy}^*(f) = S_{yy}(f)$; therefore, the multiple-coherence function is equal to unity. This statement is true only under noise-free ideal conditions when there is a true linear relationship occuring in the multiple-input single-output case. However, in the general case of a system exhibiting some nonlinearities, or affected by extraneous noise, the multiple-coherence function will be less than unity and will always be subject to the relation

$$0 \leq \gamma_{yx}^2 \leq 1 \tag{6.9}$$

The multiple-coherence function represents the fraction of the output power at frequency f that can be attributed to linear relationships in the model of Figure 6.1. Therefore, the linearity of a system can be tested by computing the multiple coherence function; the closer the value of γ^2_{yx} is to unity the closer the system is to linearity.

To give the reader a feeling of the behaviour of the coherence function under non-ideal conditions, we consider the simple case of a single-input linear system. The coherence function of this system is equal to unity. However, if the measurements of the input were contaminated by noise, the coherence function becomes less than unity. Assume that the noise power at a particular frequency is 10% of the signal power at that frequency. Due to this noise, the coherence value at that particular frequency drops to 0.91. This indicates that the coherence function is a sensitive measure of the deviation of a system from the ideal noise-free linear conditions.

6.3.3 Computation of the multiple-Coherence Function

In practice, equation (6.8) cannot be used directly to estimate the multiple-coherence function because the values of $H_i(f)$, $i=1,2,\ldots,q$, are unknown. An alternative formula can be obtained by manipulating equations (6.3)

through (6.8)). This formula makes use of the (q+1)x(q+1) augmented spectral matrix defined by

$$\underline{\underline{S}}_{yxx}(f) = \begin{bmatrix} S_{yy}(f) & S_{y1}(f) & S_{y2}(f) & \cdots & S_{yq}(f) \\ S_{1y}(f) & S_{11}(f) & S_{12}(f) & \cdots & S_{1q}(f) \\ S_{2y}(f) & S_{21}(f) & S_{22}(f) & \cdots & S_{2q}(f) \\ \vdots & \vdots & \vdots & & \vdots \\ \vdots & \vdots & \vdots & & \vdots \\ S_{qy}(f) & S_{q1}(f) & S_{q2}(f) & \cdots & S_{qq}(f) \end{bmatrix} \qquad (6.10)$$

and the multiple-coherence function is estimated using the equation

$$\gamma^2_{yx}(f) = 1 - [S_{yy}(f)S^{yy}(f)]^{-1} \qquad (6.11)$$

where $S^{yy}(f)$ denotes the first diagonal element of the matrix $\underline{\underline{S}}^{-1}_{yxx}(f)$.

Equation (6.11) was implemented by the author in the form of a computer program which computed the multiple coherence function for any system that had up to 10 inputs. A Fast Fourier Transform algorithm (FFT) was used to compute all the spectral density functions of equation (6.10), at discrete frequencies determined by the sampling rate of the signals. An important consideration in the use of the FFT algorithm to compute the spectral density estimates is that frequency smoothing had to be employed in order to reduce the estimation errors and improve the consistency of the estimates.

The need for frequency smoothing can be demonstrated by applying the Fourier transform to a Gaussian random signal. Because of the linearity of the Fourier transform, both the real and imaginary parts of the Fourier coefficients of the signal are also Gaussian random variables. The spectral density estimates are then obtained by computing the squares of the magnitudes of the Fourier coefficients. In other words, the spectral density estimates are obtained by adding the squares of two Gaussian variables. Consequently, the spectral density estimates have Chi-square distributions with two degrees of freedom. This number of degrees of freedom is too small and unacceptable for most purposes because it results in inconsistent estimates with substantial estimation errors. In fact, using the FFT estimates with 2 degrees of freedom results in coherence function estimates of unity regardless of the input and output signals (Bendat and Piersol, 1971).

For this study, the spectral density estimates obtained by the FFT algorithm were not used directly; frequency smoothing was first employed in order to increase the number of degrees of freedom. This was achieved by using the processed EMG signals corresponding to 4 walk cycles from each run. The spectral density coefficients were estimated for each cycle, and then the estimates at corresponding frequencies were averaged over the 4 walk

cycles. This resulted in the increase of the number of degrees of freedom to 8. Further increase was obtained by averaging the neighbouring coefficients. In the original computations of the spectral density coefficients, the frequency increment was 0.25 Hz; this increment was increased to 2.0 Hz by averaging each 8 neighbouring coefficients. Consequently, the number of degrees of freedom was increased to 64.

In the analysis, data from three normal subjects, walking at various speeds, was used to compute the multiple-coherence functions for different EMG processors. Experiments were conducted on each subject when he walked at four different speeds; the speeds were 0.8, 1.0, 1.2, and 1.6 m/s.

Three different multiple-input single-output systems were analyzed for each experimental run. These were:

(1) The hip-joint system: Processed EMG signals from the rectus femoris, biceps femoris, semitendinosus, and semimembranosus muscles were considered as the inputs to the hip-joint system, and the total muscle torque at the hip was considered as the output.

(2) The knee-joint system: Processed EMG signals from the rectus femoris, vastus lateralis, vastus medialis, biceps femoris, semitendinosus, semimembanosus, and gastrocnemius muscles were

treated as the inputs to the knee-joint system, and the output was the muscle torque at the knee joint.

(3) The ankle-joint system: Processed EMG signals from the gastrocnemius, soleus, and tibialis anterior muscles were considered as the inputs to the ankle-joint system, and the total muscle torque at the ankle joint was considered as the output.

In order to illustrate the severe nonlinearity of the systems under consideration when raw EMG signals are used, the multiple-coherence function was computed, at various frequencies, for the ankle-joint system with raw EMG signals as inputs. The results of these computations are shown in Figure 6.2, from which it is clear that the system is highly nonlinear. At a frequency of 3 Hz, the output power that can be attributed to linear relationships is only 30% of the total output power. At all other frequencies, the system exhibits even less linearity than that at 3 Hz.

Because of the obvious nonlinearity of the systems we are dealing with, nonlinear processors must be employed in an attempt to remove some of the nonlinearities inherent in these systems. In addition, smoothing of the processed EMG signals must be performed in order to limit the power in the signals to the low frequency range of the output signals (muscle torques).

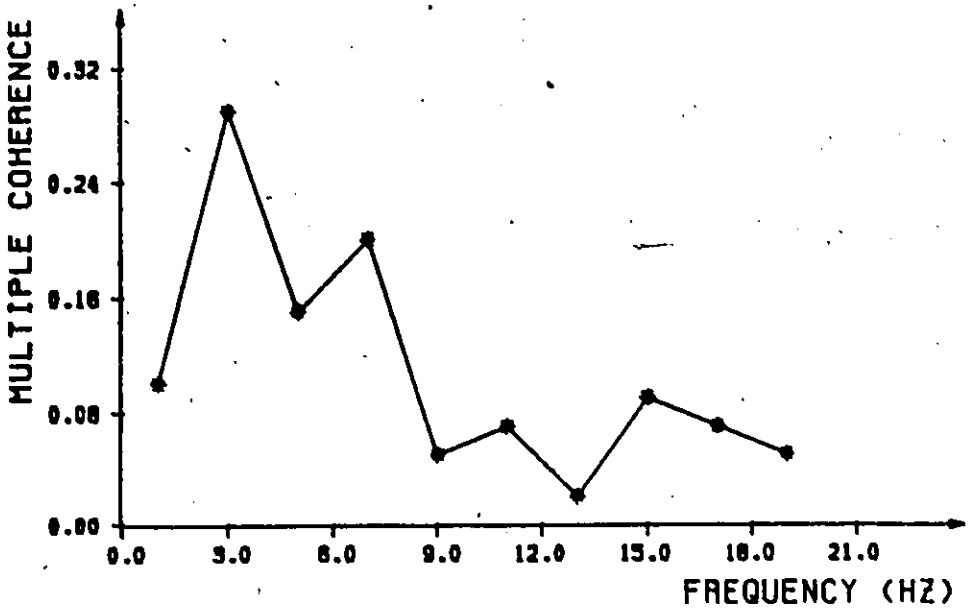

Figure 6.2
Coherence function of the ankle-joint system when raw EMG signals are used as inputs

Five different EMG processing strategies were studied. Each processing strategy consisted of a detector and a smoothing filter. The smoothing filter was simulated by a moving-average window in which the window length was varied in order to control the amount of smoothing. This is equivalent to passing the signals through a low-pass R-C filter whose cutoff frequency is varied by changing the time constant (Naumann, 1978). All the detectors considered had one property in common; that is they all removed the negative excursions of the raw EMG signals. This was an important consideration in view of the fact that although

EMG signals are bipolar, the negative excursions do not indicate negative muscle forces. Muscles can only produce forces in the direction in which they contract. The detectors used for processing EMG signals were:

(1) Half-wave rectifier, $(X + |X|)/2$.

(2) Full-wave rectifier, $(|X|)$.

(3) Square-law detector, (X^2).

(4) Square-root-law detector, $(\sqrt{|X|})$.

(5) Root-mean-square detector (RMS), $(\sqrt{\overline{X^2}})$.

Assessment of each EMG processing strategy was carried out in the following steps:

(1) Raw EMG signals from the leg muscles were processed and smoothed using a moving-average window of a particular length.

(2) The multiple-coherence function was computed for each joint system with the appropriate processed EMG signals as inputs. The resulting coherence estimates, at various frequencies, were averaged to give a single "coherence parameter". These computations were performed for each joint system of

each of the three subjects when they walked at various speeds. Altogether, 36 "coherence parameters" were computed for each window length.

(3) The 36 "coherence parameters" were averaged to give an "average coherence" value at a particular window length. The average coherence was then plotted as a function of window length. The windows used varied in length between 0 and 200 ms.

The above procedure was repeated for each processing strategy. Figures 6.3 to 6.7 show the plots of average coherence versus window length for the various EMG processors tested. The bars indicate the one-standard-deviation limits of the 36 data points used in the computation of each average coherence value. Most of the curves have one feature in common: they show that the average coherences corresponding to short windows have rather small values and that average coherence values increase with the increase in window length; the average coherence reaches a peak corresponding to a window length in the range between 100 and 150 ms, then average coherence values become smaller at longer windows (above 150 ms).

This can be explained in view of the fact that short windows do not provide enough smoothing of the processed signals to limit the signal power to the frequency range of

the output signal. On the other hand, long windows provide too much smoothing that results in the loss of useful information contained in the signals. It is clear from the figures that the RMS processor (Figure 6.7) with a 140 ms window results in the best linearity characteristics among all the processors tested. At a window length of 140 ms, the average output power that can be attributed to linear relationships constitutes about 85% of the total output power. Figure 6.8 shows EMG signals from the various muscles, after being processed using the RMS processor with a 140 ms window.

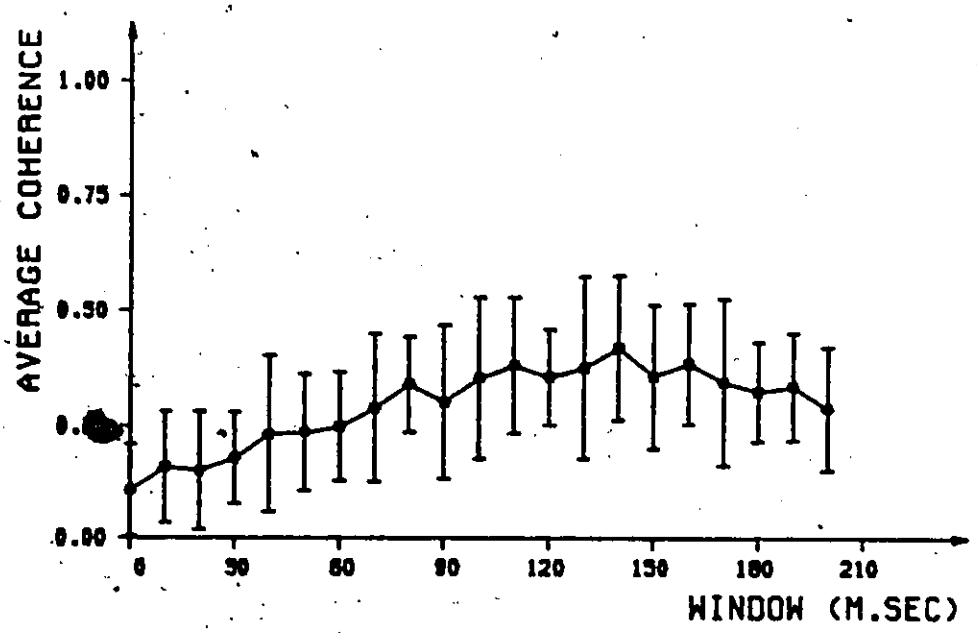

Figure 6.3
Average coherence for half-wave rectifier

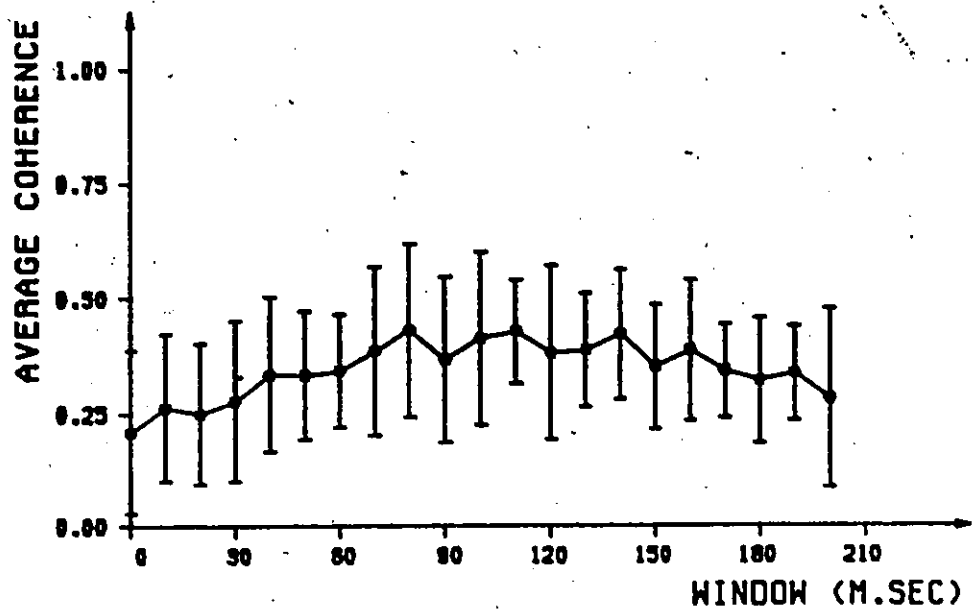

Figure 6.4
Average coherence for full-wave rectifier

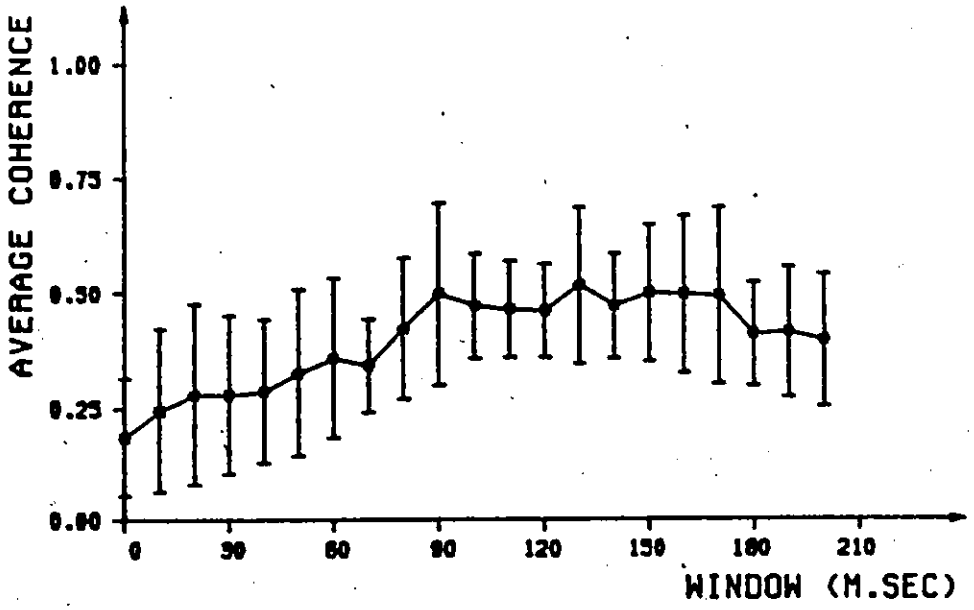

Figure 6.5
Average coherence for square-law detector

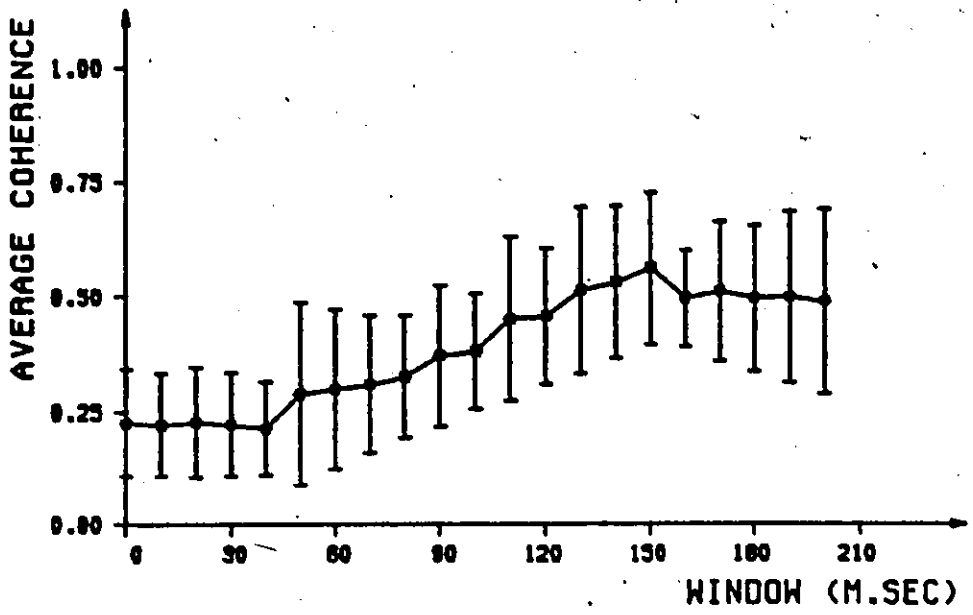

Figure 6.6
Average coherence for square-root-law detector

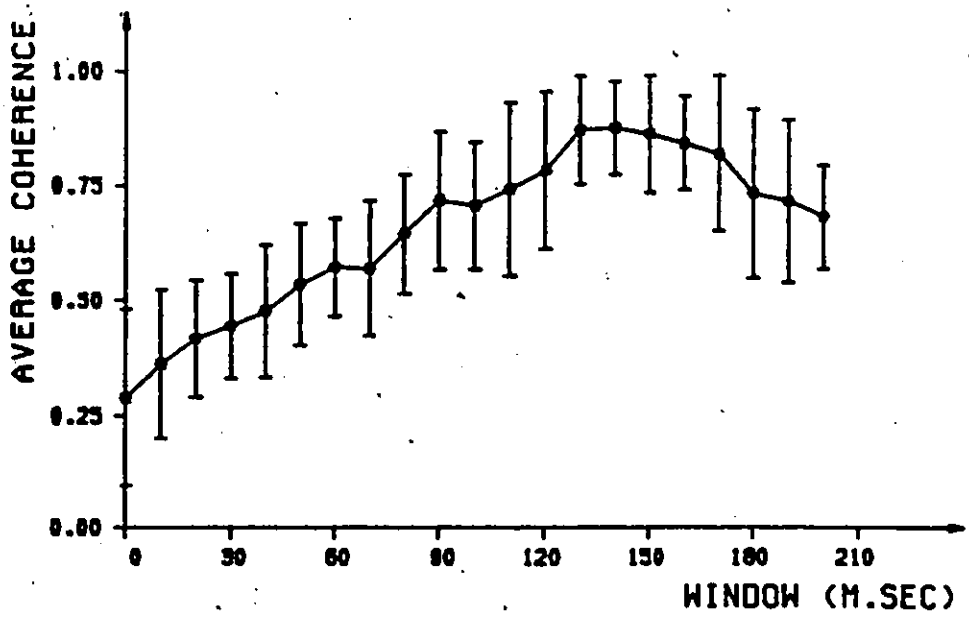

Figure 6.7
Average coherence for root-mean-square detector

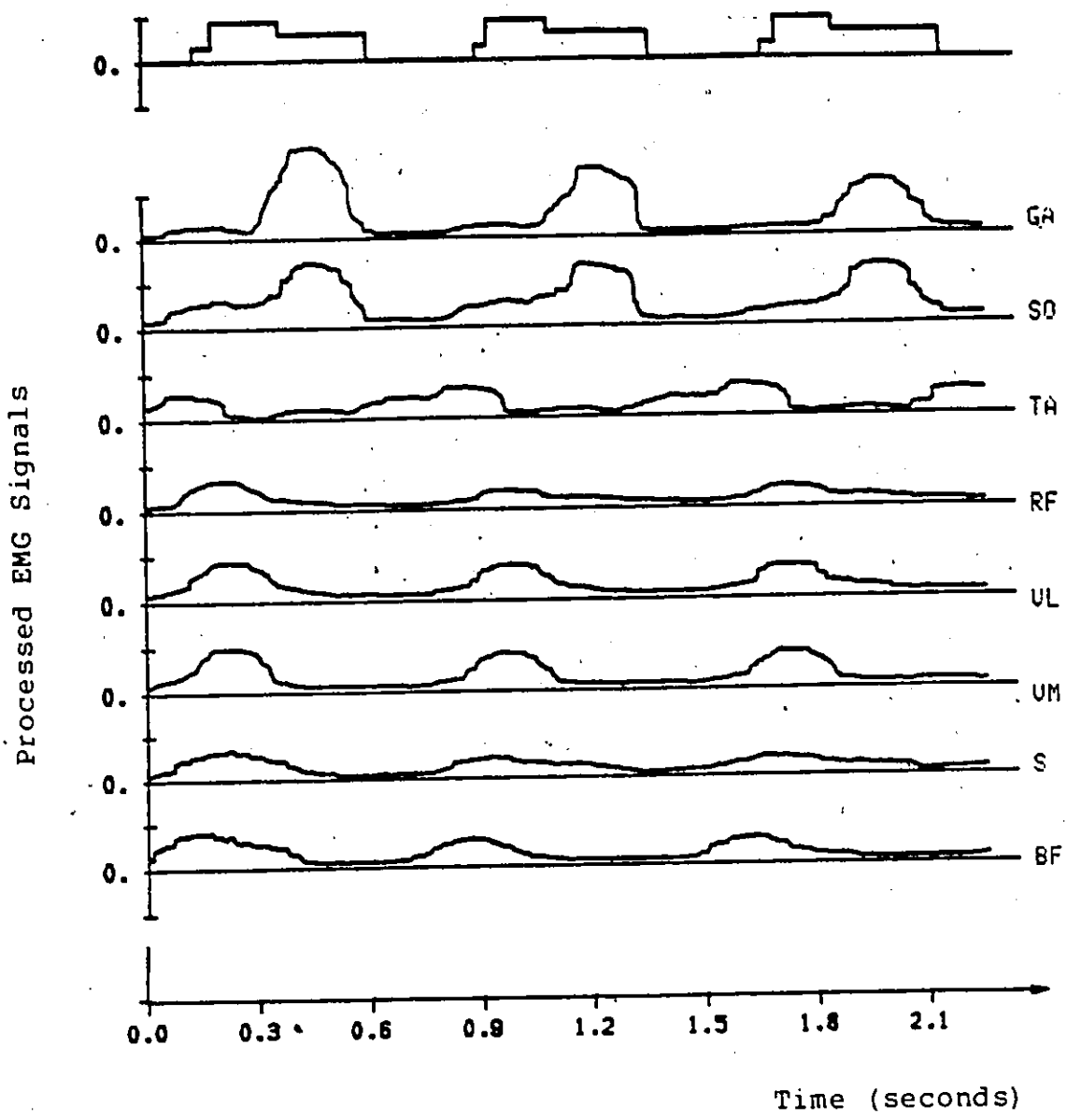

Figure 6.8
Processed EMG signals from various muscles
using the RMS detector with 140 ms window

(GA: Gastrocnemius, SO: Soleus, TA: Tibialis Anterior,
RF: Rectus Femoris, VL: Vastus Lateralis, VM: Vastus
Medialis, S: Semitendinosus, BF: Biceps Femoris)
(scale: .1 mV/div)

6.3 Transfer-Function Modeling Of the Locomotor System

Having determined the processing strategy that achieves the best linearity of the joint systems as compared to the other strategies tested, we can now proceed to analyze these systems as approximately linear systems. Naturally, some errors will be introduced because of the residual nonlinearities that the RMS processor did not remove from the joint systems. These errors will be discussed when the results obtained using the assumption of linearity are compared to the measurements obtained by other researchers.

The relationship between the inputs to a joint system (processed EMG signals) and the output of the system (muscle torque) can be easily obtained by computing transfer-function models using the spectral relations discussed in the preceding section. In the following section, the equations used in the estimation of transfer functions of linear systems are given.

6.3.1 General Transfer-Function Relations of Linear Systems

Transfer functions of a multiple-input single-output linear system are obtained by computing the vector

$$\underline{H}(f) = [H_1(f) \quad H_2(f) \quad \ldots\ldots \quad H_q(f)] \tag{6.12}$$

The elements of this vector are obtained using the relation

$$\underline{H}'(f) = \underline{S}_{xx}^{-1}(f)\underline{S}'_{xy}(f) \tag{6.13}$$

where ' denotes transposition and $\underline{S}_{xx}(f)$ is the qxq spectral matrix given by

$$\underline{S}_{xx}(f) = \begin{bmatrix} S_{11}(f) & S_{12}(f) & \cdots & S_{1q}(f) \\ S_{21}(f) & S_{22}(f) & \cdots & S_{2q}(f) \\ \vdots & \vdots & & \vdots \\ S_{q1}(f) & S_{q2}(f) & \cdots & S_{qq}(f) \end{bmatrix} \tag{6.14}$$

and $\underline{S}_{xy}(f)$ is the vector $[S_{1y}(f) \quad S_{2y}(f) \quad \ldots \quad S_{qy}(f)]$, where all the spectral quantities in the above equations are the same as those used earlier in the computation of multiple-coherence functions.

Estimation errors present in the computation of the transfer functions $H_i(f)$, i=1,2,....,q, are obtained using the following equation (Bendat and Piersol, 1971):

$$|\hat{H}_i(f) - H_i(f)|^2 \leq \hat{r}_i^2(f) \tag{6.15}$$

where

$$\hat{r}_i^2(f) = \frac{2q}{n-2q} (F_{n1,n2;\alpha}) \frac{[\ 1 - \hat{\gamma}_{yx}^2(f)\ ]\ \hat{S}_y(f)}{[\ 1 - \hat{\gamma}_{ix}^2(f)\ ]\ S_i(f)} \tag{6.16}$$

where

$\hat{H}_i(f)$ = estimate of $H_i(f)$

$\hat{S}_y(f)$ = power spectrum estimate of the output y(t)

$\hat{S}_i(f)$ = power spectrum estimate of the input $x_i(t)$

$\hat{\gamma}^2_{yx}(f)$ = sample estimate of the multiple-coherence function between the output y(t) and all the measured inputs

$\hat{\gamma}^2_{ix}(f)$ = sample estimate of the multiple coherence function between the input $x_i(t)$ and all the other inputs excluding $x_i(t)$

q = number of inputs

n = number of degrees of freedom of each spectral estimate

$F_{n1,n2;\alpha}$ = 100α percentage point of an F distribution with n1=2q and n2=n-2q degrees of freedom.

Hence, the $(1-\alpha)$ confidence intervals for the gain factor $|H_i(f)|$ and the phase factor $\phi_i(f)$ of the transfer function $H_i(f)$ are given for each frequency f and each input-output path i=1,2,...,q, by

$$|\hat{H}_i(f)| - \hat{r}_i(f) \leq |H_i(f)| \leq |\hat{H}_i(f)| + \hat{r}_i(f) \qquad (6.17)$$

$$\hat{\phi}_i(f) - \Delta\hat{\phi}_i(f) \leq \phi_i(f) \leq \hat{\phi}_i(f) + \Delta\hat{\phi}_i(f) \qquad (6.18)$$

where the phase error $\Delta\hat{\phi}_i(f)$ is calculated from

$$\Delta\hat{\phi}_i(f) = \sin^{-1}(\hat{r}_i(f)/|\hat{H}_i(f)|) \qquad (6.19)$$

Equations (6.12) through (6.19) provide all the

necessary information for the estimation of the transfer functions of a multiple-input single-output linear system. Notice that all the spectral quantities in equation (6.14), except the diagonal elements, are complex variables. This means that equation (6.13) involves the inversion of a complex matrix. A simple procedure for finding the inverse of a complex matrix can be found in the book by Otnes and Enochson (1972). Also, notice that equation (6.16) shows that the estimation error can be greatly reduced by increasing the number of degrees of freedom of the spectral estimates.

6.3.2 Computation of the Transfer Functions

In the preceding section, the transfer function relations of a linear system were presented. These relations were implemented in the form of computer programs which were used to find the transfer-function models of the joint systems discussed earlier. Because of the limited computer memory available, the computations were performed in several successive steps as follows

(1) The muscle torque at each joint was computed as outlined in Chapter 5.

(2) The EMG signals from muscles crossing the joints were

processed using the RMS processor with a 140 ms window.

(3) The spectral density functions, required for the solution of equation (6.13), were estimated using the FFT algorithm. The number of degrees of freedom of the estimates was 64. This number of degrees of freedom was obtained by using frequency smoothing as outlined in Section 6.2.3.

(4) The transfer functions between the inputs and the output were estimated using equation (6.13). Also, the various multiple coherence functions were estimated.

(5) The errors in the estimates of the transfer functions were computed using equation (6.15). The 95% confidence intervals of the estimates at various frequencies were computed

Transfer functions of the hip, knee and ankle joint systems were computed using the procedure outlined above. The values of $H_i(f)$, $i=1,2,\ldots,q$, were estimated at discrete frequencies in the range between 0 and 20 Hz with 2 Hz intervals. The hip-joint system consisted of three inputs and a single output. The inputs were the processed EMG signals from the major muscle groups responsible for rotation of the hip joint. The knee-joint system consisted

of six inputs and one output, while the ankle-joint system consisted of three inputs and a single output.

Results of the computations were stored in computer files for later use in the estimation of muscle torques during the stance phase. The intermediate results of the transfer-function computations were not included in this thesis because there was no concise way of displaying these results. For example, the knee-joint system consisted of six different paths between the inputs and the output, and every path had a different transfer-function model at various frequencies. In addition, these results would not be of any use to other researchers because they only apply to a particular subject walking at a particular speed. Also, electrode positioning usually varies slightly from one experiment to the other. In fact, it was found that the transfer function models, obtained for the three subjects tested, were significantly different from one subject to the other.

In this study, our objective was to utilize the transfer-function models obtained for a particular subject, in the prediction of muscle torques for the same subject during stance. The procedure had to be repeated for each different subject, and whenever the same subject walked at a different speed. Therefore, the variability of the model parameters from one subject to the other was not of any

concern to us in this work.

Before the transfer functions, obtained for the swing phase, could be applied to the stance phase, we had to make sure that the systems under consideration were time-invariant. However, the available information about the stance phase was insufficient to test the time-invariance of the systems through the whole walk cycle. The only test that could be performed was to check the time-invariance during the swing phase.

Tests of time-invariance of the joint systems during the swing phase were performed in the following steps:

(1) The swing phase was divided into 3 equal intervals, and the inputs and output of each system were analyzed separately for each interval. Three transfer-function models were obtained for each joint.

(2) The 95% confidence intervals were computed for each parameter of the models at various frequencies.

(3) The value of each parameter of every model was compared to the corresponding parameters of the other two models. If the differences between the parameters were small enough, they were attributed to estimation errors, and the system was considered to be time-invariant. In other words, if the 95% confidence intervals of two corresponding parameters

were overlapping, the two parameters were considered to be estimates of the same constant transfer-function parameter.

The above test was applied to all the parameters of the models of the three joint systems to check whether the systems were time-invariant or not. The systems corresponding to the hip and ankle joints were found to be approximately time-invariant. Most of the parameters of these two systems did not exhibit any variability that could not be attributed to estimation errors. The largest "significant" change in the parameters of these systems, that could not be attributed to estimation errors, was found to be 15%. On the other hand, the knee-joint system showed greater variability in its parameters. The largest change in a parameter of the knee-joint system was found to be 35%. This means that when the knee-joint system is used, with the assumption that it is time-invariant, some errors should be expected in the results. The degree of severity of these errors will be discussed when the models are used to predict muscle torques and floor-reaction forces during the stance phase.

The variability of the parameters of the knee-joint system could be attributed to the unique structure of the knee joint. The knee joint is constructed such that the end

of the femur is divided into two convex condyles which bear against the slightly concave condyles of the tibia. The articulating surfaces of the femural and tibial condyles do not have the same shape, so that space is left between them for the knee cartilages. This structure causes the axis of rotation of the knee joint to change when the joint is flexed. This means that the assumption, made in Chapter 5, that the shank and thigh are connected by a "hairpin" joint is only approximate. On the other hand, most of the other joints are constructed in the form of ball-and-socket joints. This structure causes the position of the axis of rotation of the joints to be almost fixed with respect to the joints. The changing axis of rotation of the knee joint was, most probably, the cause of the deviation of the knee-joint system from time-invariance.

6.4 The Lower Extremity During the Stance Phase

So far, we have confined our studies of the lower extremity to the swing phase. Because of the presence of unknown floor-reaction forces during the stance phase, the number of equations of the dynamic equilibrium of the extremity were not sufficient to find a unique solution to the problem during the stance phase. Several investigators, including Elftman (1939a), Paul (1971), and Inman (1966), were able to determine all the forces and moments acting at

the joints by measuring the floor-reaction forces using a force plate. Other researchers (Quanbury and Winter, 1974) were able to compute the floor-reaction forces acting on one extremity while the other extremity was in swing. However, they were unable to determine the reaction forces during the double-support period because the amounts of loads shared by the two extremities are indeterminate during this period.

In this section, we present a new technique for determining the floor-reaction forces without using a force plate. We make use of the models derived for the joints during the swing phase in the prediction of muscle torques during the stance phase

6.4.1 Prediction of Muscle Torques During the Stance Phase

The input-output models, derived for the joints, related processed EMG signals to muscle torques during the swing phase. If we assume that these models are also valid during the stance phase, we can make use of the measured EMG signals corresponding to the stance phase in the prediction of muscle torques.

Equations (6.1) and (6.2) related the inputs and the output of a linear system via the impulse-response functions $h_i(t)$, $i=1,2,\ldots,q$. In our analysis, the frequency-response functions $H_i(f)$, $i=1,2,\ldots,q$, were determined for each joint system. The impulse-response functions can be

obtained by applying the inverse Fourier transform to the frequency-response functions. However, in our analysis, we made use of the frequency-response functions directly. The steps performed to compute muscle torques during the stance phase were:

(1) The EMG signals from the muscles of each joint were processed in a manner identical to that used during the swing phase.

(2) The Fourier transform of each processed signal was obtained using the FFT algorithm.

(3) The Fourier transform Y(f) of the output signal of each joint (muscle torque) was computed using the relation

$$Y(f) = \sum_{i=1}^{q} H_i(f)X_i(f) \qquad (6.20)$$

where $X_i(f)$ is the Fourier Transform of the input signal $x_i(t)$.

(4) The muscle torque at each joint was obtained by applying the inverse Fourier transform to Y(f).

The above procedure was used to compute the muscle torques at the joints during the stance phase. Figure 6.9 shows the predicted muscle torques at the three joints. These torques were computed for a male subject, 26 years

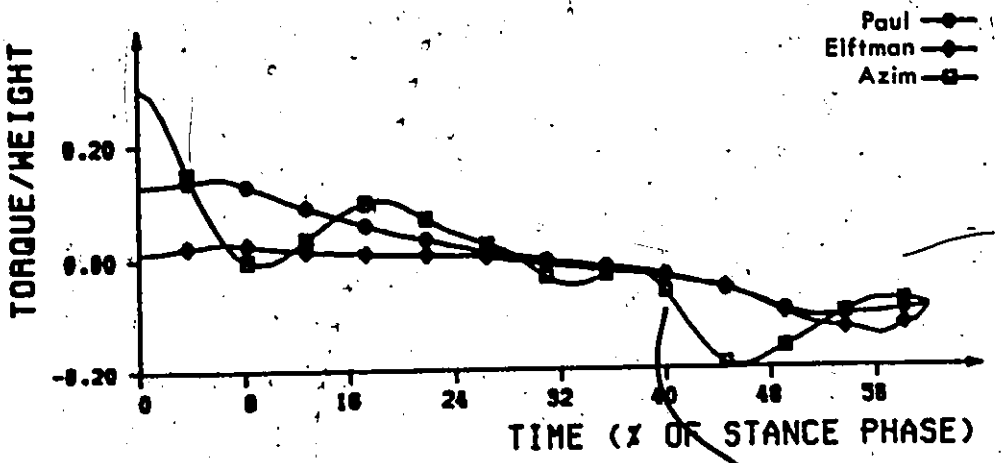

(a) Hip-joint muscle torque

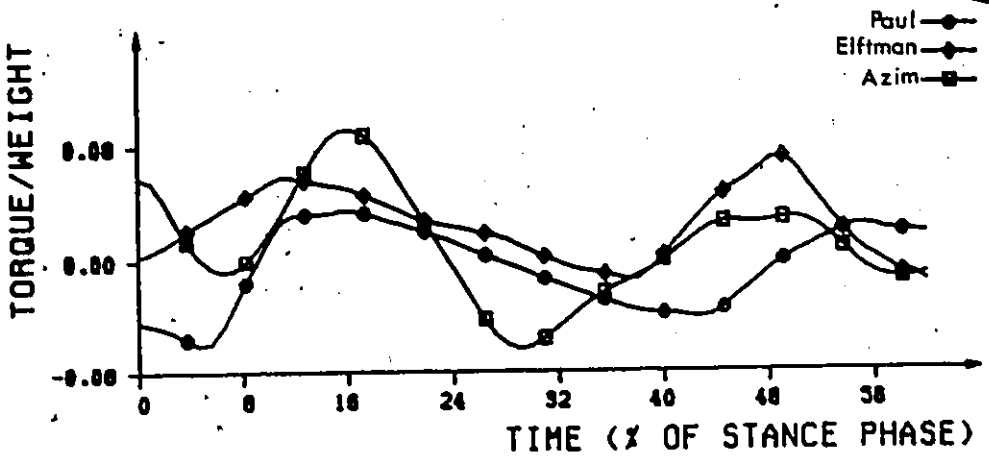

(b) Knee-joint muscle torque

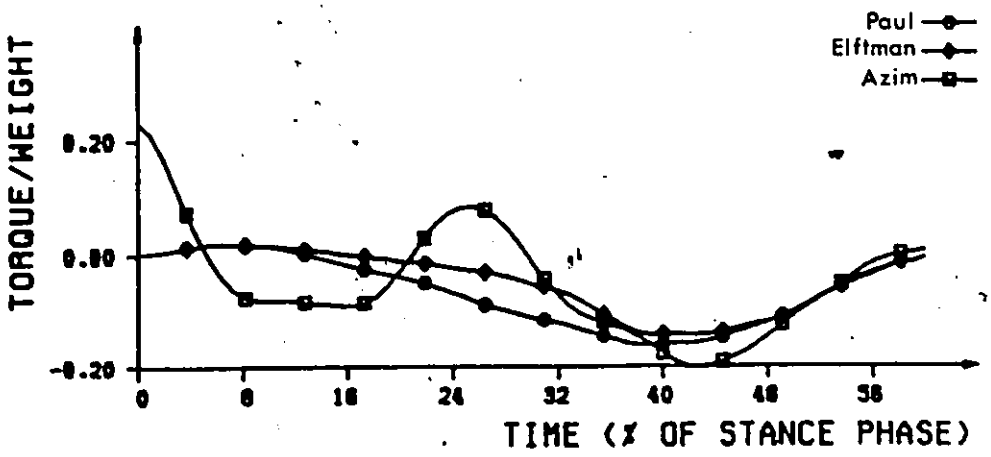

(c) Ankle-joint muscle torque

Figure 6.9
Predicted muscle torques during the stance phase
(Torque in N.m ; Weight in Kg)

old, walking at a speed of 1.2 m/s. Muscle torques measured by Elftman (1939b) and Paul (1971) were included in the figure to facilitate the comparison between our results and those obtained by other researchers. The figure shows muscle torques normalized to the weights of the subjects. It is clear from the figure that our results are, qualitatively, in good agreement with the results of other researchers. The knee-joint torque (Figure 6.9(b)), obtained by our method, shows the largest deviation from the results obtained by the other researchers. As explained earlier, this deviation could be attributed to the errors introduced by using the assumption regarding time-invariance of the knee-joint system.

Quantitative comparison between our results and those obtained by other researchers was not possible because of the different conditions under which the various experiments were conducted. One of the most important parameters that affects the muscle torques and floor-reaction forces is the speed of walking. Unfortunately, most researchers neglect to mention the walking speeds of their subjects so that other researchers could conduct their experiments under similar conditions.

6.4.2 Prediction of Floor-reaction Forces

Having determined the muscle torques at each joint, we can now analyse the kinetics of the lower extremity during the stance phase. Figure 6.10 shows the free-body diagrams of the segments of the lower extremity during the stance phase. The only difference between this figure and Figure 5.1 is that the floor-reaction forces have been added. The point of application of the floor reaction has been arbitrarily chosen at the heel. However, it should be kept in mind that the line of action of the reaction force changes during the stance phase.

Considering the thigh and shank segments, we notice that there are six unknown forces, these forces are the components of the reactions at the joints. All the other forces and torques are known. Therefore, equations (5.1) through (5.6) in Chapter 5, can be used to determine the components of the reaction force at the ankle joint (F_{x3}, F_{y3}). Once these forces have been determined, the components of the floor-reaction force can be computed by cosidering the dynamic equilibrium of the foot. That is

$$R_x = - F_{x3} - \frac{W_f}{g} \ddot{x}_3 \tag{6.21}$$

$$R_y = F_{y3} + \frac{W_f}{g} \ddot{y}_3 + W_f \tag{6.22}$$

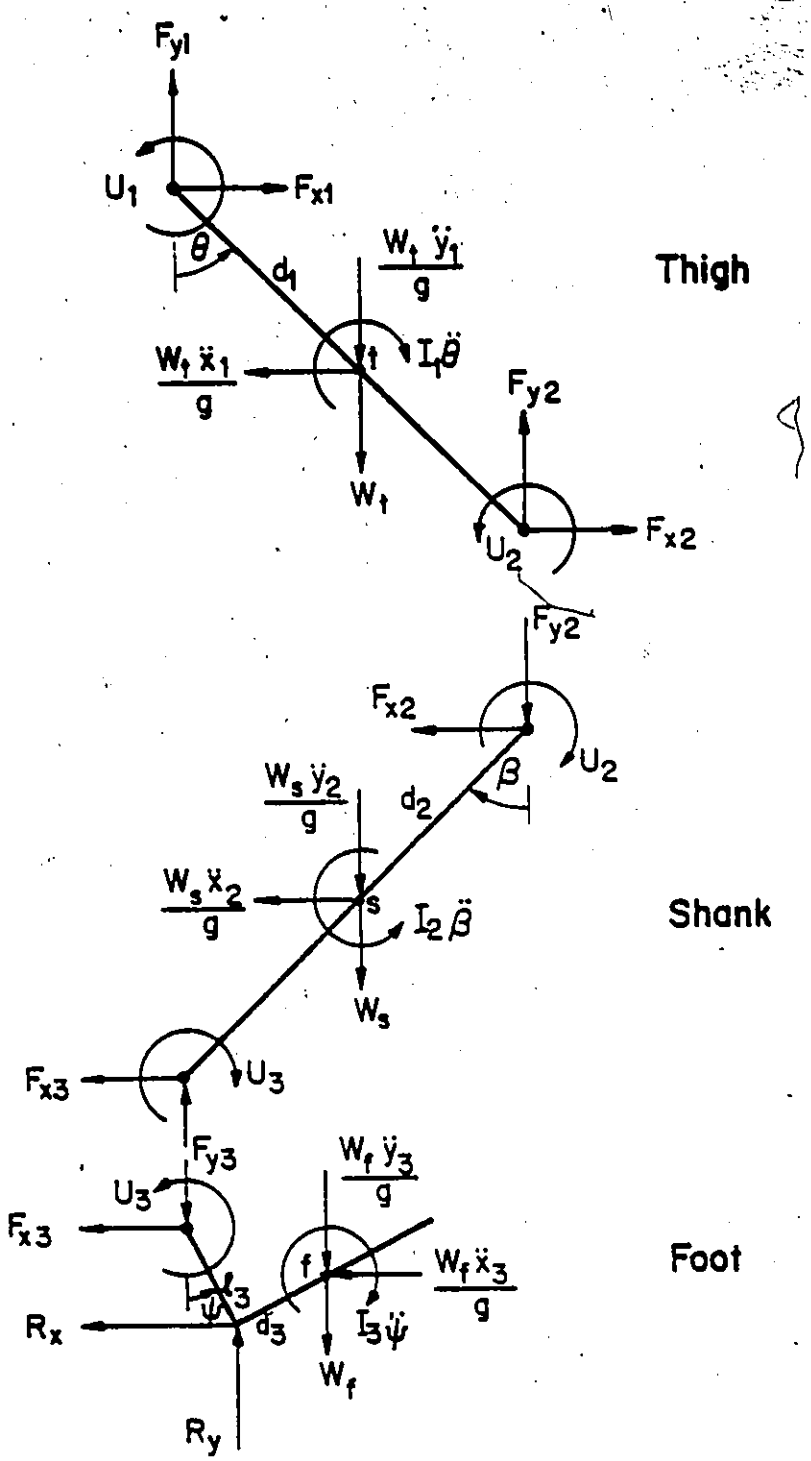

Figure 6.10
Free-body diagrams of segments of the lower extremity during the stance phase

where R_x and R_y are the components of the floor-reaction force acting on the foot.

The above equations were used to compute the floor-reaction forces shown in Figure 6.11. The figure also includes reaction forces measured by Elftman (1939a) and Inman (1966) using force plates. Figure 6.11(a) shows the vertical component of the floor-reaction force. This component exhibits two distinctive peaks. The first peak occurs after heel-strike, when the body rolls over the weight-bearing leg. The second peak occurs during the toe-only period, when the leg pushes the body up in preparation for the swing motion. Notice that the values of the reactions at the peaks exceed the body weight. This is due to the fact that in addition to gravitational forces, the body exerts forces on the floor due to acceleration. Figure 6.11(b) shows the horizontal component of the floor-reaction force which, at first, acts in the direction opposite the direction of progression, and then reverses direction near mid-stance when the center of gravity of the body moves forward of the extremity.

Again, the results obtained by our method agree, in a qualitative sense, with the results of other researchers. Deviation of our curves from the other curves could be attributed to one, or more, of the following factors:

(1) The experiments were conducted under different

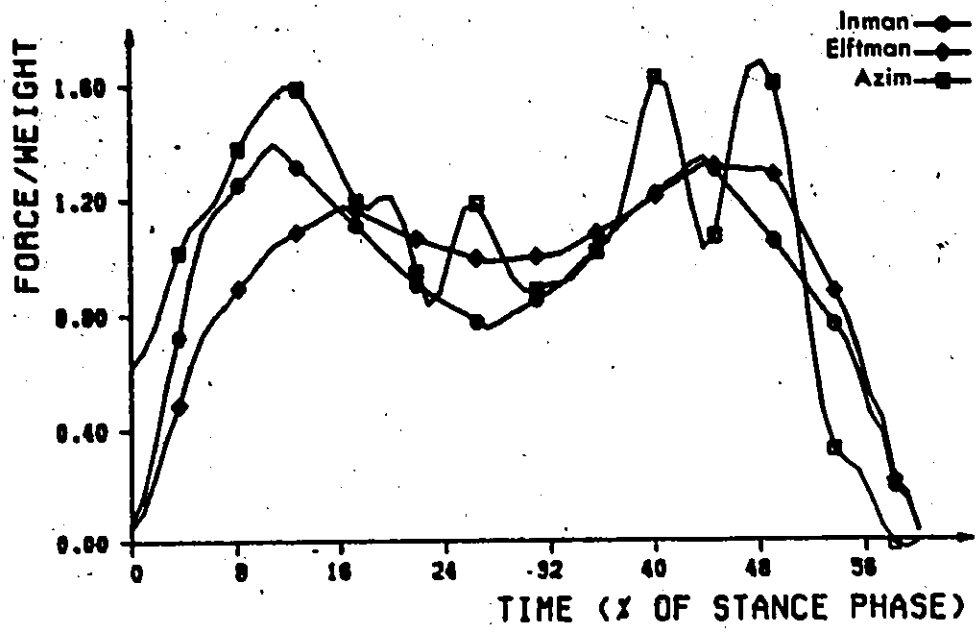

(a) Vertical component of floor-reaction force

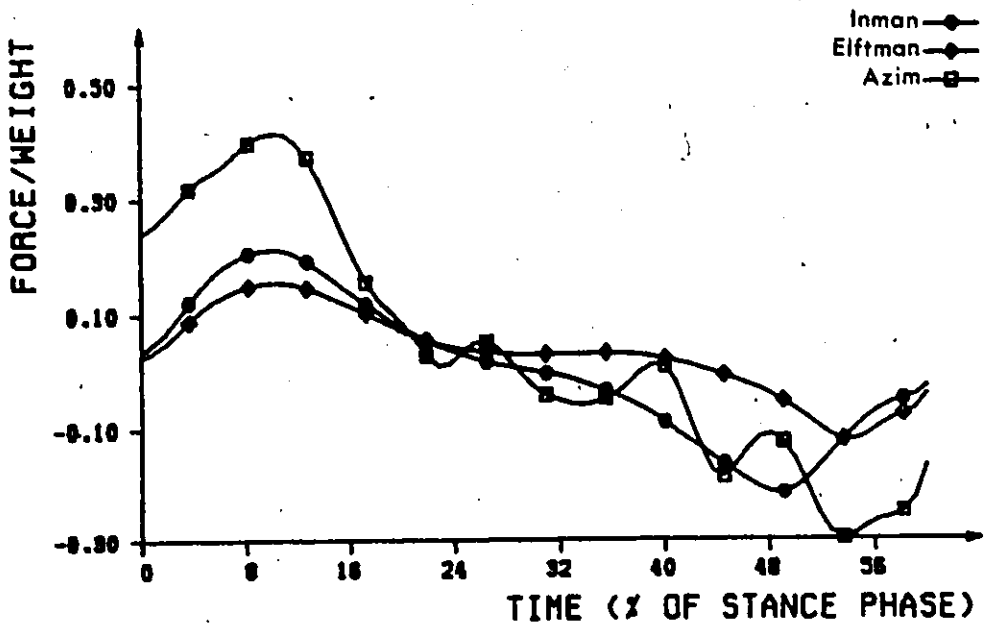

(b) Horizontal component of floor-reaction force

Figure 6.11
Predicted floor-reaction forces
(Force in N ; Weight in Kg)

conditions.

(2) The errors introduced in our results due to the assumptions of linearity and time-invariance.

(3) The use of EMG signals from a limited number of muscle groups because of the practical constraints imposed by hardware facilities.

Despite the inherent errors in our proposed technique, we believe that this is one of the first attempts to use EMG signals in the prediction of forces and torques during gait. The only other publication in this area, that we could find, was by Seireg et al. (1975) in which they tackled the problem in a different fashion. They first modeled the lower part of the body by a 7-link model and computed the forces at the various joints. They then used these forces to predict the envelopes of EMG signals from various muscles.

In this chapter, we have presented a new technique for the assessment of EMG processing strategies, based on the linearity characteristics of the locomotor system. We found that the RMS processor with a window of 140 ms results in the best linearity characteristics of the joint systems.

The joint systems were modeled as linear systems with the processed EMG signals as inputs, and the muscle torques at the joints as outputs. These models allowed us to

predict the muscle torques and floor-reaction forces during the stance phase without having to use a force plate to measure these forces.

The results we obtained, show that when EMG signals are properly processed, they can be used in the prediction of forces and torques during locomotion. The accuracy of our technique could be improved by using EMG signals from a larger number of muscle groups and developing more comprehensive models of the locomotor system.

CHAPTER 7

CONCLUSIONS

The research presented in this thesis is concerned with the analysis and processing of human gait data. Three different topics were considered. The kinematics of gait were studied, and a simple method for deriving spatial trajectories from goniometric measurements was presented. A study of the kinetics of the lower extremities was performed, and a new method for the quantitative assessment of normal and pathological gaits was proposed. Finally, methods of EMG signal processing were studied, and the feasibility of using processed EMG signals in quantitative analysis of gait was demonstrated.

Various techniques for signal processing and data acquisition were studied. Some devices were designed and constructed for use in noise reduction and multiplexing-demultiplexing of signals. Some of the major constraints on this work were imposed by hardware limitations. Sixteen channels of A/D converters were available, and eight of them were used for kinematic signals. This has limited the number of channels that could be used for EMG signals to only eight channels. Therefore, a compromise had to be

reached in the selection of muscles to be studied. Another limitation was imposed by computer memory size. Sampling of 16 channels at a rate of 500 Hz enabled us to to collect data corresponding to a maximum of 3 seconds of the subject's walk before a memory overflow occurred.

Most of the hardware problems could be solved by using an optical system to monitor the joint trajectories, which would free more channels for use in the acquisition of EMG signals from a larger number of muscles. In addition, use of one of the many new computer systems, with higher speed and the capability to access large memories, would allow a large number of walk cycles to be monitored.

Measurements of relative angular variations between segments of the lower extremities were performed using electrogoniometers. The signals were processed to reduce the noise outside of the useful frequency range of the signals. A new technique for deriving spatial trajectories from goniometric measurements was proposed and its accuracy was tested. The derivation was based on some simplifying assumptions. One of these was the assumption that pelvic rotations in both the sagittal and frontal planes were negligible. This assumption was probably the major source of error in our computations. Nevertheless, limited tests of accuracy showed that our technique resulted in errors of less than 7% in step length computations.

A study of the kinetics of the lower extremities during swing was carried out. A simple three-link model of the leg was used to compute forces and muscle torques at the joints. The rates of energy exchange between the muscles and the leg segments were computed. The total energy expended by the leg muscles during swing was studied for normal subjects and hemiplegic patients. The effect of walking speed on energy expenditure was studied, and it was found that the energy increased linearly with the square of the speed. Distinct differences were found between the relations obtained for normals and those obtained for hemiplegic patients at their early stages of recovery. Our results demonstrated the feasibility of the use of muscle energy as a quantitative measure for the assessment of gait. Data from 6 normals and 17 patients were used in the study. However, before our proposed method could be used in routine clinical assessment of patient recovery, a much larger population of normals and patients should be studied.

Electromyographic signals were collected from 8 muscles in the lower extremity. The dynamic behaviour of the locomotor system was studied. Processed EMG signals were used as inputs to the joint systems whose outputs were the muscle torques. A new technique for the evaluation of various EMG processing strategies was presented. The objective was to find the EMG processing strategy that

resulted in the best linear characteristics of the joint systems. The root-mean-square processor with 140 ms window was found to be the processor that closest met our criterion.

Transfer-function models were derived for the joint systems during the swing phase, and the models were used to predict muscle torques and floor-reaction forces during stance. Our results agreed, qualitatively, with the measurements obtained by other researchers. The errors in our results were attributed to the simplifying assumptions used in our analysis. In our experimental work, we were able to collect signals from only 8 of the leg muscles. For this reason, we had to exclude from the analysis some important muscles, such as the gluteus maximus and the iliopsoas muscles. This might be one of the major sources of errors in the results, and inclusion of these muscles in the analysis would probably improve the accuracy of our technique.

An important outcome of our work is to demonstrate that EMG signals, when properly processed, can be used in the quantitative analysis of gait. When more comprehensive studies of models of the locomotor system have been performed, EMG signals could be routinely used for the measurement of forces and moments acting at the joints.

REFERENCES

Abdel-Azim, M.S. (1975), "Modeling of the myoelectric source", M. Eng. Thesis, McMaster University.

Bajd, T., Kljajic, M., Trnkoczy, A. and Stanic, U. (1974), "Electrogoniometric measurement of step-length", Scand. J. of Rehab. Med., Vol. 6, pp. 78-80.

Bard, G.B. and Ralston, H.T. (1959), "Measurement of energy expenditure during ambulation, with special reference to evaluation of assistive devices", Arch. Phys. Med. Rehab., Vol. 40, October, pp. 415-420.

Basmajian, J.V. (1974), Muscles alive, Williams & Wilkins: Baltimore.

Beckett, R. and Chang, K. (1968), "An evaluation of the kinematics of gait by minimum energy", J. Biomechanics, Vol. 1, pp. 147-159.

Bendat, J.S. and Piersol, A.G. (1971), Random data: Analysis and measurement procedures, Wiley-Intersience: New York.

Brugger, W. (1978), "Charge-coupled-devices and computers in optical remote on-line tracking of human locomotion", Ph.D. Thesis, McMaster University.

Brunnstrom, S. (1970), Movement therapy in hemiplegia, Harper & Raw publishers: New York.

Chow, C.K. and Jacobson, D.H. (1971), "Studies of human locomotion via optimal programming", Math. Biosciences, Vol. 10, pp. 239-306.

Cooley, J.W. and Tukey, J.W. (1965), "An algorithm for the machine calculation of complex Fourier series", Mathematics of Computation, Vol. 19, No. 90, pp. 297-301.

Corcoran, P.J. and Brengelmann, G.L. (1970), "Oxygen uptake in normal and handicapped subjects, in relation to speed of walking beside velocity-controlled cart", Arch. Phys. Med. Rehab., Vol. 51, February, pp. 78-87.

Corcoran, P.J., Jebsen, R.H., Brengelmann, G.L. and Simons, B.C. (1970), "Effects of plastic and metal leg braces on speed and energy cost of hemiplegic ambulation", Arch. Phys. Med. Rehab., Vol. 51, February, pp. 69-77.

Cheng, I.S., Koozekanani, S.H. and Fatehi, M.T. (1975), " A simple computer-television interface system for gait analysis", IEEE Trans. Biomed. Eng., May, pp. 259-261.

Crosby, P.A. (1978), "Use of surface electromyogram as a measure of dynamic force in human limb muscles", Med. Biolog. Eng. Comput., Vol. 16, pp. 519-534.

Dempster, W.T. (1955), "Space requirements of the seated operator", WADC Tech. Report, 55-159.

Elftman, H. (1939a), "Forces and energy changes in the leg during walking", Am. J. Physiol., Vol. 125, No. 2, pp. 339-356.

Elftman, H. (1939b), "The function of the muscles in locomotion", Am. J. Physiol., Vol. 125, No. 2, pp. 357-366.

Grieve, D.W. (1968), "Gait patterns and the speed of walking", Biomedical Engineering, Vol. 3, March, pp. 119-122.

Hershler, C. (1977), "Quantitative electromyographic and goniometric analysis of normal and pathological human gaits", Ph.D. Thesis, McMaster University.

Hilburn, J.L. and Johnson, D.F. (1973), Manual of active filter design, McGraw-Hill: New York.

Hilderbrand, F.B. (1956), Introduction to numerical analysis, McGraw-Hill: New York, pp. 82-84.

Hollinshead, W.H. (1976), Functional anatomy of the limbs and back, Saunders: Philadelphia.

Inman, V.T. (1966), "Human locomotion", Can. Med. Assoc. J., Vol. 94, pp. 1047-1054.

Kasvand, T. and Milner, M. (1972), "Pattern recognition applied to measurement of human limb positions during movement", Journal of Cybernetics, Vol. 2, No. 1, pp. 66-78.

Kasvand, T., Milner, M., Quanbury, A.Q. and Winter, D.A. (1976), "Computers and the kinesiology of gait", Comp. Biol. Med., Vol. 6, pp. 111-120.

Katz, B. (1966), Nerve, muscle, and synapse, McGraw-Hill: New York.

Kljajic, M. and Trnkoczy, A. (1978), "A study of adaptive control principle orthoses for lower extremities", IEEE Trans. Sys. Man Cyb., Vol. SMC-8, April, pp. 313-321.

Kreifeldt, J.G. and Sumner, Y. (1974), "A signal-to noise investigation of nonlinear electromyographic processors" IEEE Trans. Biomed. Eng., Vol. BME-21, July, pp. 298-308.

Lamoreux, L.W. (1971), "Kinematic measurements in the study of human walking", Bull. Prosth. Res., BPR 10-15, Spring, pp. 3-84.

Liberson, W.T (1965), "Biomechanics of gait: a method of study", Arch. Phys. Med. Rehab., Vol. 46, January, pp. 37-48.

Miller, M. and Seireg, A. (1977), "Effect of load, speed and activity history on the EMG signals from the intact human muscles", J. Bioengineering, Vol. 1, pp. 147-155.

Milner, M., Basmajian, J.V. and Quanbury, Q. (1971), "Multifactorial analysis of walking by electromyography and computers", Am. J. Phys. Med., Vol. 50, No. 5, pp. 235-258.

Milner, M. Dall, D., McConnell, V.A., Brennan, P.K. and Hershler, C. (1973), "Angle diagrams in the assessment of locomotor function", S. Afr. Med. Journal, Vol. 47, pp. 951-957.

Murray, M.P. and Clarkson, B.H. (1966), "The vertical pathways of the foot during level walking", Journal of the American Physical Therapy Association, Vol. 46, No. 6, pp. 585-599.

Murray, M.P. Kory, R.C., Clarkson, B.H. and Sepic, S.B. (1966), "comparison of free and fast speed walking patterns of normal men", Am. J. Phys. Med., Vol. 45, No. 1, pp. 8-24.

Murray, M.P. (1967), "Gait as a total pattern of movement". Am. J. Phys. Med., Vol. 46, No. 1, pp. 290-333.

Naumann, S. (1978), "Electromyographic and position controlled functional electrical stimulation of the musculature about the human ankle joint", Ph.D. Thesis, McMaster University.

Otnes, R.K. and Enchoson, L. (1972), Digital time series analysis, Wiley-Intersience: New York.

Paul, J.P. (1965), "Bioengineering studies of the forces transmitted by joints (II)", In Biomechanics and Related Bioengineering Topics, Pergamon Press: London.

Paul, J.P. (1967), "Forces Transmitted by joints in the human body", Proc. Instit. Mech. Eng., Vol. 181, No. 3j, pp. 8-15.

Paul, J.P. (1971), "Comparison of EMG signals from leg muscles with the corresponding force actions calculated from walkpath measurements", Human Locomotion, The Institute of Mechanical Engineers: London, pp. 16-26.

Peizer, E. and Wright, D.W. (1971), In Human Locomotion, The Institute of Mechanical Engineers: London, pp. 196-214.

Perritt, R.Q. and Milner, M. (1976), "A simple inexpensive eight channel multiplexer for EMG in human locomotion", Med. & Biological Engineering, January, pp. 104-106.

Plagenhoef, S. (1971), Patterns of human motion, Prentice Hall: New Jersey.

Quanbury, A. and Winter, D.A. (1974), "Calculation of floor reaction forces from kinematic data during the single support phase of human gait", Fifth Can. Med. Biolog. Eng. Comput., Digest of papers, September, pp. 7.3A-7.3B.

Rader, C.M. and Gold, B. (1967), "Digital filter design techniques in the frequency domain", Proc. IEEE, Vol. 55, February, pp. 149-171.

Seireg, A. and Arvikar, R.T. (1973), "A mathematical model for the evaluation of forces in lower extremities of the musculo-skeletal system", J. Biomechanics, Vol. 6, pp. 313-326.

Seireg, A. and Arvikar, R.T. (1975), "The prediction of muscular load sharing and joint forces in the lower extremities during walking", J. Biomechanics, Vol. 8, pp. 89-102.

Sutherland, D.H. and Hagy, J.L. (1972), "Measurement of gait movements from motion picture film", J. of Bone and Joint Surgery, Vol. 54-A, No. 4, June, pp. 787-797.

Tinkoczy, A. and Bajd, T. (1975), "A simple electrogoniometric system and its testing", IEEE Trans. Biomed. Eng., May, pp. 257-259.

Welch, P.D. (1967), "The use of Fast Fourier Transform for estimation of power spectra: A method based on time-averaging over short, modified periodograms", IEEE Trans. Audio Eloctroacoust., Vol. AU-15, June, pp. 70-73.

Winter, D.A., Sidwell, H.G. and Hobson, D.A. (1974), "Measurement and reduction of noise in kinematics of locomotion", J. Biomechanics, Vol. 7, pp. 157-159.